



GE Nuclear Energy


NEDO-32725
Revision 1
Class I
DRF 0000-0006-8900
August 2002

TRACG Qualification for SBWR

Volume 2

Authors:

J. R. Fitch
D. Abdollahian
Md. Alamgir
T. Bandurski (PSI)
Y.K. Cheung
J.M. Healzer
A. Hunsbedt
A.J. Illich
L.A. Klebanov
U. C. Saxena
B. S. Shiralkar
S. Sitaraman
M. Stempniewicz (KEMA)
A. I. Yang
J. Wouters (KEMA)

Approved: 
C. J. Deacon, Manager
Advanced Reactor Projects

**IMPORTANT NOTICE REGARDING
CONTENTS OF THIS REPORT
PLEASE READ CAREFULLY**

Neither the General Electric Company nor any of the contributors to this document:

a. Makes any warranty or representation, express or implied, with respect to the accuracy, completeness, or usefulness of the information contained in this document, or that the use of any information, apparatus, method, or process disclosed in this document may not infringe privately owned rights;

or

b. Assumes any liabilities, including but not limited to nuclear liability, with respect to the use of, or for damages resulting from the use of any information, apparatus, method, or process disclosed in this document.

This work was performed partially as part of a contract between various utilities and GE for “ESBWR Development”.

ACKNOWLEDGMENT

The contributions of the following individuals to analyses which form the basis of this report are gratefully acknowledged:

G. Bianchini (ENEA)
P.F. Billig
P.K. Dill
R. E. Gamble
K. Kobayashi (JAPC)
P. Masoni (ENEA)
J. Morales (IIE)

In addition, the support of C. Heck and J. G. M. Andersen in the development of the models needed in TRACG is gratefully acknowledged. K. Miyata and T. Narazaki of JAPC, and A. Petry of GRS made contributions to several sections and also provided technical review of the document. Special recognition and acknowledgment are given to Trish Bautista, Yolanda Espino and Malin Swope for their assistance in the typing, compilation, editing and final preparation of this report. The work reported in this document was performed under an EPRI contract. The contributions of T. J. Mulford and R. T. Fernandez of EPRI are greatly appreciated.

Table of Contents

— VOLUME 1 —

	<u>Page</u>
EXECUTIVE SUMMARY	S-1
1. INTRODUCTION	1.1-1
1.1 Relationship to Generic TRACG Qualification Report	1.1-1
1.2 Relationship to Other Documents Needed for TRACG Application	1.2-1
1.3 Report Road Map	1.3-1
1.4 References	1.4-1
2. QUALIFICATION STRATEGY	2-1
2.1 Assessment Matrix and Coverage of PIRT Phenomena	2.1-1
2.1.1 Separate Effects Tests	2.1-2
2.1.2 Component Tests	2.1-3
2.1.3 Integral System Response Tests	2.1-3
2.1.4 Plant Operating Data	2.1-5
2.1.5 Summary of Test Coverage	2.1-5
2.2 References	2.2-1
3. SEPARATE EFFECTS TESTS	3.1-1
3.1 Toshiba Low Pressure Void Fraction Tests	3.1-1
3.1.1 Introduction	3.1-1
3.1.2 Test Facility and Test Matrix	3.1-1
3.1.3 Applicability of Data to SBWR	3.1-2
3.1.4 TRACG Model	3.1-3
3.1.5 Test Simulation	3.1-3
3.1.6 Results of Calculations	3.1-4
3.1.7 Summary and Conclusions	3.1-4
3.1.8 References	3.1-5
3.2 Ontario Hydro Void Fraction Tests	3.2-1
3.2.1 Introduction	3.2-1
3.2.2 Description of Ontario Hydro Void Fraction Tests	3.2-1
3.2.3 Applicability of Data to SBWR	3.2-5
3.2.4 TRACG Model	3.2-6
3.2.5 TRACG Simulation	3.2-6

Table of Contents

(continued)

	<u>Page</u>
3.2.6 Results of Calculations	3.2-7
3.2.6.1 Accuracy of TRACG Calculations	3.2-7
3.2.7 Summary and Conclusions	3.2-8
3.2.8 References	3.2-8
3.3 Summary of Separate Effects Comparisons	3.3-1
3.3.1 Void Fraction Data	3.3-1
3.3.2 PSTF Level Swell Tests	3.3-3
3.3.3 Condensation in the Presence of Noncondensibles - University Tests	3.3-4
3.3.4 Critical Flow	3.3-5
3.3.5 Frictional Pressure Drop	3.3-5
3.3.6 Critical Power	3.3-6
3.3.6.1 ATLAS Critical Power Data	3.3-6
3.3.6.2 Applicability of GEXL Correlation for Bundles with 2.8m Length	3.3-7
3.3.7 SPERT Reactivity Insertion Test	3.3-7
3.3.8 Thermal Hydraulic Stability	3.3-8
3.3.9 Flow Oscillations at Low Pressure	3.3-9
3.3.10 Humboldt Bay and Bodega Bay Pressure Suppression Test Programs	3.3-9
3.3.11 References	3.3-10
 4. COMPONENT PERFORMANCE TESTS	 4.1-1
4.1 Panthers PCC Performance	4.1-1
4.1.1 Introduction	4.1-1
4.1.2 Test Facility/Test Matrix	4.1-2
4.1.2.1 Test Facility	4.1-2
4.1.2.2 Test Matrix and Data Analysis	4.1-3
4.1.3 Applicability of Data To SBWR	4.1-5
4.1.3.1 Scope	4.1-5
4.1.3.2 SBWR	4.1-5
4.1.3.3 PANTHERS	4.1-8
4.1.3.4 PIRT Phenomena and Coverage	4.1-12
4.1.3.5 Scaling	4.1-13
4.1.3.6 Conclusion	4.1-14
4.1.4 TRACG Models and Nodalization	4.1-14
4.1.4.1 One-Tube Model	4.1-14
4.1.4.2 Eight-Tube Model	4.1-18
4.1.4.3 Six-Tube Model	4.1-19
4.1.4.4 Determination of Hydraulic Loss Factors	4.1-19
4.1.4.5 TRACG Heat Transfer Correlations	4.1-21

Table of Contents

(continued)

	<u>Page</u>
4.1.5 Test Simulation	4.1-21
4.1.5.1 Steady-State Tests	4.1-21
4.1.5.2 Transient Tests	4.1-22
4.1.5.3 Atmospheric Pressure Boundary Condition	4.1-23
4.1.6 Results and Discussion	4.1-23
4.1.6.1 Steady-State Pure-Steam Tests	4.1-24
4.1.6.2 Steady-State Steam-Air Tests	4.1-24
4.1.6.3 Transient Tests	4.1-26
4.1.6.4 Evaluation of Tube Wall Temperature Data	4.1-28
4.1.6.5 Accuracy of TRACG Calculations	4.1-34
4.1.7 Summary and Conclusions	4.1-34
4.1.7.1 Condenser Performance Under Prototypical Conditions	4.1-35
4.1.7.2 Condenser Performance under Non-Prototypical Conditions	4.1-35
4.1.7.3 Evaluation of TRACG Qualification Needs	4.1-36
4.1.8 References	4.1-38
 4.2 PANTHERS IC Performance	 4.2-1
4.2.1 Introduction	4.2-1
4.2.2 Test Facility and Test Matrix	4.2-1
4.2.2.1 Test Facility	4.2-1
4.2.2.2 Test Matrix and Data Analysis	4.2-2
4.2.3 Applicability of Data to SBWR	4.2-3
4.2.3.1 Steady-State Tests	4.2-3
4.2.3.2 Transient Tests	4.2-4
4.2.3.3 PIRT Phenomena and Coverage	4.2-4
4.2.3.4 Scaling	4.2-5
4.2.4 TRACG Model and Nodalization	4.2-5
4.2.4.1 Model Description	4.2-6
4.2.4.2 TRACG Heat Transfer Correlations	4.2-8
4.2.5 Test Simulation	4.2-8
4.2.5.1 Steady-State Tests	4.2-8
4.2.5.2 Transient Tests	4.2-9
4.2.6 Results and Discussion	4.2-9
4.2.6.1 Steady-State Tests	4.2-10
4.2.6.2 Transient Tests	4.2-10
4.2.6.3 Accuracy of TRACG Calculations	4.2-12
4.2.7 Summary and Conclusions	4.2-12
4.2.7.1 Pure Steam Condensation Performance	4.2-12
4.2.7.2 Noncondensible Accumulation and Venting	4.2-13
4.2.7.3 IC Pool Level Effects	4.2-13
4.2.7.4 Evaluation of TRACG Qualification Needs	4.2-13

Table of Contents

(continued)

	<u>Page</u>
4.2.8 References	4.2-15
4.3 PANDA PCC Performance	4.3-1
4.3.1 Introduction	4.3-1
4.3.2 Test Facility and Test Matrix	4.3-1
4.3.2.1 Test Facility	4.3-1
4.3.2.2 Test Matrix	4.3-2
4.3.3 Applicability of Data to SBWR	4.3-2
4.3.3.1 Overview of Data Applicability and Test Facility Scaling	4.3-2
4.3.3.2 PIRT Phenomena and Coverage	4.3-3
4.3.4 TRACG Model	4.3-4
4.3.5 Test Simulation	4.3-6
4.3.6 Results of Post-Test Calculations	4.3-7
4.3.6.1 Comparison of Experimental and Calculated Results	4.3-7
4.3.6.2 Effect of Reduced Pool Water Level	4.3-8
4.3.6.3 Accuracy of TRACG Calculations	4.3-8
4.3.7 Summary and Conclusions	4.3-8
4.3.7.1 Condenser Performance	4.3-8
4.3.7.2 Evaluation of TRACG Qualification Needs	4.3-9
4.3.8 References	4.3-11
4.4 Suppression Pool Stratification Tests	4.4-1
4.4.1 Introduction	4.4-1
4.4.2 Test Facility/Test Matrix	4.4-1
4.4.3 Applicability of Data to SBWR	4.4-2
4.4.3.1 General Data Applicability and Test Facility Scaling	4.4-2
4.4.3.2 PIRT Phenomena and Coverage	4.4-2
4.4.3.3 Scaling Parameters Range	4.4-3
4.4.4 TRACG Model	4.4-3
4.4.5 Test Simulation	4.4-4
4.4.6 Results of Post-Test Calculations	4.4-5
4.4.6.1 Test 5707-01	4.4-5
4.4.6.2 Test 5807-29	4.4-6
4.4.6.3 Condensation of Blowdown Steam	4.4-6
4.4.6.4 Accuracy of TRACG Calculations	4.4-6
4.4.7 Summary and Conclusions	4.4-7
4.4.8 References	4.4-7

— VOLUME 2 —

5. INTEGRAL SYSTEMS TESTS	5.1-1
5.1 GIST	5.1-4
5.1.1 Introduction	5.1-4

Table of Contents

(continued)

	<u>Page</u>
5.1.2 Description of GIST Facility and Tests	5.1-4
5.1.3 Applicability of Data to SBWR	5.1-5
5.1.3.1 General Test Facility Scaling	5.1-5
5.1.3.2 PIRT Phenomena and Coverage	5.1-6
5.1.3.3 Conclusions on Data Applicability	5.1-9
5.1.4 TRACG Model	5.1-10
5.1.5 TRACG Simulation of GIST Tests	5.1-11
5.1.5.1 Initial Conditions	5.1-11
5.1.5.2 Test Control	5.1-11
5.1.5.3 Tests Analyzed with TRACG	5.1-12
5.1.6 Results of Post-Test Calculations	5.1-13
5.1.6.1 TRACG/GIST Comparisons for Bottom Drain Break LOCA (Test A07)	5.1-13
5.1.6.2 TRACG/GIST Comparisons for Other LOCA Types	5.1-14
5.1.6.3 RPV Dome Pressure (Figures 5.1-17 through 5.1-20)	5.1-15
5.1.6.4 GDCS Flow (Figures 5.1-21 through 5.1-24)	5.1-15
5.1.6.5 Annulus Pressure Drop (Figures 5.1-25 through 5.1-28)	5.1-15
5.1.6.6 Core Pressure Drop (Figures 5.1-29 through 5.1-32)	5.1-16
5.1.6.7 Margin to Boiling Transition	5.1-16
5.1.7 Conclusions	5.1-16
5.1.8 References	5.1-16
5.2 GIRAFFE Helium Tests	5.2-1
5.2.1 Introduction	5.2-1
5.2.1.1 Purpose of Tests	5.2-1
5.2.1.2 Tests Selected for Post-Test Analysis	5.2-2
5.2.1.3 Purpose of Post-Test Analysis	5.2-3
5.2.2 Test Facility/Test Matrix	5.2-3
5.2.2.1 GIRAFFE Test Facility	5.2-3
5.2.2.2 Test Matrix	5.2-5
5.2.3 Applicability of Data to SBWR	5.2-5
5.2.3.1 General Data Applicability and Test Facility Scaling	5.2-6
5.2.3.2 PIRT Phenomena and Coverage	5.2-6
5.2.3.3 Conclusions on Data Applicability	5.2-10
5.2.4 TRACG Model	5.2-10
5.2.4.1 Nodalization of Test Facility	5.2-10
5.2.4.2 3-D Vessel Component	5.2-11
5.2.4.3 RPV and Associated Piping	5.2-11
5.2.4.4 PCC	5.2-11
5.2.4.5 Main Vent and Vacuum Breaker	5.2-12
5.2.4.6 Comparison to the SBWR Model	5.2-12
5.2.5 Test Simulation	5.2-13
5.2.5.1 Introduction	5.2-13

Table of Contents

(continued)

	<u>Page</u>
5.2.5.2 Component Heat Loss and Decay Heat	5.2-13
5.2.5.3 Initial Conditions	5.2-14
5.2.6 Results and Discussion	5.2-15
5.2.6.1 Test Results	5.2-15
5.2.6.2 General Discussion	5.2-16
5.2.6.3 Test H1	5.2-16
5.2.6.4 Test H2	5.2-18
5.2.6.5 Test H3	5.2-21
5.2.6.6 Test H4	5.2-22
5.2.6.7 Test T2	5.2-24
5.2.6.8 Accuracy of TRACG Calculations	5.2-25
5.2.7 Conclusions	5.2-25
5.2.7.1 General Conclusions	5.2-25
5.2.7.2 PIRT Conclusions	5.2-27
5.2.8 References	5.2-27
5.3 GIRAFFE Systems Interactions Tests	5.3-1
5.3.1 Introduction	5.3-1
5.3.2 Test Facility	5.3-2
5.3.2.1 The Reactor Pressure Vessel (RPV)	5.3-2
5.3.2.2 Drywell	5.3-2
5.3.2.3 Wetwell	5.3-3
5.3.2.4 GDCS Pool	5.3-3
5.3.2.5 Passive Containment Cooling System (PCCS)	5.3-3
5.3.2.6 Isolation Condenser System (ICS)	5.3-3
5.3.3 Applicability of Data to SBWR	5.3-3
5.3.3.1 General Data Applicability and Test Facility Scaling	5.3-4
5.3.3.2 PIRT Phenomena and Coverage	5.3-5
5.3.3.3 Conclusions on Data Applicability	5.3-10
5.3.4 TRACG Model	5.3-10
5.3.4.1 3-D Vessel Component	5.3-11
5.3.4.2 RPV Internals	5.3-11
5.3.4.3 RPV Piping	5.3-11
5.3.4.4 Drywell Piping	5.3-12
5.3.4.5 Wetwell Piping	5.3-12
5.3.4.6 GDCS Piping	5.3-12
5.3.4.7 IC and PCC systems	5.3-12
5.3.4.8 Comparison with SBWR Nodalization	5.3-13
5.3.5 Test Simulation	5.3-13
5.3.5.1 Introduction	5.3-13
5.3.5.2 Heat Losses in the System	5.3-13
5.3.5.3 Decay Heat	5.3-14
5.3.5.4 Initial Conditions	5.3-14

Table of Contents

(continued)

	<u>Page</u>
5.3.6 Test and TRACG Simulation Results	5.3-14
5.3.6.1 Introduction	5.3-14
5.3.6.2 Test GS1	5.3-16
5.3.6.3 Test GS2	5.3-18
5.3.6.4 Test GS3	5.3-19
5.3.6.5 Test GS4	5.3-20
5.3.6.6 Sensitivity Studies	5.3-21
5.3.7 Summary and Conclusions	5.3-22
5.3.7.1 General Conclusions	5.3-22
5.3.7.2 Conclusions Related to Key PIRT Phenomena	5.3-22
5.3.7.3 Final Observations	5.3-23
5.3.8 References	5.3-24
5.4 One-Sixth Scale Boron Mixing Tests	5.4-1
5.4.1 Introduction	5.4-1
5.4.2 Test Facility	5.4-1
5.4.3 Applicability to SBWR	5.4-2
5.4.4 TRACG Model	5.4-4
5.4.4.1 Model Description	5.4-4
5.4.4.2 Test Initial Conditions	5.4-5
5.4.5 Test Simulation	5.4-6
5.4.5.1 Model 1	5.4-7
5.4.5.2 Model 2	5.4-7
5.4.6 TRACG Results	5.4-7
5.4.6.1 Model 1	5.4-7
5.4.6.2 Model 2	5.4-8
5.4.7 Conclusions	5.4-8
5.4.7.1 General Conclusions	5.4-8
5.4.7.2 Conclusions Related to Key PIRT Phenomena	5.4-8
5.4.8 References	5.4-9
5.5 PSTF Mark III Containment Response	5.5-1
5.5.1 Introduction	5.5-1
5.5.2 Test Facility/Test Matrix	5.5-1
5.5.3 Applicability of Data to SBWR	5.5-2
5.5.3.1 General Data Applicability and Test Facility Scaling	5.5-2
5.5.3.2 PIRT Phenomena and Coverage	5.5-2
5.5.3.3 Scaling Parameters Range	5.5-3
5.5.4 TRACG Model and Nodalization	5.5-4
5.5.5 Test Simulation	5.5-4
5.5.6 Results of Post-Test Calculations	5.5-4
5.5.6.1 Results for Test 5703-01	5.5-5
5.5.6.2 Results for Test 5703-02	5.5-5
5.5.6.3 Results for Test 5703-03	5.5-5

Table of Contents

(continued)

	<u>Page</u>
5.5.6.4 Accuracy of TRACG Calculations	5.5-5
5.5.7 Summary and Conclusions	5.5-6
5.5.8 References	5.5-6
5.6 4T/Mark II Containment Response	5.6-1
5.6.1 Introduction	5.6-1
5.6.2 Test Facility/Test Matrix	5.6-1
5.6.3 Applicability of Data to SBWR	5.6-2
5.6.3.1 General Data Applicability and Test Facility Scaling	5.6-2
5.6.3.2 PIRT Phenomena and Coverage	5.6-2
5.6.3.3 Scaling Parameters Range	5.6-3
5.6.4 TRACG Model	5.6-3
5.6.5 Test Simulation	5.6-4
5.6.6 Results of Post-Test Calculations	5.6-4
5.6.6.1 Heated Drywell Tests	5.6-5
5.6.6.2 Unheated Drywell Test	5.6-7
5.6.6.3 Accuracy of TRACG Predictions	5.6-8
5.6.7 Summary and Conclusions	5.6-9
5.6.8 References	5.6-9
5.7 PANDA Transient Tests (M-Series)	5.7-1
5.7.1 Introduction	5.7-1
5.7.2 Test Facility and Test Matrix	5.7-2
5.7.3 Applicability of Data to SBWR	5.7-3
5.7.3.1 Overview of Data Applicability and Test Facility Scaling	5.7-3
5.7.3.2 PIRT Phenomena and Coverage	5.7-8
5.7.3.3 Conclusions on Data Applicability	5.7-12
5.7.4 PANDA TRACG Input Model Description	5.7-12
5.7.4.1 Wetwell, Drywell and GDCS Pool	5.7-12
5.7.4.2 RPV and Associated Piping	5.7-13
5.7.4.3 PCC and IC Condensers and Their Pools	5.7-13
5.7.4.4 Main Vents and Vacuum Breakers	5.7-14
5.7.4.5 System Line Flow Resistance	5.7-14
5.7.4.6 Component Heat Loss and Heat Capacity	5.7-15
5.7.4.7 Decay Heat	5.7-15
5.7.4.8 Comparison with SBWR Containment Model	5.7-16
5.7.4.9 Model Changes for Post-Test Analyses	5.7-17
5.7.5 TRACG Simulation of PANDA Tests	5.7-20
5.7.5.1 Initial Conditions	5.7-20
5.7.5.2 Test Control	5.7-21
5.7.5.3 Tests M3, M3A, and M3B	5.7-21
5.7.5.4 Tests M2, M10A, and M10B	5.7-22
5.7.5.5 Tests M6/8, M7, and M9	5.7-23

Table of Contents

(continued)

	<u>Page</u>
5.7.6 Results Of Post-Test Calculations	5.7-23
5.7.6.1 Tests M3, M3A and M3B	5.7-25
5.7.6.2 Tests M2, M10A and M10B	5.7-30
5.7.6.3 Other Tests	5.7-37
5.7.6.4 Accuracy of TRACG Predictions	5.7-44
5.7.7 Summary and Conclusions	5.7-44
5.7.7.1 Purpose and Scope of Post-Test Evaluation	5.7-44
5.7.7.2 Evaluation of TRACG Qualification Needs	5.7-45
5.7.7.3 Summary of Conclusions	5.7-51
5.7.8 References	5.7-52
 6. NATURAL CIRCULATION AND FLOW OSCILLATION TESTS	 6.1-1
6.1 Dodewaard Steady-State Operation	6.1-2
6.1.1 Introduction	6.1-2
6.1.2 Description of Dodewaard	6.1-2
6.1.3 Applicability of Data to SBWR	6.1-3
6.1.4 TRACG Model	6.1-5
6.1.5 TRACG Simulation	6.1-6
6.1.6 Results of Calculations	6.1-7
6.1.7 Summary and Conclusions	6.1-8
6.1.8 References	6.1-8
6.2 Analysis of February 1992 Startup of Dodewaard Natural Circulation BWR	6.2-1
6.2.1 Introduction	6.2-1
6.2.2 Dodewaard Plant and Startup Procedure	6.2-1
6.2.2.1 Brief Description of Dodewaard	6.2-1
6.2.2.2 Normal Startup Procedure	6.2-2
6.2.2.3 Sequence of Steps During February 1992 Startup	6.2-2
6.2.2.4 General Discussion of First Phase of Startup	6.2-2
6.2.2.5 Discussion of the Measurements	6.2-3
6.2.3 Applicability of the Dodewaard Startup Data to the SBWR	6.2-5
6.2.4 TRACG Model of Dodewaard for Startup Simulation	6.2-7
6.2.4.1 Model Description	6.2-8
6.2.4.2 Vessel	6.2-8
6.2.5 Simulation of the February 1992 Startup	6.2-9
6.2.5.1 Initial Conditions	6.2-9
6.2.5.2 Boundary Conditions	6.2-10
6.2.6 Qualification Results	6.2-11
6.2.6.1 Comparison of TRACG Results with Measured Data	6.2-11
6.2.6.2 Analysis of Other TRACG Results	6.2-14
6.2.6.3 General Analysis of TRACG Results	6.2-15
6.2.6.4 Discussion of the Results	6.2-18

Table of Contents

(continued)

	<u>Page</u>
6.2.6.5 Accuracy of TRACG Predictions	6.2-19
6.2.7 Conclusions/Results of the Assessment	6.2-19
6.2.7.1 General Conclusions	6.2-19
6.2.7.2 Adequacy of TRACG Models	6.2-20
6.2.8 References	6.2-20
6.3 CRIEPI Low Pressure Oscillation Tests	6.3-1
6.3.1 Introduction	6.3-1
6.3.2 Test Facility/Test Matrix	6.3-1
6.3.3 Applicability of Data to SBWR	6.3-2
6.3.4 TRACG Model	6.3-4
6.3.5 Test Simulation	6.3-4
6.3.6 Results of Post-Test Calculations	6.3-4
6.3.6.1 Accuracy of TRACG Calculations	6.3-7
6.3.7 Summary and Conclusion	6.3-7
6.3.8 References	6.3-7
6.4 PANDA Exploratory Tests	6.4-1
6.4.1 Introduction	6.4-1
6.4.2 Test Facility/Test Matrix	6.4-1
6.4.3 Applicability of Data to SBWR	6.4-3
6.4.4 TRACG Models	6.4-4
6.4.5 Test Simulation	6.4-5
6.4.6 Results of Post-Test Calculations	6.4-5
6.4.7 Summary and Conclusion	6.4-7
6.4.8 Reference	6.4-7
6.5 Summary of Low-Power Stability Analyses	6.5-1
6.5.1 Introduction	6.5-1
6.5.2 Review of Data from CRIEPI and PANDA Test Facilities	6.5-1
6.5.2.1 Sensitivity to Inlet Subcooling	6.5-2
6.5.2.2 Sensitivity to System Power	6.5-3
6.5.2.3 Sensitivity to System Pressure	6.5-3
6.5.2.4 Sensitivity to Static Head and Hydraulic Losses	6.5-3
6.5.3 Development of a Stability Map for Startup Oscillations	6.5-4
6.5.3.1 Criteria for the Upper Boundary	6.5-4
6.5.3.2 Criteria for the Lower Boundary	6.5-6
6.5.3.3 Effect of the Flashing Number	6.5-6
6.5.4 Implications for Dodewaard Startup	6.5-7
6.5.5 Implications for the SBWR Startup	6.5-8
6.5.6 Conclusions	6.5-9
6.5.7 References	6.5-10

Table of Contents

(continued)

	<u>Page</u>
7. MODELING TECHNIQUES TO ADDRESS TRACG MODEL LIMITATIONS	7.1-1
7.1 Phenomena Requiring More Modeling Detail	7.1-1
7.1.1 Passive Containment Condenser Modeling	7.1-1
7.1.2 Parallel PCC Operation	7.1-2
7.2 Phenomena Treated with Bounding Models	7.2-1
7.2.1 Operation of the Standby Liquid Control System (SLCS)	7.2-1
7.2.2 Suppression Pool Stratification	7.2-2
7.2.3 Stratification of Leakage Flow in the Wetwell Gas Space	7.2-3
7.2.4 Mixing of Drywell Noncondensable Gases	7.2-4
7.3 Conclusions	7.3-1
7.4 References	7.4-1
 8. SBWR PLANT NODALIZATION	 8.1-1
8.1 SBWR Reactor Vessel	8.1-1
8.1.1 Introduction	8.1-1
8.1.2 Evolution of SBWR Nodalization	8.1-1
8.1.3 Nodalization Rationale	8.1-2
8.1.4 Nodalization Feedback from Test Facility and BWR Plant Qualification	8.1-2
8.1.5 Nodalization for LOCA/ECCS	8.1-2
8.1.5.1 Reactor Vessel for LOCA/ECCS	8.1-3
8.1.5.2 Fuel Channels for LOCA/ECCS	8.1-4
8.1.5.3 Guide Tubes	8.1-5
8.1.5.4 Downcomer	8.1-5
8.1.5.5 GDCS Line	8.1-5
8.1.5.6 Chimney	8.1-6
8.1.5.7 Separators	8.1-6
8.1.5.8 Dryers	8.1-7
8.1.5.9 Main Steamlines for LOCA/ECCS	8.1-7
8.1.5.10 Feedwater System	8.1-8
8.1.5.11 Isolation Condensers	8.1-8
8.1.5.12 PCCS for LOCA/ECCS	8.1-8
8.1.5.13 Control System for LOCA/ECCS	8.1-9
8.1.5.14 Containment Model for LOCA/ECCS	8.1-9
8.1.6 Nodalization for Transients	8.1-9
8.1.6.1 Fuel Channels Grouping for Transients	8.1-10
8.1.6.2 Main Steamlines for Transients	8.1-10
8.1.6.3 Control System for Transients	8.1-11
8.1.7 References	8.1-11

Table of Contents

(continued)

	<u>Page</u>
8.2 Containment	8.2-1
8.2.1 RPV and Containment Volumes	8.2-1
8.2.2 One-Dimensional Components	8.2-2
8.2.2.1 Lower Drywell	8.2-3
8.2.2.2 Fuel Bundles	8.2-3
8.2.2.3 PCCS	8.2-3
8.2.2.4 ICS	8.2-4
8.2.2.5 GDCS One-Dimensional Components	8.2-4
8.2.2.6 Steamlines	8.2-4
8.2.2.7 SRVs	8.2-4
8.2.2.8 DPVs	8.2-5
8.2.2.9 LOCA Vents	8.2-5
8.2.2.10 Vacuum Breakers	8.2-5
8.2.2.11 Equalization Lines	8.2-5
8.2.2.12 RPV Pressure Taps	8.2-6
8.2.2.13 Gas Generation by Radiolysis and Metal/Water Reaction	8.2-6
8.2.2.14 DW-to-WW Bypass Leakage	8.2-6
8.2.2.15 Feedwater and Control Rod Drive Flow	8.2-6
8.2.2.16 Refill Pool	8.2-6
8.2.2.17 MSIVs	8.2-7
8.2.2.18 Components to Simulate Other Breaks	8.2-7
 9. ASSESSMENT OF TRACG QUALIFICATION	 9.1-1
9.1 Adequacy of TRACG Models	9.1-1
9.1.1 LOCA/ECCS	9.1-2
9.1.1.1 Key Safety Parameters	9.1-2
9.1.1.2 PIRT Phenomena	9.1-3
9.1.2 Transients	9.1-6
9.1.2.1 Key Safety Parameters	9.1-6
9.1.2.2 PIRT Phenomena	9.1-8
9.1.3 Stability	9.1-8
9.1.3.1 Key Safety Parameters	9.1-9
9.1.3.2 PIRT Phenomena	9.1-10
9.1.4 Containment	9.1-10
9.1.4.1 Key Safety Parameters	9.1-10
9.1.4.2 PIRT Phenomena	9.1-14
9.1.5 Plant Startup	9.1-16
9.1.5.1 Natural Circulation Flow (Startup Conditions)	9.1-17
9.1.5.2 Low Pressure Oscillations During Startup	9.1-17
9.1.6 References	9.1-18

Table of Contents

(continued)

	<u>Page</u>
9.2 Adequacy of Qualification Coverage	9.2-1
9.2.1 Reactor Vessel and Core	9.2-1
9.2.1.1 Lower Plenum	9.2-1
9.2.1.2 Bypass	9.2-2
9.2.1.3 Core	9.2-3
9.2.1.4 Guide Tubes	9.2-8
9.2.1.5 Downcomer	9.2-8
9.2.1.6 Chimney	9.2-10
9.2.1.7 Separators	9.2-11
9.2.1.8 ATWS	9.2-12
9.2.1.9 Steamline	9.2-12
9.2.1.10 Isolation Condenser	9.2-13
9.2.1.11 Stability	9.2-13
9.2.1.12 RPV	9.2-14
9.2.1.13 Interactions	9.2-14
9.2.2 Containment	9.2-15
9.2.2.1 Break	9.2-15
9.2.2.2 Main Vent	9.2-15
9.2.2.3 SRV	9.2-16
9.2.2.4 Drywell	9.2-16
9.2.2.5 Wetwell	9.2-17
9.2.2.6 PCCS	9.2-18
9.2.2.7 Drywell/Wetwell Boundary	9.2-20
9.2.2.8 Vacuum Breaker	9.2-20
9.2.2.9 Equalizing Line	9.2-21
9.2.2.10 RPV	9.2-21
9.2.2.11 DPV	9.2-21
9.2.2.12 System Interactions	9.2-21
9.2.3 References	9.2-22
 10. CONCLUSIONS	 10-1
10.1 References	10-2
 APPENDIX A Comparison Between TRACG02 and TRACG04	 A-1

List of Tables

— VOLUME 1 —

		<u>Page</u>
Table 1.2-1	Versions of TRACG used for Qualification Studies	1.2-5
Table 2.0-1	Database Used to Support TRACG Models and Qualification for SBWR	2-7
Table 2.1-1	PIRT Phenomena Added or Deleted for the LOCA/ECCS	2.1-7
Table 2.1-2	PIRT Parameters Added or Deleted for the LOCA/Containment	2.1-8
Table 2.1-3a	Separate Effects Tests for Highly Ranked Phenomena for TRACG Qualification for SBWR - Reactor and Core	2.1-9
Table 2.1-3b	Separate Effects Tests for Highly Ranked Phenomena for TRACG Qualification for SBWR - Containment	2.1-13
Table 2.1-4a	Component Tests for Highly Ranked Phenomena for TRACG Qualification for SBWR - Reactor and Core	2.1-15
Table 2.1-4b	Component Tests of Highly Ranked Phenomena for TRACG Qualification for SBWR - Containment	2.1-18
Table 2.1-5a	Integral System Tests for Highly Ranked Phenomena for TRACG Qualification for SBWR - Reactor Vessel and Core	2.1-20
Table 2.1-5b	Integral System Tests for Highly Ranked Phenomena for TRACG Qualification for SBWR - Containment	2.1-22
Table 2.1-6a	BWR Plant Data for Highly Ranked Phenomena for TRACG Qualification for SBWR - Reactor Vessel and Core	2.1-24
Table 2.1-7a	Overall TRACG Qualification Coverage of Highly Ranked Phenomena for SBWR - Reactor Vessel and Core	2.4-28
Table 2.1-7b	Overall TRACG Qualification Coverage of Highly Ranked Phenomena for SBWR - Containment	2.4-30
Table 3.1-1	Comparison of Range of Parameters for Toshiba Tests and SBWR	3.1-6
Table 3.1-2	Comparison of Toshiba Void Data with TRACG Calculations	3.1-7
Table 3.2-1	Comparison of Key Parameters in the OHT Test Facility and SBWR Chimney Partitions	3.2-9
Table 3.2-2	Comparison of TRACG/OHT Void Fraction During the Time Periods of Varying Mass Flow Rate (280°C/6.4 MPa)	3.2-9
Table 3.2-3	Assessment of TRACG Accuracy for Ontario Hydro Tests	3.2-9
Table 3.3-1	Range of Parameters for SBWR Regions	3.3-12
Table 3.3-2	Summary of Void Fraction Comparisons	3.3-13
Table 3.3-3	TRACG Calculation of Pressure Response and Level Change for PSTF Level Swell Tests	3.3-13
Table 3.3-4	TRACG Calculation of Critical Flow	3.3-14
Table 3.3-5	TRACG Calculation of Frictional Pressure Drop	3.3-14
Table 3.3-6	Calculation of Natural Circulation Flow and Power for Onset of Stability	3.3-14

List of Tables

(continued)

	<u>Page</u>
Table 4.1-1 PANTHERS/PCC Steady-State Performance Matrix at 5 kg/s Steam Flowrate for TRACG Post-Test Analysis	4.1-40
Table 4.1-2 PANTHERS/PCC Steady-State Performance Matrix at Extreme and Intermediate Ranges for TRACG Post-Test Analysis	4.1-41
Table 4.1-3 PANTHERS/PCC Transient Performance Matrix for TRACG Post-Test Analysis	4.1-41
Table 4.1-4 PANTHERS/PCC TRACG One-Tube Model Components and Junction Elevations	4.1-42
Table 4.1-5 Heat Transfer Correspondence Between Condenser Tube Cells and PCC Pool Cells	4.1-43
Table 4.1-6 PANTHERS PCC TRACG Eight-Tube Model Components	4.1-43
Table 4.1-7 TRACG Calculated Pressure Losses for Test 15_1 Compared with PANTHERS DP Measurements	4.1-44
Table 4.1-8 Functions of TRACG Components for Specifying PANTHERS/PCC Test Boundary Conditions	4.1-45
Table 4.1-9 TRACG Input Flow Rates and Properties for Noncondensable Gas Accumulation Tests	4.1-45
Table 4.1-10 PANTHERS/PCC Tests Included in Post-Test Evaluation	4.1-46
Table 4.1-11 Test Conditions for Steady-State Pure-Steam Tests Included in Post-Test Evaluation	4.1-46
Table 4.1-12 Test Conditions for Steady-State Steam-Air Tests Included in Post-Test Evaluation	4.1-47
Table 4.1-13 Comparison of Results from 8-Tube and 1-Tube TRACG Input Models for Steady-State Steam-Air Tests	4.1-47
Table 4.1-14 Comparison of Inferred PANTHERS Film Coefficients with TRACG Calculations for Pure-Steam Tests	4.1-48
Table 4.1-15a Test Conditions for Evaluation of Tube-to-Tube Variations	4.1-49
Table 4.1.15b Axial Average Wall Temperature Difference for Four Instrumented Tubes	4.1-49
Table 4.1.15c Axial Variation of External Tube Wall Temperature for Test 09_9	4.1-49
Table 4.1-16 Assessment of TRACG Accuracy for PANTHERS PCC SS Steam-Air Tests	4.1-50
Table 4.1-17 Assessment of TRACG Accuracy for PANTHERS PCC SS Pure-Steam Tests	4.1-51
Table 4.1-18 Maximum Measurement Uncertainties	4.1-51
Table 4.1-19 Maximum Measurement Uncertainty for Condenser Efficiency	4.1-52
Table 4.2-1 PANTHERS IC Test Maximum Measurement Uncertainties	4.2-16
Table 4.2-2 PANTHERS IC Steady-State Performance Matrix for TRACG Post-Test Analysis	4.2-16
Table 4.2-3 PANTHERS IC Transient Performance Matrix for TRACG Post-Test Analysis	4.2-16
Table 4.2-4 Components for Simulation of PANTHERS IC Test	4.2-17
Table 4.2-5 TRACG Input Flow Rate and Properties For Noncondensable Gas	4.2-18
Table 4.2-6 PANTHERS IC Tests Included in Post-Test Evaluation	4.2-18
Table 4.2-7 Test Conditions for Steady-State Post-Test Evaluation	4.2-18
Table 4.2-8 Comparison of PANTHERS and TRACG for Steady-State Evaluation	4.2-18
Table 4.2-9 Comparison of PANTHERS and TRACG Noncondensable Gas Inventory at 7.8 MPa for Test T12	4.2-19

List of Tables

(continued)

		<u>Page</u>
Table 4.2-10	Comparison of PANTHERS and TRACG Noncondensable Gas Inventory at 5.2 Mpa for Test T13	4.2-19
Table 4.2-11	TRACG Calculation of NC Gas Distribution at 5.23 MPa Inlet Pressure	4.2-19
Table 4.2-12	Assessment of TRACG Accuracy for PANTHERS IC Tests	4.2-20
Table 4.3-1	PANDA Steady-State PCC Performance Test Matrix	4.3-12
Table 4.3-2	Comparison of TRACG PCC Nodalizations for PANDA and SBWR. Containment Model	4.3-12
Table 4.3-3	Actual Conditions for PANDA Steady-State Performance Tests and TRACG Post-Test Calculations	4.3-13
Table 4.3-4	PCCS Inlet Velocities for TRACG Post-Test Calculations	4.3-13
Table 4.3-5	Void Fractions in Pool Cells with Liquid Levels	4.3-14
Table 4.3-6	Correspondence Between PANDA Measurements and TRACG Model Locations	4.3-14
Table 4.3-7	Maximum Measurement Uncertainties for PANDA Steady-State PCC Tests	4.3-15
Table 4.3-8	Condenser Efficiencies from PANDA Steady-State Steam-Air Tests Compared with TRACG Calculations	4.3-16
Table 4.3-9	Condenser Inlet Pressures from PANDA Steady-State Pure-Steam Tests Compared with TRACG Calculations	4.3-16
Table 4.3-10	Assessment of TRACG Accuracy for PANDA PCC Tests	4.3-17
Table 4.4-1	Comparison of PSTF and SBWR Parameters	4.4-8
Table 4.4-2	Comparison of Pool Total Thermal Energy - TRACG vs Data for Test 5807-29	4.4-9
Table 4.4-3	Assessment of TRACG Accuracy for PSTF Suppression Pool Stratification Tests	4.4-10

— VOLUME 2 —

Table 5.1-1	GIST Facility Tests Selected for TRACG Qualification	5.1-18
Table 5.1-2	GIST Nodalization vs SBWR Nodalization	5.1-19
Table 5.1-3	GIST Initial Conditions Used in TRACG Input	5.1-20
Table 5.1-4	GIST TRACG Comparison Results	5.1-20
Table 5.2-1	Test Matrix of Initial DW Conditions for GIRAFFE/Helium Tests	5.2-29
Table 5.2-2	Definition of TRACG Input Model Components	5.2-30
Table 5.2-3	Comparison of GIRAFFE/Helium and SBWR TRACG Containment Nodalization	5.2-31
Table 5.2-4	Initial Conditions for GIRAFFE/Helium Tests H1-H4	5.2-32
Table 5.2-5	Initial Conditions for GIRAFFE Test T2 ²	5.2-32
Table 5.2-6	Assessment of TRACG Accuracy for GIRAFFE Helium Tests	5.2-33
Table 5.3-1	List of 1-D Components	5.3-25
Table 5.3-2	TRACG Nodalization vs. SBWR Nodalization	5.3-27
Table 5.3-3	Initial Conditions for Test GS1 GDC Line Break, DPV Failure, IC/PCC off	5.3-28
Table 5.3-4	Initial Conditions for GS2 GDC Line Break, DPV Failure, IC/PCC on	5.3-29
Table 5.3-5	Initial Conditions for GS3 BDL Break, DPV Failure, IC/PCC on	5.3-30

List of Tables

(continued)

		<u>Page</u>
Table 5.3-6	Initial Conditions for GS4 GDC Line Break, GDC Valve Failure, IC/PCC on	5.3-31
Table 5.3-7	Ratio of the Calculated Elevation Pressure Drop to the Total Pressure Drop Results from Test GS1	5.3-32
Table 5.3-8	Summary of Test and TRACG Comparisons	5.3-33
Table 5.4-1	Dimensions and Grouping of the Channels	5.4-10
Table 5.5-1	Test Initial Conditions	5.5-7
Table 5.5-2	Comparison of PSTF and SBWR Parameters	5.5-7
Table 5.5-3	Summary of TRACG Calculations vs Measured Data	5.5-8
Table 5.5-4	Assessment of TRACG Accuracy for PSTF Mark III Tests	5.5-9
Table 5.6-1	Test Series 5101 Tests for TRACG Simulation	5.6-10
Table 5.6-2	Comparison of 4T/Mark II PSTF and SBWR Parameters	5.6-10
Table 5.6-3	Summary of TRACG Results vs Test Data	5.6-11
Table 5.6-4	Drywell Wall Steam Condensation - TRACG vs Measured Data	5.6-11
Table 5.6-5	Assessment of TRACG Accuracy for 4T Mark II Tests	5.6-12
Table 5.7-1	PANDA/TRACG VSSL01 Component Breakdown	5.7-54
Table 5.7-2	PANDA/TRACG Components with Connections to VSSL01 Cells	5.7-55
Table 5.7-3	PANDA/TRACG RPV Components	5.7-55
Table 5.7-4	PANDA/TRACG PCCS Components	5.7-56
Table 5.7-5	PANDA/TRACG ICS Components	5.7-57
Table 5.7-6	Other PANDA/TRACG Components	5.7-57
Table 5.7-7	PANDA Heater Power vs. Time for All Tests Except M7 and M9	5.7-58
Table 5.7-8	PANDA Heater Power vs. Time for Test M9	5.7-59
Table 5.7-9	Comparison of PANDA and SBWR Component Nodalizations	5.7-60
Table 5.7-10	Initial Conditions for PANDA Test M3	5.7-61
Table 5.7-11	Initial Conditions for PANDA Test M3A	5.7-61
Table 5.7-12	Initial Conditions for PANDA Test M3B	5.7-61
Table 5.7-13	Initial Conditions for PANDA Test M2	5.7-62
Table 5.7-14	Initial Conditions for PANDA Test M10A	5.7-62
Table 5.7-15	Initial Conditions for PANDA Test M10B	5.7-62
Table 5.7-16	Initial Conditions for PANDA Test M6/8	5.7-63
Table 5.7-17	Initial Conditions for PANDA Test M7	5.7-63
Table 5.7-18	Initial Conditions for PANDA Test M9	5.7-63
Table 5.7-19	PCC Instrumentation for PANDA Post-Test Evaluation	5.7-65
Table 5.7-20	DW Instrumentation for PANDA Post-Test Evaluation	5.7-66
Table 5.7-21	WW Instrumentation for PANDA Post-Test Evaluation	5.7-67
Table 5.7-22	Oxygen Probe Instrumentation for PANDA Post-Test Evaluation	5.7-68
Table 5.7-23	IC Instrumentation for Post-Test Evaluation of PANDA Test M6/8	5.7-68
Table 5.7-24	Main Vent Instrumentation for Post-Test Evaluation of PANDA Tests M10A, M10B, and M7	5.7-68
Table 5.7-25	RPV and GDCS Level Instrumentation for Post-Test Evaluation of PANDA Tests M7 and M9	5.7-69
Table 5.7-26	PANDA Measurement Uncertainties	5.7-69
Table 5.7-27	Assessment of TRACG Accuracy for PANDA Transient (M-Series) Tests	5.7-70

List of Tables

(continued)

	<u>Page</u>
Table 6.1-1	Comparison of Dodewaard and SBWR Steady-State Parameters
Table 6.1-2	Dodewaard Nodalization vs. SBWR Nodalization
Table 6.1-3	Comparison of TRACG Steady-State Calculations to Plant Parameters
Table 6.2-1	Sequence of Steps of a Regular Startup
Table 6.2-2	Sequence of Steps During February 1992 Startup
Table 6.2-3	Overview of All Available Measurement Data
Table 6.2-4	Comparison of Key Features of Dodewaard and SBWR
Table 6.2-5	Vessel Axial and Radial Nodalization
Table 6.2-6	Channel Initial Conditions
Table 6.2-7	Measurement Data Used for Initial and Boundary Conditions
Table 6.2-8	Calculation of Subcooling Number and Phase Change Number
Table 6.2-9	Assessment of TRACG Accuracy for Dodewaard Startup Tests
Table 6.3-1	Forced Flow Data Points
Table 6.3-2	Test Matrix (System Pressure = 0.2 MPa , Channel Power = 2.5 kW/chan)
Table 6.3-3	Comparison of Nondimensional Parameters Between the Test Loop and SBWR
Table 6.3-4	Assessment of TRACG Accuracy for CRIEPI Low Pressure Oscillation Tests
Table 6.4-1	Test Matrix for PANDA E-series Tests
Table 6.4-2	Major Observations from PANDA E-series Tests (Pressure)
Table 6.4-3	Major Observation from PANDA E-series Tests (Flow)
Table 6.4-4	Comparison of the Key Features of PANDA Facility and SBWR
Table 6.5-1	Dependence of the Period and Amplitude of CRIEPI Oscillations on Inlet Subcooling
Table 6.5-2	Dependence of the Upper and Lower CRIEPI Oscillatory Boundary on Channel Power (System Pressure = 0.2 MPa)
Table 6.5-3	Calculated Subcooling and Phase Change Numbers at Upper Boundary of Oscillatory Region
Table 6.5-4	Calculated Channel Inlet Subcooling at Lower Boundary of Oscillatory Region
Table 8.1-1a	Major Findings from Test Facility Nodalization Factored into the SBWR TRACG Model
Table 8.1-1b	SBWR Nodalization vs. TRACG Facility Nodalization for LOCA/ECCS and Transients
Table 8.1-1c	Justification of SBWR TRACG RPV Input Model Approach for LOCA/ECCS
Table 8.1-2	TRACG Components Used for LOCA/ECCS and Transient Decks
Table 8.1-3	SBWR TRACG Vessel Nodalization - Axial Levels (LOCA/ECCS)
Table 8.1-4	TRACG Description of the SBWR Vessel Regions (LOCA/ECCS)
Table 8.1-5	Grouping of Fuel Channels in Vessel Radial Rings (LOCA/ECCS)
Table 8.1-6	Grouping of Fuel Channels in Vessel Radial Rings (Transients)
Table 8.1-7	TRACG Description of the SBWR Containment (LOCA/ECCS)

List of Tables

(continued)

		<u>Page</u>
Table 8.2-1	Radial Ring Boundaries of VSSL Component in SBWR TRACG Containment Model	8.2-8
Table 8.2-2	Axial Level Boundaries of VSSL Component in SBWR TRACG Containment Model	8.2-9
Table 8.2-3	SBWR TRACG Containment Model Components (* denotes connection is specific to main steamlines break simulation)	8.2-10
Table 8.2-4	SBWR TRACG Containment Model Approach vs. Test Facility Modeling Approach	8.2-14
Table 8.2-5	Justification of SBWR TRACG Containment Model Approach	8.2-18
Table 9.1-1	Accuracy of TRACG Calculations for RPV Level	9.1-19
Table 9.1-2	Accuracy of TRACG Calculations for Core Void Fraction	9.1-19
Table 9.1-3	Accuracy of TRACG Calculations for Chimney, Lower Plenum and Downcomer Void Fraction	9.1-20
Table 9.1-4	Accuracy of TRACG Calculations for RPV Break Flow	9.1-21
Table 9.1-5	Accuracy of TRACG Calculations for GDCS Flow	9.1-21
Table 9.1-6	Accuracy of TRACG Calculations for IC Heat Removal	9.1-21
Table 9.1-7	Accuracy of TRACG Calculations for Natural Circulation and Stability	9.1-22
Table 9.1-8	Accuracy of TRACG Calculations for Peak Neutron Flux	9.1-22
Table 9.1-9	Accuracy of TRACG Calculations for Short-Term Containment Pressure	9.1-23
Table 9.1-10	Accuracy of TRACG Calculations for Long-Term Containment Pressure	9.1-23
Table 9.1-11	Accuracy of TRACG Calculations for DW Temperature	9.1-24
Table 9.1-12	Accuracy of TRACG Calculations for WW Gas Temperature	9.1-24
Table 9.1-13	Accuracy of TRACG Calculations for Vent Clearing Time	9.1-25
Table 9.1-14	Accuracy of TRACG Calculations for WW Liquid Temperature	9.1-25
Table 9.1-15	Accuracy of TRACG Calculations for PCC Heat Removal	9.1-26
Table 9.1-16	Accuracy of TRACG Calculations for PCC Pressure Drop	9.1-26
Table 9.1-17	Accuracy of TRACG Calculations for Natural Circulation Flow (Startup Conditions)	9.1-27
Table 9.1-18	Accuracy of TRACG Calculations of Flow Oscillations During Startup	9.1-27

List of Figures

— VOLUME 1 —

	<u>Page</u>
Figure 1.2-1 Road Map of SBWR TRACG Related Documentation	1.2-9
Figure 1.3-1 Qualification Report Roadmap	1.3-4
Figure 2.1-1 SBWR LOCA Phases and Major Test Coverage	2.1-32
Figure 3.1-1 Test Bundle Cross-Section [3.1-1]	3.1-8
Figure 3.1-2 External View of Test Section [3.1-1]	3.1-9
Figure 3.1-3 Void Measurement Section [3.1-1]	3.1-10
Figure 3.1-4 TRACG Model for Toshiba Test	3.1-11
Figure 3.1-5 TRACG Calculations of Toshiba CT Void Data (1.00 MPa and 1390 Kg/m ² -s)	3.1-12
Figure 3.1-6 TRACG Calculation of Toshiba CT Void Data (1.00 MPa and 833 Kg/m ² -s)	3.1-12
Figure 3.1-7 TRACG Calculation of Toshiba CT Void Data (0.50 MPa and 1390 Kg/m ² -s)	3.1-13
Figure 3.2-1 Schematic Diagram of the Test Facility [3.2-2]	3.2-10
Figure 3.2-2 Schematic Diagram of the Test Section [3.2-2]	3.2-11
Figure 3.2-3 Radial Void Fraction Distribution at Nominal Temperature of 280°C	3.2-12
Figure 3.2-4 Average Void Fraction as Obtained from the Gamma Densitometer Measurements Versus those Obtained using the Axial Pressure Drop Measurements at Nominal Temperature of 280°C	3.2-13
Figure 3.2-5 TRACG Model Description of OHT Test	3.2-14
Figure 3.2-6 Local Void Fluctuations (around 2000 s) at Nominal Temperature of 280°C	3.2-15
Figure 3.2-7 Local Void Fluctuations (around 2500 s) at Nominal Temperature of 280°C	3.2-16
Figure 3.2-8 Comparison of TRACG and Time-averaged Data - Average Void Fraction at Nominal Temperature of 280°C	3.2-17
Figure 3.3-1 Critical Power vs. Length (Columbia Data) [3.3-17])	3.3-15
Figure 3.3-2 Critical Power Comparisons for 2.8m GE8 Fuel Bundle – GEXL02 Correlation vs. COBRAG	3.3-16
Figure 4.1-1 Passive Containment Condenser Test Article	4.1-53
Figure 4.1-2 PANTHERS/PCC Test Facility Schematic	4.1-54
Figure 4.1-3 PCC Operational Modes	4.1-55
Figure 4.1-4 PANTHERS Representation of PCC Operational Modes	4.1-56
Figure 4.1-5 TRACG PANTHERS/PCC Qualification Points	4.1-57
Figure 4.1-6 Schematic of TRACG PANTHERS/PCC One-Tube Input Model	4.1-58
Figure 4.1-7 Nodalization of Inlet Line (TEE22)	4.1-59
Figure 4.1-8 Nodalization of Upper (PIPE92) and Lower (TEE26) Headers	4.1-60
Figure 4.1-9 Nodalization of PCC Tubes (PIPE96)	4.1-61
Figure 4.1-10 Nodalization of Drain Line (PIPE46)	4.1-62

List of Figures

(continued)

	<u>Page</u>
Figure 4.1-11 Nodalization of Vent Line (PIPE52)	4.1-63
Figure 4.1-12 Nodalization of Pools (VSSL01 and TEE40)	4.1-64
Figure 4.1-13 Nodalization of the PANTHERS/PCC Eight-Tube TRACG Model	4.1-65
Figure 4.1-14 Comparison of TRACG and PANTHERS Inlet Pressure for Pure-Steam Tests	4.1-66
Figure 4.1-15 Comparison of TRACG and Panthers Condensation Efficiency and Pressure Drop for Test 9	4.1-67
Figure 4.1-16 Comparison of TRACG and PANTHERS Condensation Efficiency and Pressure Drop for Test 15	4.1-68
Figure 4.1-17 Comparison of TRACG and PANTHERS Condensation Efficiency and Pressure Drop for Test 18	4.1-69
Figure 4.1-18 Comparison of TRACG and PANTHERS Condensation Efficiency and Pressure Drop for Test 23	4.1-70
Figure 4.1-19 Comparison of TRACG and PANTHERS Condensation Efficiency and Pressure Drop for Test 2	4.1-71
Figure 4.1-20 Comparison of TRACG and PANTHERS Condensation Efficiency and Pressure Drop for Test 17	4.1-72
Figure 4.1-21 Comparison of TRACG and PANTHERS Condensation Efficiency and Pressure Drop for Test 19	4.1-73
Figure 4.1-22 Comparison of TRACG and PANTHERS Condensation Efficiency and Pressure Drop for Test 22	4.1-74
Figure 4.1-23 Comparison of TRACG and PANTHERS Condensation Efficiency and Pressure Drop for Test 35	4.1-75
Figure 4.1-24 Comparison of TRACG and PANTHERS Condensation Efficiency and Pressure Drop for Test 2 with Heat Transfer Between Vent Line and Drain Line	4.1-76
Figure 4.1-25 Comparison of TRACG and PANTHERS Inlet Pressure for Test 51	4.1-77
Figure 4.1-26 Comparison of TRACG and PANTHERS Inlet Pressure for Test 76	4.1-78
Figure 4.1-27 Comparison of TRACG and PANTHERS Inlet Pressure for Test 78	4.1-79
Figure 4.1-28 Comparison of TRACG and PANTHERS Inlet Pressure for Test 54	4.1-80
Figure 4.1-29 Location of the PCC Instrumented Tubes and Thermocouples	4.1-81
Figure 4.1-30 Comparison of Average Tube Wall Temperature Measurements to TRACG Calculations - PANTHERS Test T15_1	4.1-82
Figure 4.1-31 Comparison of Average Tube Wall Temperature Measurements to TRACG Calculations - PANTHERS Test T43_2	4.1-83
Figure 4.2-1 Isolation Condenser Test Heat Exchanger Assembly	4.2-21
Figure 4.2-2 PANTHERS IC Test Facility Schematic	4.2-22
Figure 4.2-3 TRACG Nodalization for Simulation of PANTHERS IC Test	4.2-23
Figure 4.2-4 Comparison of TRACG and PANTHERS for Steady-State Tests	4.2-24
Figure 4.2-5 Comparison of TRACG and PANTHERS Inlet Pressure Transient for Test T12	4.2-25
Figure 4.2-6 Comparison of TRACG and PANTHERS Heat Transfer for Test T12	4.2-25
Figure 4.2-7 Comparison of TRACG and PANTHERS Inlet Pressure Transient for Test T13	4.2-26
Figure 4.2-8 Comparison of TRACG and PANTHERS Heat Transfer for Test T13	4.2-26
Figure 4.2-9 Comparison of TRACG and PANTHERS for Pool Level Test	4.2-27

List of Figures (continued)

	<u>Page</u>
Figure 4.3-1 TRACG Model of the PANDA PCCS as Modified for the Steady-State Tests	4.3-18
Figure 4.3-2 TRACG Model of the PANDA PCCS Inlet Pipe as Modified for the Steady-State Tests	4.3-18
Figure 4.3-3 TRACG Model of the PANDA PCCS Secondary Side	4.3-19
Figure 4.3-4 Comparison of TRACG Calculations of Condenser Efficiency with PANDA Measurements (Steam-Air Tests)	4.3-20
Figure 4.3-5 Comparison of TRACG Calculations of Condenser Inlet Pressure with PANDA Measurements (Pure-Steam Tests)	4.3-20
Figure 4.4-1 Pressure Suppression Test Facility - Test 5707 Series	4.4-11
Figure 4.4-2 Pressure Suppression Test Facility - Test 5807 Series	4.4-12
Figure 4.4-3 TRACG Component Layout	4.4-13
Figure 4.4-4 TRACG Modeling of Eight Degree WW Section	4.4-14
Figure 4.4-5 TRACG Modeling of Vent System	4.4-15
Figure 4.4-6 TRACG Suppression Pool Nodalization	4.4-16
Figure 4.4-7 Temperature Profile of Volume 5 - Test 5707-01	4.4-17
Figure 4.4-8 Temperature Profile of Volume 1 - Test 5807-29	4.4-18
Figure 4.4-9 Temperature Profile of Volume 2 - Test 5807-29	4.4-19
Figure 4.4-10 Temperature Profile of Volume 3 - Test 5807-29	4.4-20
Figure 4.4-11 Temperature Profile of Volume 4 - Test 5807-29	4.4-21
Figure 4.4-12 Temperature Profile of Volume 5 - Test 5807-29	4.4-22
Figure 4.4-13 Temperature Profile of Volume 6 - Test 5807-29	4.4-23

— VOLUME 2 —

Figure 5.0-1 SBWR LOCA Phases and Major Test Coverage	5.1-3
Figure 5.1-1 GIST Facility	5.1-21
Figure 5.1-2 GIST Facility - Major Flow Paths	5.1-22
Figure 5.1-3 GIST Facility -Pressure Vessel	5.1-23
Figure 5.1-4 TRACG Nodalization of GIST RPV	5.1-24
Figure 5.1-5 Nodalization of GIST Containment	5.1-25
Figure 5.1-6 TRACG Nodalization of GIST Steamlines	5.1-25
Figure 5.1-7 TRACG Nodalization for GDCS Line Calibration	5.1-26
Figure 5.1-8 GIST RPV Blowdown	5.1-27
Figure 5.1-9 Comparison of RPV Pressures (Bottom Drain Line LOCA-A07)	5.1-28
Figure 5.1-10 Comparison of Upper Drywell Pressure (Test A07)	5.1-28
Figure 5.1-11 Comparison of Wetwell Pressure (Test A07)	5.1-29
Figure 5.1-12 Comparison of GDCS Flow Rate (Test A07)	5.1-29
Figure 5.1-13 Comparison of Annulus Pressure Drop (Test A07)	5.1-30
Figure 5.1-14 Comparison of Core Pressure Drop (Test A07)	5.1-30
Figure 5.1-15 Comparison of Bypass Pressure Drop (Test A07)	5.1-31
Figure 5.1-16 Comparison of Standpipe Pressure Drop (Test A07)	5.1-31
Figure 5.1-17 Comparison of RPV Pressure (Test B01)	5.1-32
Figure 5.1-18 Comparison of RPV Pressure (Test B07)	5.1-32
Figure 5.1-19 Comparison of RPV Pressure (Test C01A)	5.1-33
Figure 5.1-20 Comparison of RPV Pressure (Test D03A)	5.1-33
Figure 5.1-21 Comparison of GDCS Flow (Test B01)	5.1-34

List of Figures (continued)

	<u>Page</u>
Figure 5.1-22 Comparison of GDCS Flow (Test B07)	5.1-34
Figure 5.1-23 Comparison of GDCS Flow (Test C01A)	5.1-35
Figure 5.1-24 Comparison of GDCS Flow (Test D03A)	5.1-35
Figure 5.1-25 Comparison of Annulus Pressure Drop (Test B01)	5.1-36
Figure 5.1-26 Comparison of Annulus Pressure Drop (Test B07)	5.1-36
Figure 5.1-27 Comparison of Annulus Pressure Drop (Test C01A)	5.1-37
Figure 5.1-28 Comparison of Annulus Pressure Drop (Test D03A)	5.1-37
Figure 5.1-29 Comparison of Core Pressure Drop (Test B01)	5.1-38
Figure 5.1-30 Comparison of Core Pressure Drop (Test B07)	5.1-38
Figure 5.1-31 Comparison of Core Pressure Drop (Test C01A)	5.1-39
Figure 5.1-32 Comparison of Core Pressure Drop (Test D03A)	5.1-39
Figure 5.1-33 Calculated Annulus Level (Test B07)	5.4-40
Figure 5.1-34 Comparison of Rod Temperatures (Test B07)	5.4-41
Figure 5.1-35 Calculated Core Axial Void Profile (Test B07)	5.4-42
Figure 5.2-1 GIRAFFE Facility Layout	5.2-34
Figure 5.2-2 TRACG Nodalization of the Vessel Component	5.2-35
Figure 5.2-3 TRACG Nodalization of the Individual Vessels	5.2-36
Figure 5.2-4 PCC Nodalization	5.2-37
Figure 5.2-5 The RPV and Piping	5.2-38
Figure 5.2-6 Suppression Chamber and Piping	5.2-39
Figure 5.2-7 GDCS Pool and Piping	5.2-40
Figure 5.2-8 Drywell and Drywell Piping	5.2-41
Figure 5.2-9 H1: Drywell and Wetwell Pressure	5.2-42
Figure 5.2-10 H1: RPV and PCC Power	5.2-42
Figure 5.2-11 H1: PCC Mass Flow Rate	5.2-43
Figure 5.2-12 H1: PCC Nitrogen Partial Pressure	5.2-43
Figure 5.2-13 H1: DW Nitrogen Partial Pressure	5.2-44
Figure 5.2-14 H1: WW Nitrogen Partial Pressure	5.2-44
Figure 5.2-15 H1: DW and WW Pressure - Sensitivity to Increased PCC Heat Transfer Area	5.2-45
Figure 5.2-16 H1: PCC Nitrogen Partial Pressure - Sensitivity to Increased PCC Heat Transfer Area	5.2-45
Figure 5.2-17 H2: Drywell and Wetwell Pressure	5.2-46
Figure 5.2-18 H2: DW and WW Pressure - Simulated Helium Updraft from LDW	5.2-46
Figure 5.2-19 H2: RPV and PCC Power - Simulated Helium Updraft from LDW	5.2-47
Figure 5.2-20 H2: PCC Mass Flow Rate - Simulated Helium Updraft from LDW	5.2-47
Figure 5.2-21 H2: PCC Helium Partial Pressure - Simulated Helium Updraft from LDW	5.2-48
Figure 5.2-22 H2: DW Helium Partial Pressure - Simulated Helium Updraft from LDW	5.2-48
Figure 5.2-23 H2: WW Helium Partial Pressure - Simulated Helium Updraft from LDW	5.2-49
Figure 5.2-24 H2: DW and WW Pressure - Sensitivity to Specifying all Helium Initially in Top of UDW	5.2-49
Figure 5.2-25 H2: DW and WW Pressure - Sensitivity to 3 Cell -Header	5.2-50
Figure 5.2-26 H2: PCC Helium Partial Pressure - Sensitivity to 3 Cell-Header	5.2-50
Figure 5.2-27 H3: Drywell and Wetwell Pressure	5.2-51
Figure 5.2-28 H3: RPV and PCC Power	5.2-51
Figure 5.2-29 H3: PCC Mass Flow Rate	5.2-52
Figure 5.2-30 H3: PCC Noncondensable Gas Partial Pressure	5.2-52

List of Figures

(continued)

	<u>Page</u>
Figure 5.2-31 H3: DW Helium Partial Pressure	5.2-53
Figure 5.2-32 H3: WW Helium Partial Pressure	5.2-53
Figure 5.2-33 H4: Drywell and Wetwell Pressure	5.2-54
Figure 5.2-34 H4: RPV and PCC Power	5.2-54
Figure 5.2-35 H4: PCC Mass Flow Rate	5.2-55
Figure 5.2-36 H4: PCC Noncondensable Gas Partial Pressure	5.2-55
Figure 5.2-37 H4: DW Helium Partial Pressure	5.2-56
Figure 5.2-38 H4: WW Helium Partial Pressure	5.2-56
Figure 5.2-39 T2: Drywell and Wetwell Pressure	5.2-57
Figure 5.2-40 T2: RPV and PCC Power	5.2-57
Figure 5.2-41 T2: PCC Mass Flow Rate	5.2-58
Figure 5.2-42 T2: PCC Nitrogen Partial Pressure	5.2-58
Figure 5.2-43 T2: DW Nitrogen Partial Pressure	5.2-59
Figure 5.2-44 T2: DW and WW Pressure - Sensitivity to Increased PCC Heat Transfer Area	5.2-59
 Figure 5.3-1 GIRAFFE Facility Layout	 5.3-34
Figure 5.3-2 RPV Internals	5.3-35
Figure 5.3-3 TRACG Vessel Nodalization	5.3-36
Figure 5.3-4 The RPV and Piping	5.3-37
Figure 5.3-5 Drywell and Drywell Piping	5.3-38
Figure 5.3-6 Wetwell and Piping	5.3-39
Figure 5.3-7 GDCS Pool and Piping	5.3-40
Figure 5.3-8 IC and PCC Models in TRACG	5.3-41
Figure 5.3-9 GS1 - RPV Dome Pressure	5.3-42
Figure 5.3-10 GS1 - DW Pressure	5.3-42
Figure 5.3-11 GS1 - WW Pressure	5.3-43
Figure 5.3-12 GS1 - RPV Dome Pressure	5.3-44
Figure 5.3-13 GS1 - DW Pressure	5.3-44
Figure 5.3-14 GS1 - WW Pressure	5.3-44
Figure 5.3-15 GS1 - Chimney Collapsed Level	5.3-45
Figure 5.3-16 GS1 - Channel Delta P	5.3-45
Figure 5.3-17 GS1 - Bypass Collapsed Level	5.3-46
Figure 5.3-18 GS1 - Downcomer Collapsed Level	5.3-46
Figure 5.3-19 GS1 - Chimney Collapsed Level	5.3-47
Figure 5.3-20 GS1 - Channel Delta P	5.3-47
Figure 5.3-21 GS1 - Bypass Collapsed Level	5.3-48
Figure 5.3-22 GS1 - Downcomer Collapsed Level	5.3-48
Figure 5.3-23 GS1 - GDCS Flow	5.3-49
Figure 5.3-24 GS1 - GDCS Flow	5.3-49
Figure 5.3-25 GS1 - GDCS - DW Break Flow	5.3-50
Figure 5.3-26 GS1 - RPV - DW Break Flow	5.3-50
Figure 5.3-27 GS1 - GDCS Pool Level	5.3-51
Figure 5.3-28 GS1 - GDCS Flow Volume	5.3-51
Figure 5.3-29 GS1 - GDCLB1 Flow Volume	5.3-52
Figure 5.3-30 GS2 - RPV Dome Pressure	5.3-53
Figure 5.3-31 GS2 - DW Pressure	5.3-53
Figure 5.3-32 GS2 - WW Pressure	5.3-54

List of Figures

(continued)

	<u>Page</u>
Figure 5.3-33	GS3 - RPV Dome Pressure 5.3-54
Figure 5.3-34	GS2 - DW Pressure 5.3-55
Figure 5.3-35	GS2 - WW Pressure 5.3-55
Figure 5.3-36	GS2 - Chimney Collapsed Level 5.3-56
Figure 5.3-37	GS2 - Channel Delta -P 5.3-56
Figure 5.3-38	GS2 - Bypass Collapsed Level 5.3-57
Figure 5.3-39	GS2 - Downcomer Collapsed Level 5.3-57
Figure 5.3-40	GS2 - Chimney Collapsed Level 5.3-58
Figure 5.3-41	GS2 - Channel Delta-P 5.3-58
Figure 5.3-42	GS2 - Bypass Collapsed Level 5.3-59
Figure 5.3-43	GS2 - Downcomer Collapsed Level 5.3-59
Figure 5.3-44	GS2 - GDCS Flow 5.3-60
Figure 5.3-45	GS2 - GDCS Flow 5.3-60
Figure 5.3-46	GS2 - GDCS - DW Break Flow 5.3-61
Figure 5.3-47	GS2 - RPV - DW Break Flow 5.3-61
Figure 5.3-48	GS2 - GDCS Pool Level 5.3-62
Figure 5.3-49	GS2 - GDCS Flow Volume 5.3-62
Figure 5.3-50	GS2 - GDCLB1 Flow Volume 5.3-63
Figure 5.3-51	GS3 - RPV Dome Pressure 5.3-64
Figure 5.3-52	GS3 - DW Pressure 5.3-64
Figure 5.3-53	GS3 - WW Pressure 5.3-65
Figure 5.3-54	GS3 - RPV Dome Pressure 5.3-65
Figure 5.3-55	GS3 - DW Pressure 5.3-66
Figure 5.3-56	GS3 - WW Pressure 5.3-66
Figure 5.3-57	GS3 - Chimney Collapsed Level 5.3-67
Figure 5.3-58	GS3 - Channel Delta-P 5.3-67
Figure 5.3-59	GS3 - Bypass Collapsed Level 5.3-68
Figure 5.3-60	GS3 - Downcomer Collapsed Level 5.3-68
Figure 5.3-61	GS3 - Chimney Collapsed Level 5.3-69
Figure 5.3-62	GS3 - Channel Delta -P 5.3-69
Figure 5.3-63	GS3 - Bypass Collapsed Level 5.3-70
Figure 5.3-64	GS3 - Downcomer Collapsed Level 5.3-70
Figure 5.3-65	GS3 - GDCS Flow 5.3-71
Figure 5.3-66	GS3 - GDCS Flow 5.3-71
Figure 5.3-67	GS3 - BDL Flow 5.3-72
Figure 5.3-68	GS3 - GDCS Pool Level 5.3-72
Figure 5.3-69	GS3 - GDCS Flow Volume 5.3-73
Figure 5.3-70	GS3 - BDLB Flow Volume 5.3-73
Figure 5.3-71	GS4 - RPV Dome Pressure 5.3-74
Figure 5.3-72	GS4 - DW Pressure 5.3-74
Figure 5.3-73	GS4 - WW Pressure 5.3-75
Figure 5.3-74	GS4 - RPV Dome Pressure 5.3-75
Figure 5.3-75	GS4 - DW Pressure 5.3-76
Figure 5.3-76	GS4 - WW Pressure 5.3-76
Figure 5.3-77	GS4 - Chimney Collapsed Level 5.3-77
Figure 5.3-78	GS4 - Channel Delta - P 5.3-77
Figure 5.3-79	GS4 - Bypass Collapsed Level 5.3-78

List of Figures

(continued)

	<u>Page</u>
Figure 5.3-80 GS4 - Downcomer Collapsed Level	5.3-78
Figure 5.3-81 GS4 - Chimney Collapsed Level	5.3-79
Figure 5.3-82 GS4 - Channel Delta-P	5.3-79
Figure 5.3-83 GS4 - Bypass Collapsed Level	5.3-80
Figure 5.3-84 GS4 - Downcomer Collapsed Level	5.3-80
Figure 5.3-85 GS4 - GDCS Flow	5.3-81
Figure 5.3-86 GS4 - GDCS Flow	5.3-81
Figure 5.3-87 GS4 - GDCS - DW Break Flow	5.3-82
Figure 5.3-88 GS4 - RPV - DW Break Flow	5.3-82
Figure 5.3-89 GS4 - GDCS Pool Level	5.3-83
Figure 5.3-90 GS4 - GDCS Flow Volume	5.3-83
Figure 5.3-91 GS4 - GDCLB1 Flow Volume	5.3-84
Figure 5.3-92 GS3 - No Heat Loss: RPV Pressure	5.3-85
Figure 5.3-93 GS3 - No Heat Loss: DW Pressure	5.3-85
Figure 5.3-94 GS3 - No Heat Loss: WW Pressure	5.3-86
Figure 5.3-95 GS2 - RPV Dome Pressure	5.3-87
Figure 5.3-96 GS2 - DW Pressure	5.3-87
Figure 5.3-97 GS2 - SC Pressure	5.3-88
Figure 5.3-98 GS2 - RPV Dome Pressure	5.3-88
Figure 5.3-99 GS2 - DW Pressure	5.3-89
Figure 5.3-100 GS2 - SC Pressure	5.3-89
Figure 5.3-101 GS2 - Chimney Collapsed Level	5.3-90
Figure 5.3-102 GS2 - Channel Delta-P	5.3-90
Figure 5.3-103 GS2 - Bypass Collapsed Level	5.3-91
Figure 5.3-104 GS2 - Downcomer Collapsed Level	5.3-91
Figure 5.3-105 GS2 - Chimney Collapsed Level	5.3-92
Figure 5.3-106 GS2 - Channel Delta - P	5.3-92
Figure 5.3-107 GS2 - Bypass Collapsed Level	5.3-93
Figure 5.3-108 GS2 - Downcomer Collapsed Level	5.3-93
Figure 5.3-109 GS2 - GDCS Flow	5.3-94
Figure 5.3-110 GS2 - GDCS Flow	5.3-94
Figure 5.3-111 GS2 - GDCS - DW Break Flow	5.3-95
Figure 5.3-112 GS2 - RPV - DW Break Flow	5.3-95
Figure 5.3-113 GS2 - GDCS Pool Level	5.3-96
Figure 5.3-114 GS2 - GDCS Flow Volume	5.3-96
Figure 5.3-115 GS2 - GDCLB1 Flow Volume	5.3-97
Figure 5.3-116 GS1 - Upper DW Air Pressure	5.3-98
Figure 5.3-117 GS1 - Lower DW Air Pressure	5.3-98
Figure 5.3-118 GS1 - WW Air Pressure	5.3-99
 Figure 5.4-1 Schematic of the One-Sixth Scale BWR-5 Facility	 5.4-11
Figure 5.4-2 TRACG Nodalization Diagram	5.4-12
Figure 5.4-3 Channel at 41-in. Center: Well-Mixed Model	5.4-13
Figure 5.4-4 Channel at 55-in. Middle: Well-Mixed Model	5.4-13
Figure 5.4-5 Channel at 41-in. Periphery: Well-Mixed Model	5.4-14
Figure 5.4-6 Bypass 41-in. Center: Well-Mixed Model	5.4-14
Figure 5.4-7 Bypass 55-in. Middle: Well-Mixed Model	5.4-15

List of Figures (continued)

	<u>Page</u>
Figure 5.4-8 Bypass 41-in Periphery: Well-Mixed Model	5.4-15
Figure 5.4-9 Lower Plenum at 14-in.: Well-Mixed Model	5.4-16
Figure 5.4-10 Upper Plenum Center: Well-Mixed Model	5.4-16
Figure 5.4-11 Channel at 41-in. Center: Conservative Model	5.4-17
Figure 5.4-12 Channel at 55-in. Middle: Conservative Model	5.4-17
Figure 5.4-13 Channel at 41-in. Periphery: Conservative Model	5.4-18
Figure 5.4-14 Bypass 41-in. Center: Conservative Model	5.4-18
Figure 5.4-15 Bypass 55-in. Middle: Conservative Model	5.4-19
Figure 5.4-16 Bypass 41-in. Periphery: Conservative Model	5.4-19
Figure 5.4-17 Lower Plenum at 14-in.: Conservative Model	5.4-20
Figure 5.4-18 Upper Plenum Center: Conservative Model	5.4-20
Figure 5.4-19 Non-Dimensional Parameters	5.4-21
 Figure 5.5-1 Pressure Suppression Test Facility (PSTF) Schematic	 5.5-10
Figure 5.5-2 PSTF TRACG Component Layout	5.5-11
Figure 5.5-3 TRACG Model of PSTF Suppression Pool	5.5-12
Figure 5.5-4 TRACG Vent System Model - PSTF and SBWR	5.5-13
Figure 5.5-5 Drywell Pressure Response - TRACG vs Measured Data, Test 5703-01	5.5-14
Figure 5.5-6 Drywell Pressure Response - TRACG vs Measured Data, Test 5703-02	5.5-15
Figure 5.5-7 Drywell Pressure Response - TRACG vs Measured Data, Test 5703-03	5.5-16
 Figure 5.6-1 Pressure Suppression Test Facility Schematic	 5.6-13
Figure 5.6-2 TRACG Simulation of PSTF/Mark II	5.6-14
Figure 5.6-3 PSTF Steam Generator and Blowdown Line	5.6-15
Figure 5.6-4 TRACG Nodalization of 4T/Mark II PSTF	5.6-16
Figure 5.6-5 Drywell Pressure Response For Test 5101-34 - TRACG vs Measured Data	5.6-17
Figure 5.6-6 Wetwell Airspace Pressure For Test 5101-34 - TRACG vs Measured Data	5.6-18
Figure 5.6-7 Drywell-to-Wetwell Pressure Differential For Test 5101-34 - TRACG vs Measured Data	 5.6-19
 Figure 5.7-1 PANDA Test Facility Schematic	 5.7-71
Figure 5.7-2 PANDA Vessel Component Nodalization Diagram	5.7-72
Figure 5.7-3 RPV, IC, and Connected Piping Nodalization Diagram	5.7-73
Figure 5.7-4 PCCS (PCC1) Nodalization Diagram	5.7-74
Figure 5.7-5 PCCS and ICS Pools Nodalization Diagram	5.7-85
Figure 5.7-6 Main Vent (DW2 to WW2) Nodalization Diagram	5.7-86
Figure 5.7-7 Vacuum Breaker (DW2 to WW2) Nodalization Diagram	5.7-87
 5.7 Attach. Comparison of TRACG Predictions with PANDA Test Data	 5.7A-1
	through 5.7A-233/5.7A-234
 Figure 6.1-1 Dodewaard RPV with Internals (Left) and with Measurement Equipment (Right)	 6.1-13
Figure 6.1-2 TRACG Model for Dodewaard Steady-State and Transient Analysis	6.1-14
Figure 6.1-3 Axial Power Distribution at End of Cycle 23	6.1-15

List of Figures

(continued)

		<u>Page</u>
Figure 6.2-1	Comparison of the Power-Pressure Path of the February 1992 Startup with a Regular Startup (From [6.2-1])	6.2-33
Figure 6.2-2	TRACG Nodalization Diagram of Dodewaard for Startup Simulation	6.2-34
Figure 6.2-3	Axial Power Distribution Used for Startup Simulation	6.2-35
Figure 6.2-4	Comparison of Measured and Calculated Thermal Power	6.2-36
Figure 6.2-5	Comparison of Measured and Calculated Pressure	6.2-37
Figure 6.2-6	Comparison of Measured and Calculated Steam Flow	6.2-38
Figure 6.2-7	Comparison of Measured and Calculated Water Level	6.2-39
Figure 6.2-8	Comparison of Measured and Calculated Downcomer Local Subcooling	6.2-40
Figure 6.2-9	Comparison of Measured and Calculated Downcomer Velocity	6.2-41
Figure 6.2-10	Comparison of Measured and Calculated Short Range Downcomer Pressure Differences DP1 and DP2	6.2-42
Figure 6.2-11	Comparison of Measured and Calculated Long Range Downcomer Pressure Difference DP3	6.2-43
Figure 6.2-12	Comparison of Measured and Calculated Bypass Temperature	6.2-44
Figure 6.2-13	Comparison of Measured and Calculated Bypass Velocity	6.2-45
Figure 6.2-14	Comparison of Measured and Calculated Sparger Flow	6.2-46
Figure 6.2-15	Calculated Local Subcooling in the Hot Channel (Channel 79) and its Chimney (Ring 2)	6.2-47
Figure 6.2-16	Calculated Void Fraction at the Exit of the Hot Channel	6.2-48
Figure 6.2-17	Calculated Core-and-Bypass-Averaged Void Fraction	6.2-49
Figure 6.2-18	Calculated Liquid Velocity in the Hot Channel (Channel 79 Ring 2)	6.2-50
Figure 6.2-19	Calculated Liquid Velocity at Channel Entrance for all Four Channels	6.2-51
Figure 6.2-20	Calculated Liquid Axial Velocity in the Bypass	6.2-52
Figure 6.2-21	Calculated Void Fractions and Velocities in Channel 81 and Chimney Ring 2 (Zoomed-In 5-Minute Period)	6.2-53
Figure 6.3-1	Schematic Diagram of the CRIEPI Thermal Hydraulic Test Facility	6.3-11
Figure 6.3-2	Schematic Diagram of the Pressure Drop Measurement Location	6.3-12
Figure 6.3-3	Sketch of CRIEPI Circulation Flow for Various Values of Inlet Subcooling	6.3-13
Figure 6.3-4	TRACG Model of CRIEPI Test Facility	6.3-14
Figure 6.3-5	Channel Inlet Pressure Drop (Region 1,2)	6.3-15
Figure 6.3-6	Channel Exit Pressure Drop (Region 5,6)	6.3-15
Figure 6.3-7	Chimney (lower part) Pressure Drop (Region 7)	6.3-16
Figure 6.3-8	Chimney (exit) Pressure Drop (Region 8)	6.3-16
Figure 6.3-9	Steady-State Flow Comparison (P = 0.2MPa)	6.3-17
Figure 6.3-10	Steady-State Flow Comparison (P = 0.5MPa)	6.3-17
Figure 6.3-11	Circulation Flow as a Function of Inlet Subcooling	6.3-18
Figure 6.3-12	Power - Inlet Subcooling Stability Map	6.3-18
Figure 6.3-13	Single Flow Peak	6.3-19
Figure 6.3-14	Chimney Void Fraction Distribution	6.3-19
Figure 6.3-15	Chimney Void Fraction Distribution	6.3-20
Figure 6.3-16	Chimney Temperature Distribution (Tl = Liquid Temperature; Ts = Saturation Temperature)	6.3-20
Figure 6.3-17	Chimney Temperature Distribution Tl = Liquid Temperature; Ts = Saturation Temperature)	6.3-21
Figure 6.3-18	Mechanism of Low Pressure Oscillations	6.3-21

List of Figures (continued)

		<u>Page</u>
Figure 6.3-19	Void Fraction at Different Chimney Locations	6.3-22
Figure 6.3-20	Channel Inlet and Chimney Exit Mass Flow Perturbations	6.3-22
Figure 6.3-21	Implicit - Explicit Scheme Comparison	6.3-23
Figure 6.3-22	Time Step Sensitivity	6.3-23
Figure 6.3-23	Node Size Sensitivity	6.3-24
Figure 6.4-1	PANDA RPV Schematic	6.4-12
Figure 6.4-2	Test E1A: Pressure at the Top of the RPV (solid) and in the PCC3 Inlet Line (dash)	6.4-13
Figure 6.4-3	Test E1A: Flow from the RPV to PCC3 (solid) and from PCC3 to the GDCS Pool (dash)	6.4-13
Figure 6.4-4	Test E1B: Pressure at the Top of the RPV (solid) and in the PCC3 Inlet Line (dash)	6.4-14
Figure 6.4-5	Test E1B: Flow from the RPV to PCC3 (solid) and from PCC3 to the GDCS Pool (dash)	6.4-14
Figure 6.4-6	Test E1C: Pressure at the Top of the RPV (solid) and in the PCC3 Inlet Line (dash)	6.4-15
Figure 6.4-7	Test E1C: Flow from the RPV to PCC3 (solid) and from PCC3 to the GDCS Pool (dash)	6.4-15
Figure 6.4-8	Test E2: Pressure at the Top of the RPV (solid) and in the PCC3 Inlet Line (dash)	6.4-16
Figure 6.4-9	Test E2: Flow from the RPV to PCC3 (solid) and from PCC3 to the GDCS Pool (dash)	6.4-16
Figure 6.4-10	Test E3: Pressure at the Top of the RPV (solid) and in the PCC3 Inlet Line (dash)	6.4-17
Figure 6.4-11	Test E3: Flow from the RPV to PCC3 (solid) and from PCC3 to the GDCS Pool (dash)	6.4-17
Figure 6.4-12	Test E3: Liquid Temperature at the Chimney Inlet	6.4-18
Figure 6.4-13	Base TRACG Model of PANDA RPV	6.4-19
Figure 6.4-14	Simplified TRACG Model of PANDA RPV	6.4-20
Figure 6.4-15	TRACG Simulation of Test E1C: 1) PCC3 Flow (solid; 2) Steam Flow into the Steam Dome (dash)	6.4-21
Figure 6.4-16	TRACG Simulation of the Test E1C: RPV Pressure at 1) Top; 2) Bottom	6.4-21
Figure 6.4-17	TRACG Simulation of the Test E1C: Liquid temperature at 1) Channel Inlet; 2) Chimney Inlet	6.4-22
Figure 6.4-18	TRACG Simulation of the Test E2: 1) PCC3 Flow (solid); 2) Steam Flow into the Steam Dome (dash)	6.4-22
Figure 6.4-19	TRACG Simulation of the Test E2: RPV Pressure at 1) Top; 2) Bottom	6.4-23
Figure 6.4-20	Flow Dependency on Inlet Subcooling (K) for Test E1C: 1) 0.6; 2) 0.4; 3) 0.15; 4) -0.6; 5) -1.35; 6) -1.4	6.4-23
Figure 6.4-21	Circulation Flow for Test E2	6.4-24
Figure 6.5-1	Measured CRIEPI Circulation Flow (P = 0.2 MPa, q = 2.5 kW/chan, Inlet subcooling = 5.1 K)	6.5-13
Figure 6.5-2	Measured CRIEPI Chimney Inlet Temperature (P = 0.2 MPa, q = 2.5 kW/chan , Inlet subcooling = 5.1 K)	6.5-13

List of Figures (continued)

	<u>Page</u>
Figure 6.5-3 Measured CRIEPI Upper Chimney Void Fraction (P = 0.2 MPa, q = 2.5 kW/chan , Inlet subcooling = 5.1 K)	6.5-14
Figure 6.5-4 TRACG Simulation: 1 - Nondimensional Circulation Flow; 2 - Nondimensional Chimney Inlet Temperature; 3 - Chimney Exit Void Fraction	6.5-14
Figure 6.5-5 Measured Chimney Inlet Temperature for PANDA Exploratory Test E1C	6.5-15
Figure 6.5-6 CRIEPI Data: Stability Maps at Various System Pressures	6.5-15
Figure 6.5-7 TRACG Simulation: Dependence of Subcooling Number on Phase Change Number at the Upper Boundary of the Oscillatory Region	6.5-16
Figure 6.5-8 CRIEPI Data: Dependence of Subcooling Number on Phase Change Number at the Upper Boundary of the Oscillatory Region	6.5-16
Figure 6.5-9 TRACG Simulation: Sensitivity of Circulation Flow to Chimney Height at Zero Inlet Subcooling	6.5-17
Figure 6.5-10 TRACG Simulation: Dependence of the Flow Oscillation Period on Flashing Number	6.5-17
Figure 6.5-11 TRACG Simulation: Sensitivity of Circulation Flow to System Pressure at Zero Inlet Subcooling	6.5-18
Figure 6.5-12 TRACG Model with Five Channel-Chimney Regions	6.5-19
Figure 6.5-13 Core Flow Calculated with Multiple Channel TRACG Model	6.5-20
Figure 7.2-1 SBWR Boron Concentrations Estimated Using TRACG Models	7.2-6
Figure 7.2-2 TRACG SBWR Drywell Model	7.2-7
Figure 8.1-1 Evolution of SBWR/TRACG Nodalization for LOCA/ECCS and Transients	8.1-23
Figure 8.1-2 Schematic of the LOCA/ECCS Model Showing the RPV and the Containment Nodalization	8.1-24
Figure 8.1-3 SBWR RPV Nodalization for LOCA/ECCS	8.1-25
Figure 8.1-4 Nodalization of an SBWR Fuel Channel	8.1-26
Figure 8.1-5 Nodalization of GDSCS Piping	8.1-27
Figure 8.1-6 Nodalization of SBWR Steamline System for LOCA/ECCS	8.1-28
Figure 8.1-7 Nodalization for SBWR Feedwater System	8.1-29
Figure 8.1-8 Nodalization of Steam Separators	8.1-29
Figure 8.1-9 Nodalization for SBWR IC and DPV System	8.1-30
Figure 8.1-10 Nodalization of Main Steamline System for SBWR Transients	8.1-31
Figure 8.2-1 TRACG Model of SBWR Containment -RPV	8.2-24
Figure 8.2-2 TRACG Model of SBWR Containment - IC and PCC	8.2-25
Figure 8.2-3 TRACG Model of SBWR Containment - DW and GDSCS	8.2-26
Figure 8.2-4 TRACG Model of SBWR Containment - WW	8.2-27
Figure 8.2-5 TRACG Model of SBWR Containment - Configured for Main Steamline Break	8.2-28
Figure 9.1-1 SBWR Stability Map	9.1-28

Nomenclature and Abbreviations

Nomenclature

English Letters

Symbols	Description	Units
A	Cross-sectional flow area	m^2
B	Specific buoyancy flux defined in Eq. 2.1-22b	m^4/s^3
C_0	Drift flux model distribution parameter	*
C	Concentration	*
c_i	Interfacial shear parameter	*
c_p	Specific heat at constant pressure	J/kg K
d	Characteristic length	m
D	Diameter	m
D_h	Hydraulic diameter	m
e	Specific internal energy	J/kg
F/A^2	Sum of loss coefficients divided by area ² (Eq. 2.1-24b)	$1/m^4$
f	Darcy friction factor	*
f_2	Parameter defined in Eq. 2.1-4	*
f_3	Parameter defined in Eq. 2.1-1	*
f_4	Parameter defined in Eq. 2.1-1	*
$f(X_i)$	Designates an arbitrary function of arguments X_i	*
G	Mass flux	kg/m^2s
g	Acceleration due to gravity	$9.81 m/s^2$
H	Submergence head	m
h	Specific enthalpy	J/kg
h_{fg}	Latent heat of vaporization	J/kg
Δh	Specific enthalpy difference	J/kg
h	Heat transfer coefficient	$J/m^2 K$
h_y	Heat transfer coefficient with noncondensibles	$J/m^2 K$
J_j	Volumetric flow rate	m^3/s
J_o	Volumetric injection flow rate in pool	m^3/s
K	Form loss coefficient	*
k	Thermal conductivity	J/ m K
k_μ	Coefficient in Eq. (2.1-22a)	*
L	Pipe or pipe segment length	m
L	Hydrostatic or gravity head	m
L_0	Characteristic length	m
L/A	Sum of pipe segment lengths divided by area (Eq. 2.1-25b)	m^{-1}
n	Number of free or wall jets	*
ΔP	Pressure difference	Pa

* = dimensionless

Nomenclature and Abbreviations

(continued)

\dot{P}	Rate of pressure change	Pa/s
P^*	Pressure parameter defined in Eq. 2.1-10	Pa
Q	Heat rate	W
R	Radius	m
T	Temperature	K
ΔT	Temperature difference, form defined by Eq. 2.1-6	K
t	Time	s
t_0	Charateristic time	s
u	Fluid velocity	m/s
u_e	Characteristic entrainment velocity	m/s
u_0	Characteristic transport velocity	m/s
V_{gj}	Drift flux velocity	m/s
v	Specific volume	m ³ /kg
W	Mass flow rate	kg/s
ΔW	Differential mass flow rates between channels	kg/s
X	Steam quality	*
X	Distance from centerline	m
y	Mass fraction	*
Z	Characteristic distance from submerged vent	m
z	Axial coordinate along flow path	m

Greek Letters

Symbols	Description	Units
α	Void fraction	*
$\Delta\alpha$	Void fraction difference	*
β	Coefficient of thermal expansion	K ⁻¹
μ	Viscosity	kg/m s
ρ	Density	kg/m ³
σ	Surface tension	kg/s ²
τ	Time constant	s

Nondimensional Groups

Symbols	Description
N_{Ku}	Kutateladze Number, defined by Eq. 2.1-2
$N_{Bi} = h d/k_s$	Biot Number
N_{Fr}	Froude Number, defined by Eq. 2.1-16
N_{fl}	Flashing Number, defined in Section 6.2.3
N_{Gr}	Grashof Number, defined by Eq. 2.1-19

Nomenclature and Abbreviations

(continued)

$N_{Nu} = h d/k$	Nusselt Number
$N_{Nu,dlt}$	Droplet Nusselt Number, defined by Eq. 2.1-13
$N_{Nu,fb,low\ flow}$	Film Boiling Nusselt Number at low flow
$N_{Pr} = c_p \mu/k_f$	Prandtl Number
N_{PCH}	Phase change Number, defined by Eq. 2.1-17
$N_{Nu,fb,dist. dlt}$	Film Boiling Nusselt Number, form given in Table 2.1-1
N_{Eu}	Euler Number, form defined by Eq. 2.1-9b
$N_\rho = \rho_g/\rho_l$	Density Ratio Number
$N_{Re} = \rho V D_h/\mu$	Reynolds Number
N_{sub}	Subcooling Number, defined by Eq. 2.1-18
$N_{We,dlt}$	Droplet Weber Number, defined by Eq. 2.1-14
$N_{Ra} = N_{Gr} N_{Pr}$	Rayleigh Number
N_{Ri}	Richardson Number, defined by Eq. 2.1-9
Π_{GM}	Nondimensional group, defined by Eq. 2.1-1
Π_{IN}	Inertia pressure number, defined by Eq. 2.1-26
Π_P	Nondimensional group, defined by Eq. 2.1-1
Π_V	Nondimensional group, defined by Eq. 2.1-1
$\Pi_{PCH,stored}$	Phase change group-heat stored in structures, defined by Eq. 2.1-3
$\Pi_{PCH,decht}$	Phase change group-core decay heating, defined by Eq. 2.1-7
$\Pi_{Q,stored}$	Heat addition group-heat stored in structures, defined by Eq. 2.1-4
$\Pi_{Q,misc}$	Heat addition group-miscellaneous sources
$\Pi_{Q,decht-losses}$	Heat addition group-net core decay heating, defined by Eq. 2.1-8
Π_t	Time scale group, defined by Eq. 2.1-3
Π_{sub}	Subcooling group, form defined by Eq. 2.1-5
Π_{subm}	Submergence pressure number, defined by Eq. 2.1-23
Π_W	Inventory addition group, form defined by Eq. 2.1-11
Π_{Wh}	Enthalpy flow group, form defined by Eq. 2.1-12
Π_{mech}	Mechanical compression group, form defined by Eq. 2.1-10
Π_{loss}	Pressure loss number, defined by Eq. 2.1-25
Π_{hyd}	Hydrostatic head group, defined by Eq. 2.1-24
Π_{bj}^S	Free buoyant jet mixing time ratio, defined by Eq. 2.1-21a
Π_{bl}^S	Wall buoyant jet mixing time ratio, defined by Eq. 2.1-21b

Subscripts

avg	Average value
BP	Bypass
bj	Free buoyant jet
bl	Wall buoyant jet
c	Core

Nomenclature and Abbreviations

(continued)

ch	Chimney
DW	Drywell
DC	Downcomer
decht	Decay heat
decht-losses	Decay heat less heat losses
dlt	Droplet
GDCS	Gravity-Driven Cooling System
GT	Guide tube
G,g	Gas phase
EQ	Equalization line
FW	Feedwater
f	Fluid
fg	Phase change
fb	Film boiling
fuel	Fuel
hx	Heat exchanger
LP	Lower Plenum
L,l	Liquid phase
L/G	Change from Liquid to Gas
leak	Leakage flow
i	Refers to component or location “i”
j	Refers to component or location “j”
MV	Main Vent
max	Maximum value
mod	Model (Test Facilities)
N/C	Noncondensibles
o	Initial value
0	Characteristic value
PCC	Passive Containment Cooling Condenser
p	Prototype (SBWR)
ppm	Parts per million
rest	Restriction
RPV	Reactor Pressure Vessel
SRV	Safety-Relief Valve
r	Refers to a reference quantity
SL	Steam Line
sat	Saturation
sep	Separator
sub	Vent submergence
sp	Spray
UTP	Upper Tie Plate
VB	Vacuum Breaker
W	Wall

Nomenclature and Abbreviations

(continued)

WW	Wetwell
wall	Wall of structure
y	Refers to heat transfer coefficient in gas with N/C
∞	Refers to temperature away from wall

Additional subscripts are defined in the text or are self-explanatory

Superscripts

'	Denotes derivative with respect to pressure
.	Denotes derivative with respect to time
+	Nondimensional variable normalized to its initial value
◦	Nondimensional parameter normalized to reference value
S	Specific (for a well defined geometry)

Abbreviations

ADS	Automatic Depressurization System
ADW	Annular Drywell
ALPHA	Advanced LWR Passive Heat Removal and Aerosol Program
ATLAS	Fuel bundle thermal hydraulic test facility at GE
ATWS	Anticipated Transients Without Scram
ATRAC	Computer input deck generator for TRACG
BAF	Bottom of Active Fuel
BDL	Bottom Drain Line
BDLB	Bottom Drain Line Break
BT	Boiling Transition
BWR	Boiling Water Reactor
CANDU	Canadian Deuterium Uranium reactor
CHF	Critical Heat Flux
CCFL	Counter Current Flow Limiting
CRD	Control Rod Drive
CRGT	Control Rod Guide Tube
CRIEPI	Central Research Institute for Electric Power Industry
DBA	Design Basis Accident
DPV	Depressurization Valve
DRF	Design Record File
DSA	Double sided heat Slabs
DW	Drywell
ECCS	Emergency Core Cooling System
ECPR	Experimental Critical Power Ratio
ENEA	Italian national agency for new technology, energy and environment
EOC	End of Cycle

Nomenclature and Abbreviations

(continued)

EQL	Equalization Line
EBWR	Experimental Boiling Water Reactor
FIST	Full Integral Simulation Test
FRIGG	Facility used for fuel channel thermal-hydraulic tests in Sweden
GDC	Gravity-Driven Cooling
GDCS	Gravity-Driven Cooling System
GDCL	GDCS Line
GDLB	GDCS Line Break
GE	General Electric Company
GIRAFFE	Gravity-Driven Integral Full-Height Test for Passive Heat Removal
GIST	GDCS Integrated Systems Test
GTBP	Guide Tube Bypass
HPCS	High Pressure Core Spray
H2TS	Hierarchical Two-Tier Scaling
HVL	Horizontal Vent Line
IC	Isolation Condenser
ICS	Isolation Condenser System
IST	Integral System Test
I.D.	Inner Diameter
JAPC	Japan Atomic Power Company
JPI	Jet Pump Injection
KEMA	Dutch company for engineering and consultancy services
KSP	Kuhn-Schrock-Peterson correlation
LDW	Lower Drywell
LOCA	Loss-of-Coolant Accident
LWRSIM	Light water reactor simulation code used by the Dutch
L/D	Length to Diameter ratio
ln()	Natural logarithm with base e=2.718282
MDW	Middle Drywell-center, annular section of DW
MIT	Massachusetts Institute of Technology
MPR	Minimum Pressure Regulator
MSL	Main Steam Line
MSLB	Main Steam Line Break
MSIV	Main Steam line Isolation Valve
NB	No-Break
NDT	Nondestructive Test
NRC	Nuclear Regulatory Commission
N/C	Noncondensibles
O.D.	Outer Diameter
OHT	Ontario Hydro Technologies
PANACEA	BWR core simulator code
PANDA	Passive Nachwarmeabfuhr-und Drueckabbau-Testanlage
PANTHERS	Performance Analysis and Testing of Heat Removal Systems

Nomenclature and Abbreviations

(continued)

PCC	Passive Containment Condenser
PCCS	Passive Containment Cooling System
PCT	Peak Clad Temperature
PCV	Primary Containment Vessel
RHR	Residual Heat Removal
PIRT	Phenomena Identification and Ranking Table
RSA	Control rod drive flow
PSI	Paul Scherrer Institute
PSTF	Pressure Suppression Test Facility
RPV	Reactor Pressure Vessel
RWCU	Reactor Water Cleanup
RZS	Reactor water cleanup flow
SBWR	Simplified Boiling Water Reactor
SC	Pressure Suppression Chamber
SET	Separate Effects Test
SDC	Shutdown Cooling
SLCS	Standby Liquid Control System
SIET	Societa Informazioni Esperienze Termoidrauliche
SIT	Systems Interaction Tests
SP	Suppression Pool
SPERT	Reactivity insertion transient test facility at Idaho National Laboratory
SRV	Safety-Relief Valve
SSAR	Standard Safety Analysis Report
TAF	Top of Active Fuel
TAPD	SBWR Test and Analysis Program Description
TCS	Turbine Control Valve
TCV	Turbine Stop/Control Valves
TLTA	Two Loop Test Apparatus
TRACG	Transient Reactor Analysis Code, GE version
TSV	Turbine Stop Valve
UCB	University of California at Berkeley
UDW	Upper Drywell
VB	Vacuum Breaker
WL	Water Level
WW	Wetwell
1-D	One-dimensional
Π -group	Refers to a nondimensional group in text

5. Integral Systems Tests

This section covers the integral systems tests (ISTs) that have been analyzed to qualify TRACG for SBWR application. Integral systems tests are more complex than separate effects and component performance tests. The overall system response depends not only on the performance of the individual analytical models in TRACG, but also on the complex interactions between these models. The primary purpose of the ISTs, therefore, is to assess TRACG predictions of the phenomena and component interactions, and how they affect the overall system response. The secondary purpose is to provide additional information useful for the qualification of individual models in TRACG. As discussed in Section 2, the qualification of the highly ranked PIRT phenomena in the ISTs will be mostly through the evaluation of these phenomena in a top-down sense (i.e., a global evaluation of how the effects of these phenomena on the system response are predicted in relationship to other important effects).

The tests included in this section are all LOCA tests (covering both the primary system and containment) with the exception of the boron mixing test, which is useful for analysis of anticipated transients without scram (ATWS). Integral systems and plant data related to plant startup are covered in Section 6.

The GIST, GIRAFFE and PANDA tests were performed specifically for the SBWR. Figure 5.0-1 shows the relationship of these test programs to the phases of the SBWR LOCA transient. As discussed in Section 2.1 of this report, prior tests performed in support of the earlier BWR designs have also been used to fill in gaps in the SBWR-specific test program. Specifically, tests were not performed for the initial blowdown phase of the SBWR, because no new phenomena are introduced in this phase prior to Gravity-Driven Cooling System (GDSCS) initiation. A large database of tests exists for the early blowdown phase. TRACG has been qualified against data from the TLTA [5.0-1] and FIST [5.0-2] facilities for the reactor vessel phenomena (vessel depressurization, blowdown flow and regional inventories). The results of this analysis are documented in the generic TRACG qualification report [5.0-3] and are not repeated here. On the containment side, extensive series of tests were conducted in the Pressure Suppression Test Facility (PSTF) in San Jose, CA. Comparisons against representative Mark III and Mark II tests are shown in Sections 5.5 and 5.6, respectively. The objective of this analysis is to validate TRACG predictions of the containment response in the early blowdown period.

Section 5.1 contains comparisons between TRACG and test data from the GIST facility. GIST is a scaled simulation of the SBWR and includes components simulating the RPV and containment. The GDSCS is a key feature of the GIST facility. GIST covers the late blowdown and early GDSCS phases of the LOCA.

Section 5.2 contains the results of TRACG analysis of the GIRAFFE Helium tests. GIRAFFE is a scaled simulation of the SBWR and includes components simulating the RPV, containment, PCCS, GDSCS and ICS. These tests cover the PCCS or long-term phase of the LOCA transient. The emphasis is on the containment response. Tests were conducted with nitrogen and helium in the drywell to investigate the effects of both heavier-than-steam and lighter-than-steam noncondensable gases on PCC performance and containment response.

Section 5.3 examines the GIRAFFE Systems Interaction Tests (SIT). These tests cover the late blowdown and GDCS periods of the LOCA transient. The emphasis in these tests was on systems interactions with respect to RPV parameters (pressure response and inventory distribution). Interactions between the GDCS, PCCS, ADS and ICS were present in these tests.

Comparisons of TRACG predictions with the boron mixing data from the 1/6th Scale Boron Mixing Facility at Vallecitos are discussed in Section 5.4. A salt solution was injected into the upper plenum of a scaled BWR/5 model, and its transport into the bypass, core and lower plenum regions was tracked. The salt solution simulated the density difference resulting from the injection of cold borated water in an ATWS event.

Sections 5.5 and 5.6, respectively, contain comparisons of TRACG predictions with Mark III and Mark II containment simulations. These tests were performed in the PSTF. The Mark III tests provide data on drywell pressurization and horizontal vent-clearing phenomena. The Mark II tests can be used to assess wetwell pressurization during the early blowdown transient.

Section 5.7 compares TRACG predictions with data from the PANDA tests. These are large-scale tests of the SBWR containment response to a large steamline break in the PCCS or long-term phase of the LOCA transient. One of the tests (M9) also provides data for the GDCS phase of the transient. A number of parameters were explored in the PANDA M Series of tests, including the effects of asymmetric steam discharge, combined IC and PCC operation, leakage between the drywell and wetwell, and PCC startup with the drywell filled with noncondensable gas.

References

- [5.0-1] Md. Alamgir, *BWR Refill-Reflood Program Task 4.8 - TRAC-BWR Model Qualification: BWR Safety Analysis Final Report* (NUREG/CR-2571), July 1983.
- [5.0-2] W.S. Hwang, Md. Alamgir and Wm. A. Sutherland, *BWR FIST Phase I Test Results*, NUREG/CR-3711, November 1983.
- [5.0-3] J.G.M. Andersen et. al, *TRACG Qualification*, NEDE-32177P, Revision 2, January 2000.

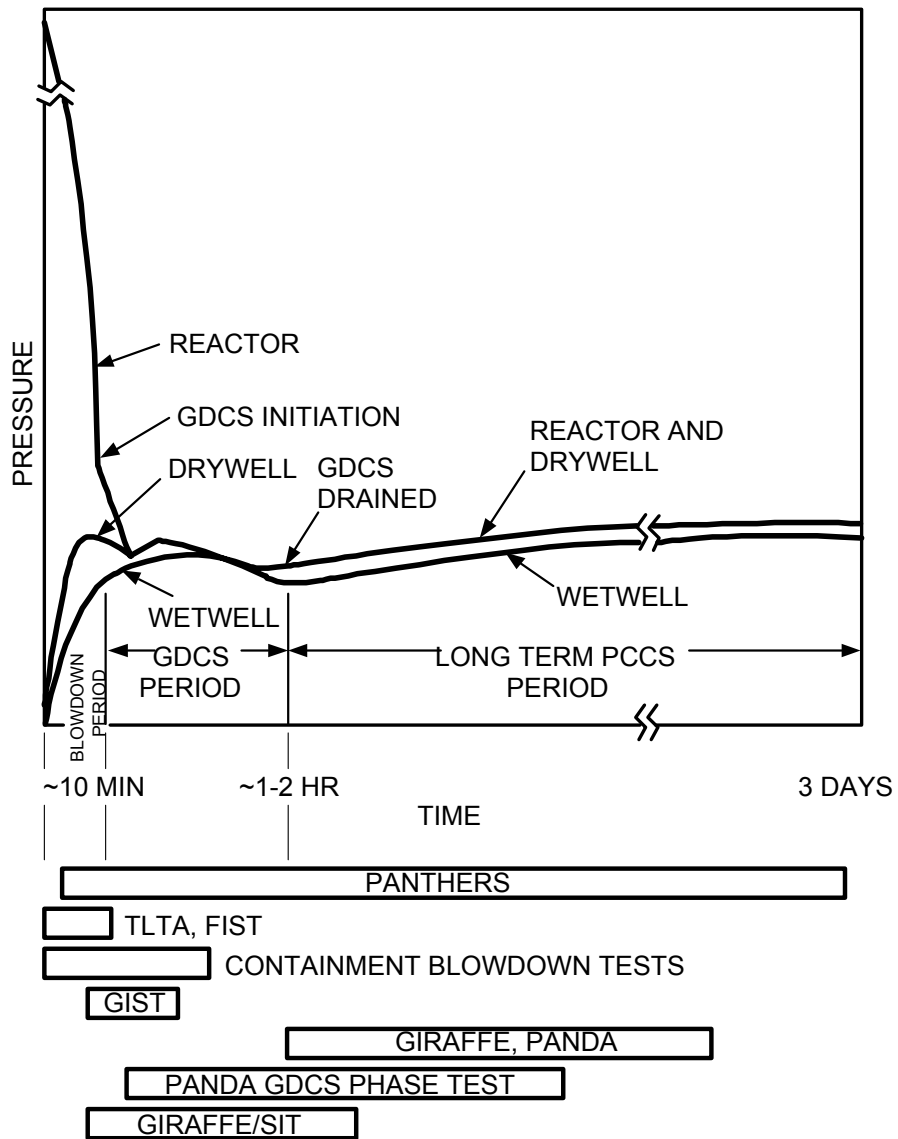


Figure 5.0-1 SBWR LOCA Phases and Major Test Coverage

5.1 GIST

5.1.1 Introduction

The objective of this section of the qualification was to assess the overall capability of TRACG to predict the GIST facility response to a variety of LOCA initiating events. The main areas of interest were the effectiveness of the modeling of the GDCS, the RPV, and the containment in the late blowdown and GDCS periods of the LOCA transient. At this time, low flow (natural circulation) and low pressure (below 1.068 MPa) conditions exist in the RPV. The qualification consisted of post-test calculations with TRACG and comparison against the GIST data.

Large and small liquid line break LOCA tests, steamline break LOCA tests, power transient simulations, and tests to determine natural circulation flow characteristics have been completed. The test results and data evaluations have been reported in References 5.1-1 and 5.1-2. Five tests were selected for TRACG analysis. These represent the base case LOCAs in the steam line, GDCS line and a bottom break in the Reactor Water Cleanup (RWCU) Line. In addition, a No-Break case with loss of feedwater, and a steamline break with low initial inventory were analyzed.

5.1.2 Description of GIST Facility and Tests

The GDCS Integrated Systems Test (GIST) facility was built at the GE Nuclear Energy site in San Jose, California. All significant plant features which could affect the performance of the GDCS were included in the design. Since the containment pressure and the GDCS pool water level determine the start of the GDCS initiation, the containment (both drywell and wetwell) was simulated in the tests. The focus in these tests was the GDCS system performance and the RPV/containment integrated system response for the low pressure (1.068 MPa and below) range of the LOCA blowdown phase.

The GIST facility, shown schematically in Figure 5.1-1, is a full-height, one-five hundred eighth (1/508) volumetric scale model of the March 1987 SBWR conceptual design. As depicted in Figures 5.1-2 and 5.1-3, GIST has cylindrical vessels simulating regional volumes of the SBWR and has interconnecting piping thermally-hydraulically scaled to simulate the Automatic Depressurization System (ADS), the GDCS lines and LOCA conditions such as a Main Steamline Break (MSLB), a GDCS Line Break (GDLB), and a vessel Bottom Drain Line Break (BDLB). GIST was scaled on power/volume basis with the full-height, and volumetric scaling of regions as well as scaled flow areas in key regions. As shown in the scaling report [5.1-5], this scaling basis results in a well-scaled, real-time response in the GIST facility (i.e., for the key parameters of changes in level, pressure, temperature and velocity). Detailed descriptions of design and operation of the GIST facility are contained in Reference 5.1-3.

The GIST depressurization tests selected for qualification study represented a full variety of the type of initiating event (break types), a wide range of initial liquid inventories in the pressure vessel, variations of the containment initial conditions and a variation in the degree of availability of the GDCS. These tests provided a significant challenge to TRACG in terms of LOCA type, the rate of blowdown, the vessel-containment integrated system response, the

GDCS response, the vessel reflood, and the core thermal-hydraulic response under low pressure natural circulation conditions.

Table 5.1-1 summarizes the tests selected for qualification study. The motivation for selecting each test is stated. Section 3.4 of Reference 5.1-1 provides additional detail on these and all of the GIST facility tests. The key measurements in the tests were the RPV, drywell and wetwell pressures; the level in the RPV annulus; and GDCS flow rate. The uncertainties in these measurements were estimated to be:

RPV Pressure: ± 14 kPa

Drywell Pressure: ± 7 kPa

Wetwell Pressure: ± 6 kPa

Annulus Pressure Drop: ± 0.85 kPa

GDCS mass flux: ± 9.5 kg/m²-s

5.1.3 Applicability of Data to SBWR

This section describes how the GIST tests provided data relevant for validation of computer code models used to analyze the post-LOCA performance of the SBWR. The overall scaling approach for the GIST test facility is discussed in Section 5.1.3.1. Descriptions of the significant PIRT phenomena and the associated parameters that this test was to provide data for are given in Section 5.1.3.2. The applicable PIRT phenomena for this test are listed in the TAPD [5.1-4] and summarized in Table 2.1-5a of this report. An explanation of how the test covered a particular PIRT phenomenon in terms of physical parameter ranges is given immediately following each PIRT phenomenon description.

5.1.3.1 General Test Facility Scaling

[

Redacted

]

[

Redacted

]

5.1.3.2 PIRT Phenomena and Coverage

[

Redacted

]

[

Redacted

]

[

Redacted

]

[

Redacted

]

5.1.3.3 Conclusions on Data Applicability

[

Redacted

]

5.1.4 TRACG Model

[

Redacted

]

[

Redacted

]

5.1.5 TRACG Simulation of GIST Tests

[

Redacted

]

5.1.5.1 Initial Conditions

[

Redacted

]

5.1.5.2 Test Control

[

Redacted

]

[

Redacted

]

5.1.5.3 Tests Analyzed with TRACG

Five GIST tests were selected for TRACG analysis.

Test B01 is the reference Main Steamline Break case. It results in a rapid RPV blowdown and inventory loss. The steamline break is the most limiting break for containment pressure. The TRACG model configuration for the steamline break is shown in Figure 5.1-6.

Test B07 is a Main Steamline Break with low initial RPV inventory. It resulted in core uncover and subsequent heatup.

Test C01A is a GDCS Line Break test. This test has the minimum availability of GDCS - one line broken and second line unavailable due to valve failure. The break flow is discharged into the annular drywell region.

Test A07 is a Bottom Drain Line Break case. This test has a small, low liquid line break, with the slowest blowdown and recovery. The bottom drain line break represents the largest LOCA below the elevation of the core. In this test, the low pressure DPVs were assumed to be failed. The break location is in the lower drywell.

Test D03A is a No Break test. The test was run with a high decay heat. With no break, there is no containment back pressure to aid the GDCS flow. Table 5.1-3 presents the key initial conditions obtained from GIST data that were used in the TRACG simulations. In addition to the initial conditions, the break configuration needed to be modeled individually for the different break locations.

5.1.6 Results of Post-Test Calculations

5.1.6.1 TRACG/GIST Comparisons for Bottom Drain Break LOCA (Test A07)

Overall, TRACG shows good prediction of the pressures, the GDCS flow rate and timing, and annulus inventory. Other regional inventories are predicted with acceptable accuracy. These comparisons indicate that TRACG has adequate models of the relevant thermal-hydraulic phenomena.

[

Redacted

]

[

Redacted

]

5.1.6.2 TRACG/GIST Comparisons for Other LOCA Types

[

Redacted

]

[

Redacted

]

5.1.6.3 RPV Dome Pressure (Figures 5.1-17 through 5.1-20)

[

Redacted

]

5.1.6.4 GDCS Flow (Figures 5.1-21 through 5.1-24)

[

Redacted

]

5.1.6.5 Annulus Pressure Drop (Figures 5.1-25 through 5.1-28)

[

Redacted

]

5.1.6.6 Core Pressure Drop (Figures 5.1-29 through 5.1-32)

[

Redacted

]

5.1.6.7 Margin to Boiling Transition

[

Redacted

]

5.1.7 Conclusions

TRACG calculates the performance of the GIST facility with acceptable accuracy over the expected range of break sizes and initial conditions. The calculations included system pressures (RPV, drywell and wetwell), regional mass distribution of the two-phase fluid within the vessel, GDCS onset time and the GDCS flow rate. The key parameters of RPV pressure and core inventory were calculated accurately, particularly after the early drainage of the downcomer mass into the annulus.

Data were obtained to qualify TRACG for the highly ranked PIRT phenomena, as discussed in Section 5.1.3. The ranges of these parameters in the tests were acceptable for use in SBWR qualification. The effects of these phenomena were assessed mostly in a top-down fashion, (i.e. in terms of their effects on such parameters as pressures, inventories and pressure drops).

5.1.8 References

- [5.1-1] P.F. Billig, *Simplified Boiling Water Reactor (SBWR) Program Gravity-Driven Cooling System (GDCS) Integrated Systems Test - Final Report*, GE Nuclear Energy, GEFR-00850, October 1989.

- [5.1-2] Md. Alamgir, J.G.M. Andersen, A.I. Yang and B.S. Shiralkar, *TRACG prediction of Gravity-Driven Cooling System Response in the SBWR/GIST Facility LOCA Tests*, ANS Transactions, 62, pp. 665-668, November 1990.
- [5.1-3] J.M. Mross, *Final Test Report: Testing of the Gravity-Driven Cooling System for the Simplified Boiling Water Reactor*, GE Nuclear Energy, NEDO-31680, July 1989.
- [5.1-4] B.S. Shiralkar, et al., *SBWR Test and Analysis Program Description*", NEDC-32391P, Rev. C, August 1995.
- [5.1-5] R.E. Gamble, et al., *Scaling of the SBWR Related Tests*, NEDC-32288P, Rev. 1, October 1995.
- [5.1-6] P. F. Billig, et al., *SBWR Testing Summary Report*, NEDC-32606P, Rev. 0, August 2002.

Table 5.1-1
GIST Facility Tests Selected for TRACG Qualification

I	B01 Main Steamline Break	
	A	Rapid RPV Blowdown
	B	Rapid RPV Inventory Loss
	C	Most Limiting LOCA Condition
II	B07 Main Steamline Break	
	A	Lowest Initial RPV Inventory
	B	Core Uncovery and Subsequent Heatup
III	C01A GDSCS Line Break	
	A	Minimum Availability of GDSCS
	B	Drywell Depressurization
	C	Wetwell-to-Drywell Vacuum Breaker Operation
	D	Shows Total Integrated System Response
IV	A07 Bottom Drain Line Break	
	A	Slowest Blowdown and Recovery
	B	Largest LOCA Below the Core
	C	No Low Pressure DPV's
V	D03A No Break	
	A	No Containment Backpressure to Aid GDSCS
	B	High "Appendix A" Decay Heat

Table 5.1-2
GIST Nodalization vs. SBWR Nodalization

[

Redacted

]

**Table 5.1-3
GIST Initial Conditions Used in TRACG Input**

	B01	B07	C01A	A07	D03A
Drywell Pressure (MPa)	0.198	0.199	0.198	0.196	0.101
Drywell Water Level (meter above Bottom)	0.127	0.142	0.140	0.132	0.150
Wetwell Pressure (MPa)	0.150	0.150	0.150	0.138	01.01
Wetwell Water Level (meter above Bottom)	5.974	6.014	6.014	5.974	5.982
Vessel Dome Pressure (MPa)	1.060	1.057	1.058	1.060	1.065
Vessel Level (meter above Bottom)	8.636	7.620	8.814	8.814	8.814
Available GDCS Lines	3	1	2	3	3
DPV's Available	All	All	All	1/2	All

**Table 5.1-4
GIST TRACG Comparison Results**

[

Redacted

]

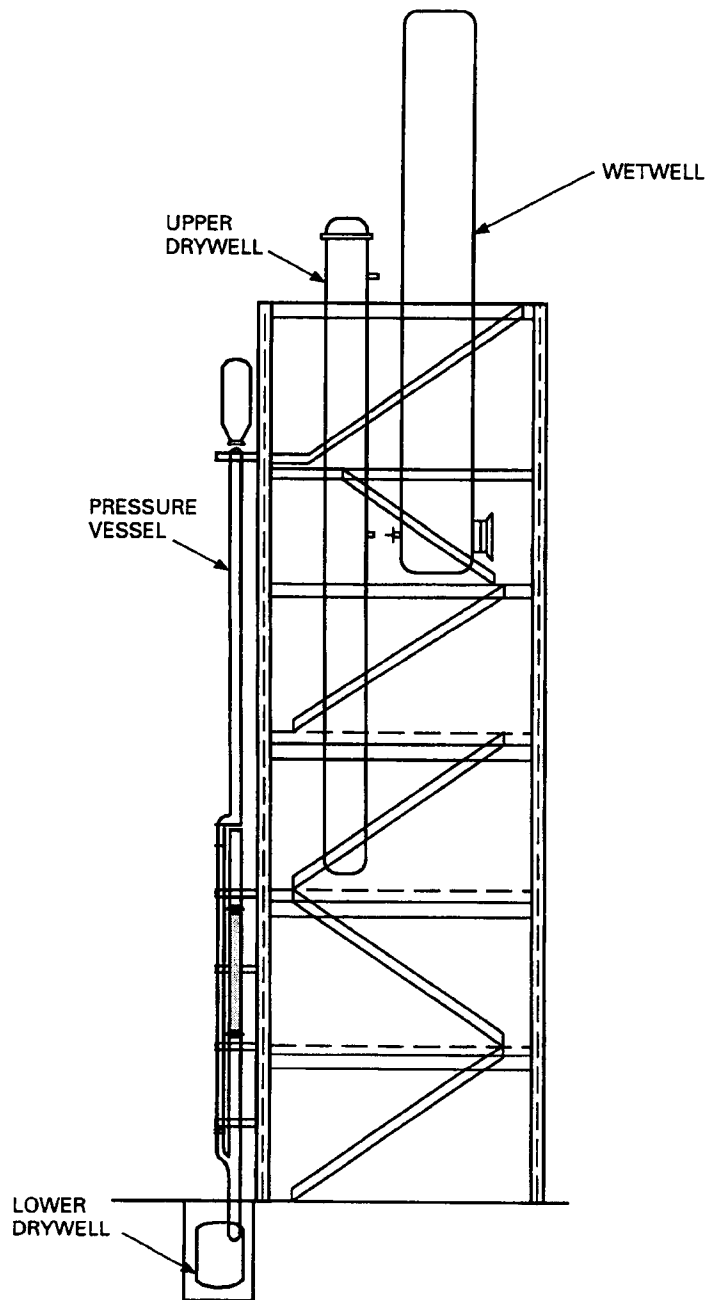


Figure 5.1-1 GIST Facility

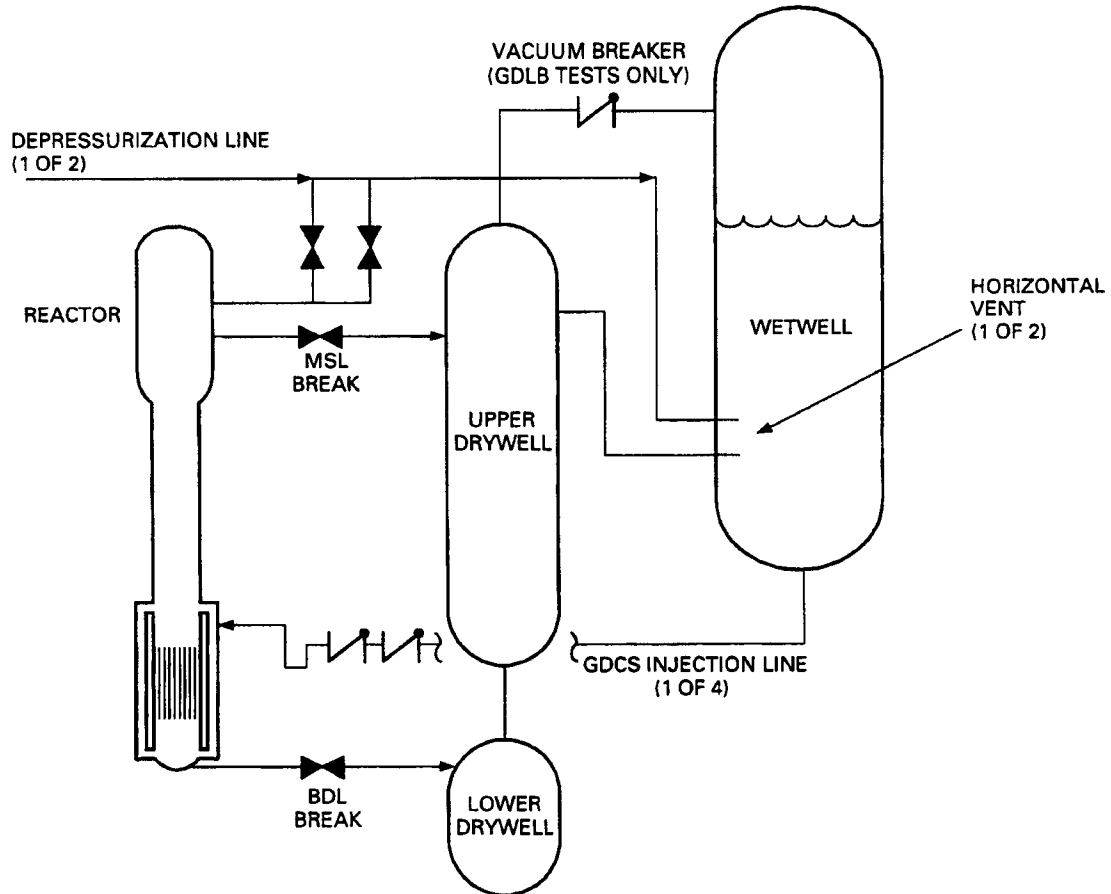


Figure 5.1-2 GIST Facility - Major Flow Paths

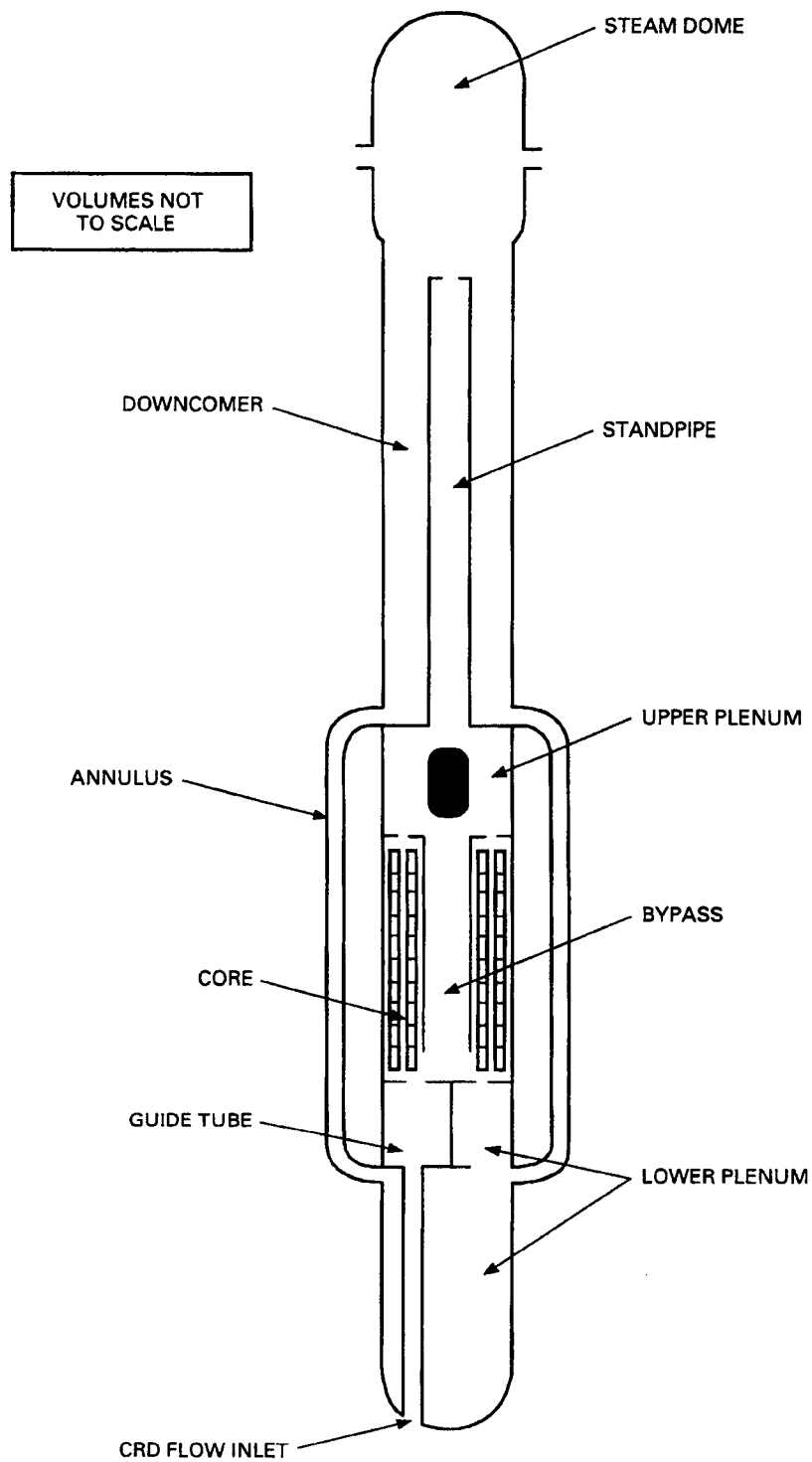


Figure 5.1-3 GIST Facility - Pressure Vessel

[

Redacted

]

Figure 5.1-4 TRACG Nodalization of GIST RPV

[

Redacted

]

Figure 5.1-5 Nodalization of GIST Containment

[

Redacted

]

Figure 5.1-6 TRACG Nodalization of GIST Steam lines

[

Redacted

]

Figure 5.1-7 TRACG Nodalization for GDCS Line Calibration

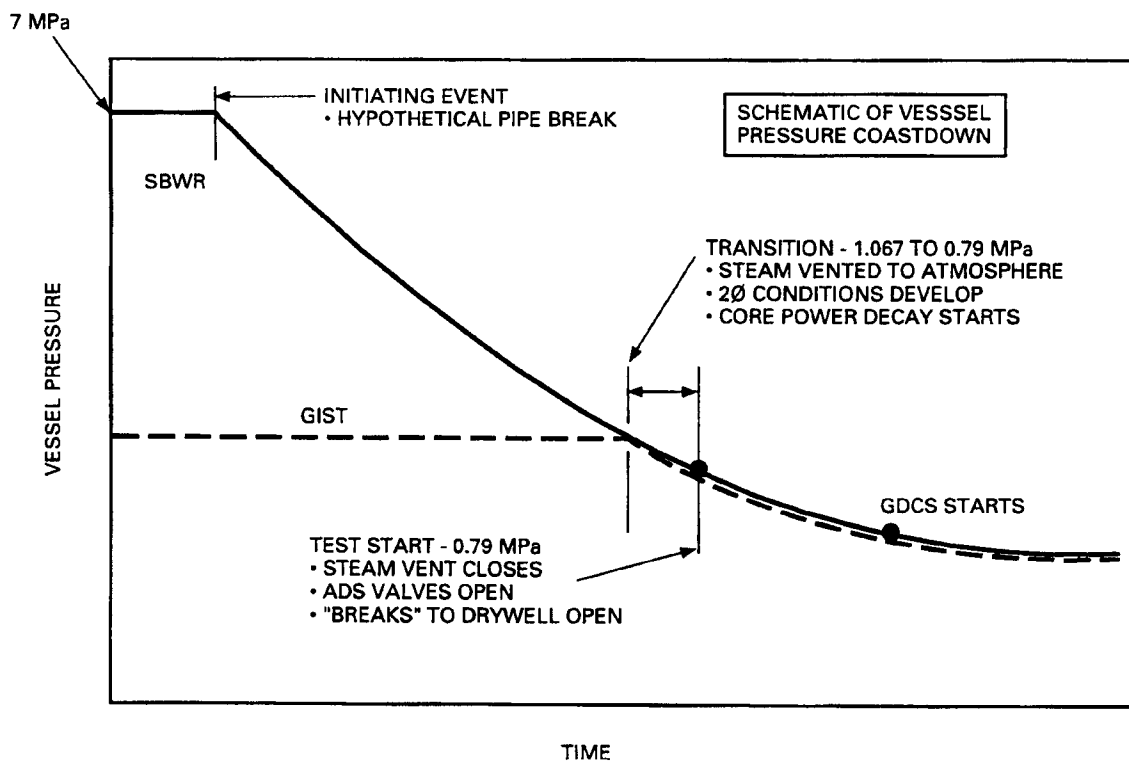


Figure 5.1-8 GIST RPV Blowdown

[

Redacted

]

Figure 5.1-9 Comparison of RPV Pressures (Bottom Drain Line LOCA-A07)

[

Redacted

]

Figure 5.1-10 Comparison of Upper Drywell Pressure (Test A07)

[

Redacted

]

Figure 5.1-11 Comparison of Wetwell Pressure (Test A07)

[

Redacted

]

Figure 5.1-12 Comparison of GDCS Flow Rate (Test A07)

[

Redacted

]

Figure 5.1-13 Comparison of Annulus Pressure Drop (Test A07)

[

Redacted

]

Figure 5.1-14 Comparison of Core Pressure Drop (Test A07)

[

Redacted

]

Figure 5.1-15 Comparison of Bypass Pressure Drop (Test A07)

[

Redacted

]

Figure 5.1-16 Comparison of Standpipe Pressure Drop (Test A07)

[

Redacted

]

Figure 5.1-17 Comparison of RPV Pressure (Test B01)

[

Redacted

]

Figure 5.1-18 Comparison of RPV Pressure (Test B07)

[

Redacted

]

Figure 5.1-19 Comparison of RPV Pressure (Test C01A)

[

Redacted

]

Figure 5.1-20 Comparison of RPV Pressure (Test D03A)

[

Redacted

]

Figure 5.1-21 Comparison of GDCS Flow (Test B01)

[

Redacted

]

Figure 5.1-22 Comparison of GDCS Flow (Test B07)

[

Redacted

]

Figure 5.1-23 Comparison of GDCS Flow (Test C01A)

[

Redacted

]

Figure 5.1-24 Comparison of GDCS Flow (Test D03A)

[

Redacted

]

Figure 5.1-25 Comparison of Annulus Pressure Drop (Test B01)

[

Redacted

]

Figure 5.1-26 Comparison of Annulus Pressure Drop (Test B07)

[

Redacted

]

Figure 5.1-27 Comparison of Annulus Pressure Drop (Test C01A)

[

Redacted

]

Figure 5.1-28 Comparison of Annulus Pressure Drop (Test D03A)

[

Redacted

]

Figure 5.1-29 Comparison of Core Pressure Drop (Test B01)

[

Redacted

]

Figure 5.1-30 Comparison of Core Pressure Drop (Test B07)

[

Redacted

]

Figure 5.1-31 Comparison of Core Pressure Drop (Test C01A)

[

Redacted

]

Figure 5.1-32 Comparison of Core Pressure Drop (Test D03A)

[

Redacted

]

Figure 5.1-33 Annulus Level Position (Test B01)

[

Redacted

]

Figure 5.1-34 Comparison of Rod Temperatures (Test B07)

[

Redacted

]

Figure 5.1-35 Calculated Core Axial Void Profile (Test B07)

5.2 GIRAFFE Helium Tests

5.2.1 Introduction

5.2.1.1 Purpose of Tests

As part of the validation effort for the application of the TRACG code to SBWR applications, calculations have been performed to simulate tests being conducted at various facilities around the world. One such facility is the GIRAFFE facility at the Toshiba Corporation in Kawasaki City in Japan. The facility is described in detail in Reference 5.2-1, and a schematic of the plant is shown in Figure 5.2-1. This study pertains to a series of five tests conducted at the GIRAFFE facility to provide data on the containment performance during the long-term PCCS phase of a LOCA.

The purpose of the GIRAFFE Helium test program was to demonstrate the operation of the Passive Containment Cooling System (PCCS) operating in the Post-Accident containment environments in the presence of both lighter-than-steam and heavier-than-steam noncondensable gases. The results demonstrate the SBWR containment thermal-hydraulic performance, heat removal capability and provide additional data for the qualification of the containment response calculations in the presence of the noncondensable gases mentioned above by using the TRACG04 computational code.

The GIRAFFE Helium tests are chiefly focused on the SBWR primary containment vessel (PCV) pressure response and the PCCS cooling capabilities during the part of the post-accident transient which follows the termination of subcooled water injection into the reactor pressure vessel (RPV) from the Gravity Driven Cooling System (GDCS). This period starts at approximately one hour after reactor scram. At this time after the LOCA, the RPV is sufficiently depressurized such that its pressure is essentially equalized to that of the PCV. During this period, the principal means of removing the decay heat from the PCV is via the PCCS.

This section is divided into two main portions. The first provides a detailed description of the GIRAFFE TRACG model; the second presents the results of the analysis for the five tests. A brief description of the four Helium tests (H1-H4) and the Tie Back test (T2) is included in the introduction. A more detailed description, along with a discussion of instrumentation, shakedown, data acquisition, and test control, is found in References 5.2-1 and 5.2-2.

The test objectives of the GIRAFFE Helium Test Program were:

- Demonstrate the operation of a passive containment cooling system in the presence of a lighter-than-steam noncondensable gas, including demonstrating the process of purging noncondensibles from PCC condenser. (*Concept Demonstration*)

[

Redacted

]

- Provide a database for computer codes used to simulate SBWR containment system performance in the presence of a lighter-than-steam noncondensable gas, including potential systems interaction effects. (Integral Systems Tests)

[Redacted]

- Provide a tie-back test, which includes the appropriate Quality Assurance documentation to repeat a previous GIRAFFE test, thereby reinforcing the validity of the previous GIRAFFE testing.

[Redacted]

5.2.1.2 Tests Selected for Post-Test Analysis

The five tests analyzed are:

Test H1

The purpose of this test is to provide a base case with initial conditions for the SBWR containment at one hour from the initiation of a LOCA caused by a rupture of the main steam line. At the start of this test, the drywell contains a mixture of steam and nitrogen. This case demonstrates the operation of the PCCS without the presence of helium.

Test H2

The purpose of this test is to demonstrate the effects of a lighter-than-steam noncondensable gas on the operation of the PCCS. The test is a repeat of H1, but with helium replacing the total volume of nitrogen in the drywell. The results from this test can be compared to H1 results in order to determine the effects of a lighter-than-steam noncondensable gas on the PCCS.

Test H3

The purpose of this test is to demonstrate the effects of a high concentration of a lighter-than-steam noncondensable gas on the operation of the PCCS. This test confirms the efficacy of the PCCS for conditions resulting from a significant amount of metal-water reaction. For this test, an estimated initial bounding concentration of hydrogen is simulated; the initial mass of helium in the drywell is based on assuming that approximately 20% of the hydrogen generated by a 100% SBWR metal-water reaction is initially in the drywell.

Test H4

The purpose of this test is to confirm the assumption that the hydrogen generated by the metal water reaction will not permanently build up in the PCCS condensers. In order to confirm this, helium was continuously injected into the upper drywell for the first hour of the test until a total amount of helium equal to that used for H3 was reached.

Test T2

The purpose of this test is to provide additional data for comparison by demonstrating the PCCS operation with an initial nitrogen concentration in the drywell that is higher than H1.

In summary, Tests H1 and T2 used only nitrogen, Test H2 used only helium, and Tests H3 and H4 used a combination of nitrogen and helium.

[

Redacted

]

The present discussion focuses on the post-test phase of the calculations where TRACG04 was used, actual test conditions were simulated and the calculations compared with test data. The study describes the facility, the TRACG models used in the simulation and, finally, the comparisons of TRACG calculations with the test data.

5.2.1.3 Purpose of Post-Test Analysis

The purpose of conducting the post-test analysis was to provide a basis for comparing TRACG04 calculations with Toshiba test results for the cases described above with the objective of confirming the adequacy of TRACG to predict the SBWR ECCS performance during the late blowdown phase of the LOCA. Sensitivity studies can then be conducted with the intent of explaining differences between the facility results and the TRACG analysis. The remainder of this section deals with a brief comparison of the SBWR modeling with the GIRAFFE nodalization, plus presentation and discussion of the results of the post-test analysis. The applicability of the results to the SBWR is also discussed.

5.2.2 Test Facility/Test Matrix

5.2.2.1 GIRAFFE Test Facility

The GIRAFFE test facility is a 1/400 scale model of the SBWR (1:1 in height and 1:400 in cross-sectional area). Figure 5.2-1 shows a schematic of the facility. The principal components are the RPV, the wetwell pool, the drywell, the GDCS pool, and the PCC pool. Greater detail of the facility can be found in Reference 5.2-1.

5.2.2.1.1 The Reactor Pressure Vessel

The pressure vessel is 20.723m in height and has an inner diameter of 0.34m with an 8 mm thick wall. The bottom of the vessel in GIRAFFE is at 0.808m from the ground level. The vessel contains a heat generating core composed of an 8x8 matrix of heater rods enclosed in a square 2 mm thick stainless steel channel 0.136m per side. The heated length is 2.44m, with an unheated length at the top of 0.467m length. The top of the heater rods (equivalent to the top of active fuel) is at 3.2m elevation from the bottom of the vessel. The bottom part of the channel is connected to an annular region representing the guide tube/bypass. At an elevation 3.667m from the bottom of the vessel, both the channel and the guide tube/bypass merge into the chimney. The chimney extends to an elevation of 11.008m. The GDCS return line is at an elevation of 5.008m, the DPV at an elevation of 16.048m and the main steam line at 17.243m. The RPV and associated piping are shown in Figure 5.2-5.

5.2.2.1.2 Drywell

The drywell in the facility consists of three distinct regions: the upper drywell (UDW), the middle drywell or annular region (MDW), and the lower drywell (LDW). The total height of the drywell is 18.145m with a total volume of 12.2 m³.

The UDW is 3.307m in height, has an inner diameter of 1.779m and a wall thickness of 8 mm. The UDW has several connections with other vessels in the system (Figure 5.2-8). The horizontal vent line and the vacuum breaker line connect the UDW to the wetwell. The PCC steam supply line is connected to the top of the UDW. The lines representing the DPV and the main steam line are connected to the RPV. The UDW is also connected to the GDCS pool to equalize the pressure in the two components.

The MDW is 11.122m in height with an I.D. of 0.512m. For the Helium tests, this part of the drywell system has no connections.

The LDW has a lower most part of 0.508m in height and an I.D. of 2.0m and a narrower top part of 3.2m in height and an I.D. of 0.416m. As with the MDW, there are no connections at this section for the Helium tests.

5.2.2.1.3 The Wetwell

The wetwell (WW) is 11.871m in height with an I.D. of 1.4m. The WW is connected to the drywell through the horizontal vent line and the vacuum breaker line. The PCC gas vent line ends in the wetwell. For the Helium tests, the pool is filled to a height such that the PCC vent line is submerged to a depth of 0.9m. This represents the SBWR submergence at normal water level (0.75m), increased by 0.15m to account for mass addition to the pool during the early blowdown. The wetwell chamber and associated piping are shown in Figure 5.2-6.

5.2.2.1.4 The GDCS Pool

The GDCS has a height of 5.714m and an I.D. of 0.773m. The GDCS has three connections for the helium tests. The condensate return line to the RPV emerges vertically from the pool

bottom. The PCC drain water return line empties into the GDSCS with a U-tube. The equalization line connects with the UDW (Figures 5.2-7 and 5.2-8).

5.2.2.1.5 The Passive Containment Cooling System (PCCS)

The PCCS is a heat exchanger that consists of a steam box at the top and a water box at the bottom with three heat exchanger tubes connecting them (see Figure 5.2-4). The insulated steam box is 0.97m long and the uninsulated water box is 1.1m long. The heat exchanger tubes are 1.8m long with a 51-mm O.D. The steam supply line from the UDW enters the steam box and the vent and drain lines are connected to the water box. The whole assembly is immersed in the PCC pool, which has a total volume of 5.1 m³. The water level for the pool is sufficient to cover the entire heat exchanger assembly. The pool has a steam vent to the atmosphere.

5.2.2.2 Test Matrix

The test matrix is shown in Table 5.2-1. The test initial conditions for Test H1 were derived from a TRACG calculation for SBWR at one hour into the LOCA. The thermodynamic conditions at this point in the transient are fairly well stabilized, and steam production from the RPV resumes following the draining of the GDSCS pools into the RPV. A noncondensable concentration of about 4% by volume is calculated in the drywell by TRACG due to nitrogen return as a result of vacuum breaker openings in the GDSCS period. Test T2 provides an upper bound on the initial nitrogen concentration with a value of 14% by volume. The other three tests include a light gas (helium) to simulate the effects of hydrogen in the containment. All three tests were performed with helium concentrations higher than would be consistent with the assumptions for Design Basis Accidents. Test H2 replaced the volume of nitrogen (4%) in Test H1 with helium to provide a direct comparison with H1. Tests H3 and H4 had much higher concentrations of helium, and test the performance of the PCCS to successfully clear the light gas to the wetwell. Test H3 was initialized with an initial drywell concentration of 20% helium and 4% nitrogen. Test H4 was run with helium injection over one hour to achieve the same amount of mass of helium at the end of the hour as initially present in Test H3.

Table 5.2-4 shows the initial conditions for the tests as well as the measurement accuracies for the various parameters. The gas sample measurements made in the lower drywell, upper drywell and wetwell gas space had an uncertainty of $\pm 3\%$ in the determinations of the percent concentrations of helium, nitrogen and steam.

5.2.3 Applicability of Data to SBWR

This section describes how the GIRAFFE Helium tests provided data relevant for validation of computer code models used to analyze the containment performance of the SBWR. The general applicability of the data to the SBWR, the overall scaling approach and the test objective for the GIRAFFE Helium test facility are discussed in Section 5.2.3.1.

Descriptions of each of the PIRT phenomena that this test was to provide data for are given in Section 5.2.3.2. The applicable PIRT phenomena for this test were listed in the TAPD Report [5.2-6]. An updated version of the original list is given in Table 2.1-5b of this report. An

explanation of how the test covered a particular PIRT phenomenon in terms of physical parameter ranges is given immediately following each PIRT phenomenon description.

5.2.3.1 General Data Applicability and Test Facility Scaling

[

Redacted

]

5.2.3.2 PIRT Phenomena and Coverage

[

Redacted

]

[

Redacted

]

[

Redacted

]

[

Redacted

]

Test	Location	He (vol %)	N ₂ (vol %)
H1	LDW	<0.1 - 0.1	4.4 - 34.7
	UDW	<0.1 - 0.2	<0.1 - 1.4
H2	LDW	1.3 - 10.8	<0.1 - 0.1
	UDW	0.1 - 1.5	<0.1
H3	LDW	18.1 - 47.2	2.4 - 5.9
	UDW	0.2 - 6.6	<0.1 - 0.7
H4	LDW	0.3 - 12.3	8.3 - 26.5
	UDW	0.1 - 2.6	<0.1 - 1.1
T2	LDW	<0.1	14.4 - 49.6
	UDW	<0.1	0.1 - 3.1

[

Redacted

]

[

Redacted

]

Test	He (vol %)	N ₂ (vol %)
H1	<0.1	85.7 - 87.5
H2	1.4 - 2.8	83.2 - 84.8
H3	3.0 - 12.8	74.9 - 82.1
H4	0.3 - 15.1	72.5 - 85.0
T2	<0.1	84.1 - 85.6

[

Redacted

]

5.2.3.3 Conclusions on Data Applicability

[

Redacted

]

5.2.4 TRACG Model

5.2.4.1 Nodalization of Test Facility

[

Redacted

]

Redacted

5.2.4.2 3-D Vessel Component

Redacted

5.2.4.3 RPV and Associated Piping

Redacted

5.2.4.4 PCC

Redacted

[

Redacted

]

5.2.4.5 Main Vent and Vacuum Breaker

[

Redacted

]

5.2.4.6 Comparison to the SBWR Model

[

Redacted

]

[

Redacted

]

5.2.5 Test Simulation

5.2.5.1 Introduction

[

Redacted

]

5.2.5.2 Component Heat Loss and Decay Heat

[

Redacted

]

5.2.5.3 Initial Conditions

[

Redacted

]

[

Redacted

]

5.2.6 Results and Discussion

5.2.6.1 Test Results

[

Redacted

]

5.2.6.2 General Discussion

[

Redacted

]

[

Redacted

]

5.2.6.3 Test H1

5.2.6.3.1 H1 Test Results

[

Redacted

]

[

Redacted

]

5.2.6.3.2 Comparison with Analysis

[

Redacted

]

[

Redacted

]

5.2.6.3.3 Sensitivity to Increased PCC Heat Removal

[

Redacted

]

5.2.6.4 Test H2

5.2.6.4.1 H2 Test Results

[

Redacted

]

[

Redacted

]

5.2.6.4.2 Comparison with Analysis

[

Redacted

]

5.2.6.4.3 TRACG Calculations with Modified Analysis Procedure

[

Redacted

]

5.2.6.4.4 Sensitivity to Confinement of Helium to the Top of Drywell

[

Redacted

]

5.2.6.4.5 Sensitivity to Multi-Cell Modeling of the PCC Headers

[

Redacted

]

[

Redacted

]

5.2.6.5 Test H3

5.2.6.5.1 Test Results

[

Redacted

]

[

Redacted

]

5.2.6.5.2 Comparison with Analysis

[

Redacted

]

5.2.6.6 Test H4

5.2.6.6.1 Test Results

[

Redacted

]

[

Redacted

]

5.2.6.6.2 Comparison with Analysis

[

Redacted

]

5.2.6.7 Test T2

5.2.6.7.1 Test Results

[

Redacted

]

5.2.6.7.2 Comparison with Analysis

[

Redacted

]

[
Redacted
]

5.2.6.7.3 Sensitivity Study on PCC Heat Removal

[
Redacted
]

5.2.6.8 Accuracy of TRACG Calculations

[

Redacted

]

5.2.7 Conclusions

5.2.7.1 General Conclusions

[

Redacted

]

[

Redacted

]

[Redacted]

5.2.7.2 PIRT Conclusions

[

Redacted

]

5.2.8 References

- [5.2-1] M. Herzog, *GIRAFFE SBWR Helium Series Test Report*, NEDC-32608P Rev. 0, Class 3, June 1996.
- [5.2-2] *GIRAFFE Helium Test Specification*, GENE 25A5677, Rev. 1, May 10, 1995,
- [5.2-3] *Shakedown Test Series*, Toshiba TOGE 110-T18, May 1995,
- [5.2-4] *Report on Result of Measurement Analysis*, KKS 0706-0 3140, June 1995. (Filed in DRF No. T15-00013)
- [5.2-5] R.E. Gamble et al., *Scaling of the SBWR Related Tests*, NEDC-32288P, Rev. 1, October 1995.
- [5.2-6] *SBWR Test and Analysis Program Description*, NEDC-32391P, Rev. C, August 1995.
- [5.2-7] A.J. Illich, *Blind Analysis for GIRAFFE Helium Tests H1 - H4*, Attachment to MFN 159-95, August 1995.

- [5.2-8] *SBWR Testing Summary Report*, NEDC-32606P, Rev. 0, August 2002.
- [5.2-9] J. G. M. Andersen, et al., *TRACG Model Description*, NEDE-32176P, Rev. 2, December 1999.

Table 5.2-1
Test Matrix of Initial DW Conditions for GIRAFFE Helium Tests

GIRAFFE Test No	Helium Injection Rate (kg/sec)	Nitrogen Partial Press (kPa)	Steam Partial Press (kPa)	Helium Partial Press (kPa)
H1	0	13	281	0
H2	0	0	281	13
H3	0	13	214	67
H4	0.00027	13	281	0
T2	0	38	228	0

Table 5.2-2
Definition of TRACG Input Model Components

[

Redacted

]

Table 5.2-3
Comparison of GIRAFFE Helium and SBWR TRACG Containment Nodalization

[

Redacted

]

Table 5.2-4
Initial Conditions for GIRAFFE Helium Tests H1-H4

Parameter	Value	Tolerance	Measurement Accuracy
RPV Pressure (kPa)	295	6	± 2.6 kPa
Initial Heater Power (kW)	66 + heat loss compensation	1	± 1 kW
RPV Water Level (m)*	12.0	0.15	± 0.06 m
Drywell Pressure (kPa)	294	4	± 2.6 kPa
Wetwell Pressure (kPa)	285	4	± 2.6 kPa
Wetwell Nitrogen Pressure (kPa)	240	4	± 2 kPa*
GDCS Gas Space Pressure (kPa)	294	4	± 2.6 kPa
GDCS Nitrogen Pressure (kPa)	274	4	± 2 kPa*
Wetwell Temperature (K)	352	2	± 1 K
PCC Pool Temperature (K)	373	2	± 1 K
GDCS Pool Temperature (K)	333	2	± 1 K
GDCS Pool Level (m)	In equilibrium with RPV level		± 0.03 m
Wetwell Level ¹ (m)	3.25	0.075	± 0.005 m
PCC Pool Collapsed Water Level * (m)	23.2	0.075	± 0.04 m
PCC Vent Line Submergence	0.95	0.075	± 0.005 m

* Based on saturated vapor pressure

Table 5.2-5
Initial Conditions for GIRAFFE Test T2²

Parameter	Value	Tolerance
RPV Pressure (kPa)	267	6
Drywell Pressure (kPa)	266	4
Wetwell Pressure (kPa)	257	4
Wetwell Nitrogen Pressure (kPa)	212	4
GDCS Gas Space Pressure (kPa)	266	4
GDCS Nitrogen Pressure (kPa)	246	4

Notes for Tables 5.2-4 and 5.2-5:

¹ Referenced to the Top of Active Fuel (TAF)

² Conditions same as in Table 5.2-4 unless noted.

Table 5.2-6
Assessment of TRACG Accuracy for GIRAFFE Helium Tests

[

Redacted

]

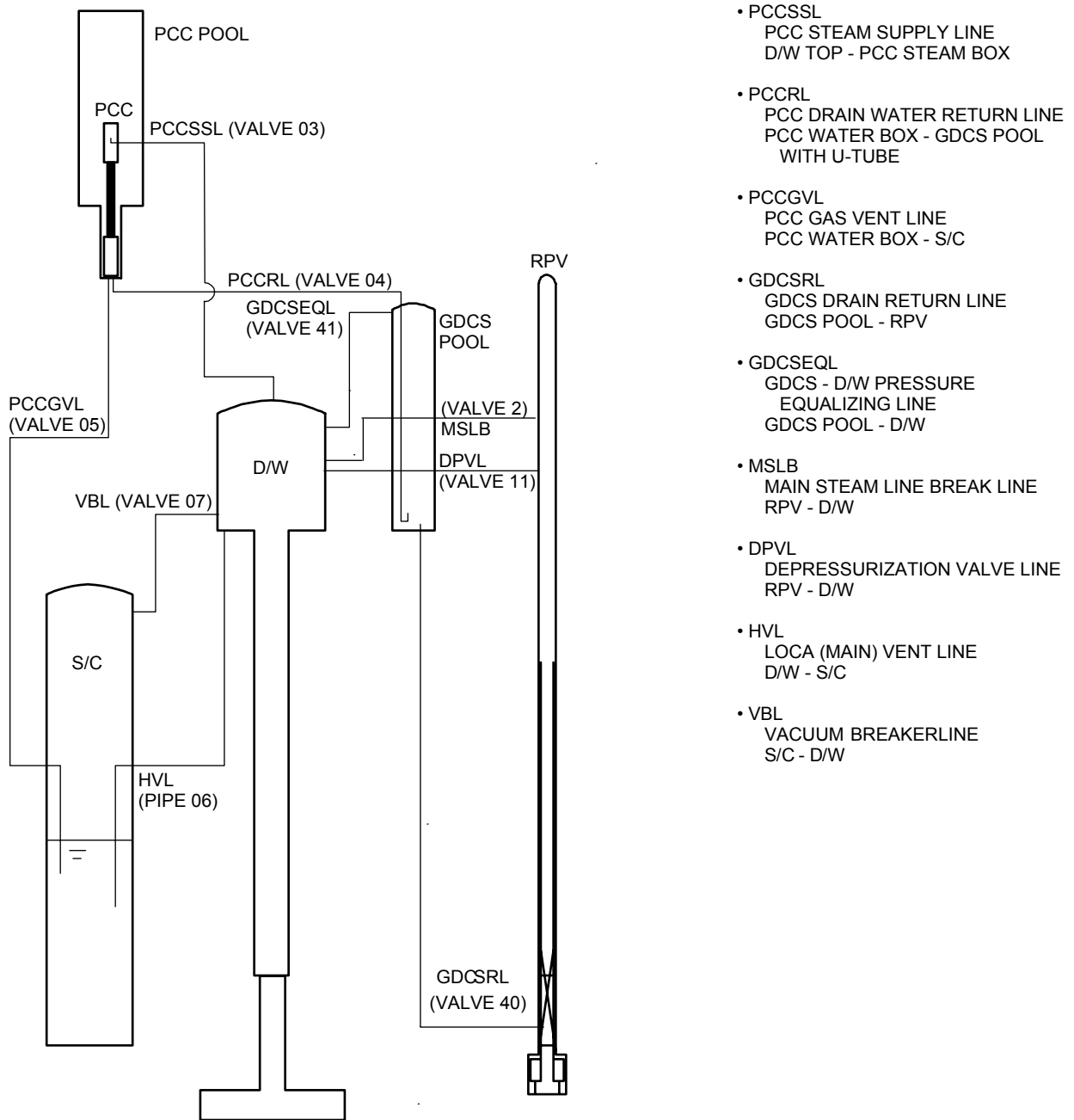


Figure 5.2-1 GIRAFFE Facility Layout

Figures 5.2-2 through 5.2-44

Pages 5.2-35 through 5.2-59

Redacted

5.3 GIRAFFE Systems Interactions Tests

5.3.1 Introduction

As part of the validation effort for application of the TRACG code to SBWR, calculations have been performed to simulate tests conducted at various facilities around the world. One such test facility is the GIRAFFE facility [5.3-1] at Toshiba Corporation in Kawasaki, Japan. This study pertains to a series of four tests conducted at the GIRAFFE facility, to provide a database on the performance of the SBWR ECCS during the Late Blowdown/ GDCS Transition/Reflood phases of a LOCA, with specific focus on potential systems interaction effects.

The four tests had initial conditions representing those at approximately 10 minutes after the initiation of a postulated LOCA. The tests lasted approximately two hours. The containment and vessel initial conditions were based on the corresponding SBWR TRACG LOCA case at the time the RPV pressure is 1.034 MPa. The basis for the tests is described in the TAPD [5.3-2, Table A.3-23]. A brief description of each test is given below:

- Test GS1, the base case, is a GDCS line break with one DPV failure and no PCC or IC operation. This set of test conditions resulted in the lowest predicted chimney water level.
- Test GS2 is the same as Test GS1 except that the PCC and IC are operational during the test. Test results can be compared with Test GS1 for potential systems interactions associated with the IC and PCC.
- Test GS3 is a bottom drain line break with a single DPV failure. The IC and PCC were operational. This test represents the case with the fastest water level recovery.
- Test GS4 is a GDCS break with a GDCS valve failure in one of the other two GDCS lines. The IC and PCC were operational. This test produced the slowest rate of recovery of the chimney water level.

[

Redacted

]

The results presented here focus on the post-test phase (the second phase) of the calculations where actual test conditions are simulated and the calculations compared with test data. The objective of the study is to confirm the adequacy of TRACG to predict the SBWR ECCS performance during the Late Blowdown/ GDCS Transition/ Reflood phases of the LOCA. The study describes the facility, the TRACG models used in the simulation and, finally, the comparisons of TRACG predictions with the test data. The applicability of the data to the SBWR is also discussed.

5.3.2 Test Facility

The GIRAFFE test facility is operated by Toshiba Corporation in Kawasaki, Japan and is a 1/400 scale model of the SBWR (1:1 in height and 1:400 in cross-sectional area). Figure 5.3-1 shows a schematic of the facility. The principal components are the RPV, the wetwell, the drywell, the GDCS pool, and two pools, one containing the isolation condenser and the other containing the Passive Containment Cooling System (PCCS). The valve and pipe numbers indicated in Figure 5.3-1 refer to components representing these features in the TRACG model. A more detailed description of the facility can be obtained from Reference 5.3-1.

5.3.2.1 The Reactor Pressure Vessel (RPV)

The pressure vessel is 20.72m in height and has an inner diameter of 0.34m with a 8 mm thick wall. The bottom of the vessel in GIRAFFE is 0.808m from the ground level and all elevations shown (Figure 5.3-2) are from the ground level. The vessel contains a heat generating core composed of an 8x8 matrix of heater rods enclosed in a square 2 mm thick stainless steel channel of side 0.136 m (internal dimension). The heated length is 2.44m, with an unheated length at the top of 0.467m length. The top of the heater rods (equivalent to the top of active fuel) is at 3.2m elevation from the bottom of the vessel. The internals of the RPV are shown in Figure 5.3-2. The unrodded part of the channel at the bottom is 0.76m in length and is connected to an annular region representing the guide tube/bypass (GTBP), by two small leak holes (Figure 5.3-2). At an elevation of 4.475m (3.667m from the vessel bottom), both the channel and the GTBP merge into the chimney. The chimney extends to an elevation of 11.008m (10.2m from the vessel bottom) and has a 2 mm thick wall. The channel and GTBP assembly sits on a ring with six holes on its circumference through which water from the downcomer enters the channel. The GDCS return line is at an elevation of 5.008m (4.2m from the vessel bottom). The line representing the SRVs and DPVs is at an elevation of 16.048m and the main steamline is at 17.243m.

5.3.2.2 Drywell

The drywell in the facility consists of three distinct regions: the upper drywell (UDW), the middle drywell or annular region (MDW), and the lower drywell (LDW). The total height of the drywell is 18.145m and the total volume is 12.2 m³.

The UDW is 3.307m in height, has an inner diameter of 1.779m and a wall thickness of 8 mm. The UDW has several connections with other vessels in the system (Figure 5.3-1). The horizontal vent line and the vacuum breaker line connect the UDW to the wetwell (WW), the former connecting to the suppression pool and the latter connecting to the WW airspace. The PCC steam supply line is connected to the top of the UDW. The line representing the SRV/DPV system is connected to the RPV, as is the main steam break line. The UDW is also connected to the top of the GDCS pool to equalize the pressures in the two components.

The MDW is 11.122m in length with an I.D. of 0.512m. This part of the drywell system contains lines representing both parts of a GDCS Line Break (GDLB) - one from the RPV and one from the GDCS pool.

The LDW has a lower part 0.508m in height with an I.D. of 2.0m and a narrower top part of I.D. 0.416m and a length of 3.2m. The break line representing a bottom drain line break is connected from the bottom of the RPV to the LDW. There is an orifice plate at the interface of the bottom of the MDW and the top of the LDW. This orifice is sized to represent the vertical vent pipes in the SBWR that connect the UDW to the LDW.

5.3.2.3 Wetwell

The WW or suppression chamber (S/C in Figure 5.3-1) is 11.871m in height with an I.D. of 1.4m. The WW is connected to the drywell through the horizontal vent line and the vacuum breaker line. The PCC gas vent line ends in the suppression pool. For the GIRAFFE/SIT, the suppression pool has water to an initial level of 3.15m above the top of active fuel. This translates to the horizontal vent line having a submergence of 1.6m and the PCC vent line a submergence of 0.85m.

5.3.2.4 GDSC Pool

The GDSC pool in the facility has a height of 5.714m and an I.D. of 0.773m. The GDSC line to the RPV and the line representing the GDSC break into the MDW emerge vertically down from the pool bottom and branch out at an elevation of about 0.5m from the pool bottom. The PCC drain line empties out into the GDSC pool. The pool had an initial water level of 16.3m above TAF for all the four tests.

5.3.2.5 Passive Containment Cooling System (PCCS)

The PCCS consists of steam box at the top and a water box at the bottom with three heat exchanger tubes connecting them. The steam box is 0.97m long and the water box is 1.1m long. The heat exchange tubes are 1.8m long with a total outside heat transfer area of 0.8618 m^2 . The steam supply line from the UDW enters the steam box and the vent and drain lines are connected to the water box. A tube sleeve encloses this system except for the bottom 0.55m of the water box. The whole assembly is immersed in the PCC pool, which has total volume of 5.1 m^3 . The water level in the pool for all tests was set at 1.242m from the top of the pool. The pool has a steam vent to the atmosphere.

5.3.2.6 Isolation Condenser System (ICS)

The ICS is very similar to the PCCS except that the heat exchanger tubes are 2.4m long. In this series of tests only one of the three tubes was used, thus presenting a total outside heat transfer area of 0.3830 m^2 . The steam supply line from the RPV enters the steam box at the top and the drain line returns the condensate to the RPV. There is no line corresponding to the PCC vent line in the IC. The IC pool level was the same as the PCC pool level.

5.3.3 Applicability of Data to SBWR

[

Redacted

]

[

Redacted

]

5.3.3.1 General Data Applicability and Test Facility Scaling

[

Redacted

]

Component Volumes (m³)	GIRAFFE	SBWR	Ratio
RPV bottom to TAF	0.375	137.2	366
RPV bottom to Top of Chimney	0.994	396.9	399
Total RPV	1.94	615.0	317
DW	12.2	5503	451
WW Air Space	9.9	3819	386
WW Water	8.4	3253	387
GDCS Water	2.4	1056	440

Component Height (m)	GIRAFFE	SBWR	Ratio
Core: BAF-TAF	2.44	2.74	1.12
Core: BAF- Top of Fuel	2.91	3.19	1.09
Chimney	6.53	6.56	1.00
Horiz. Vent Submergence	1.6	1.6	1.00

[

Redacted

]

[

Redacted

]

5.3.3.2 PIRT Phenomena and Coverage

[

Redacted

]

[

Redacted

]

[

Redacted

]

[

Redacted

]

[

Redacted

]

[

Redacted

]

5.3.3.3 Conclusions on Data Applicability

[

Redacted

]

5.3.4 TRACG Model

[

Redacted

]

[Redacted]

5.3.4.1 3-D Vessel Component

5.3.4.2 RPV Internals

5.3.4.3 RPV Piping

[Redacted]

5.3.4.4 Drywell Piping

5.3.4.5 Wetwell Piping

5.3.4.6 GDCS Piping

5.3.4.7 IC and PCC systems

[

Redacted

]

5.3.4.8 Comparison with SBWR Nodalization

[

Redacted

]

5.3.5 Test Simulation

5.3.5.1 Introduction

[

Redacted

]

5.3.5.2 Heat Losses in the System

[

Redacted

]

[

Redacted

]

5.3.5.3 Decay Heat

[

Redacted

]

5.3.5.4 Initial Conditions

[

Redacted

]

5.3.6 Test and TRACG Simulation Results

5.3.6.1 Introduction

[

Redacted

]

[

Redacted

]

Measured Quantity	Uncertainty
RPV Pressure (kPa)	± 6.4
DW Pressure (kPa)	± 2.6
WW Pressure (kPa)	± 2.6
Chimney Level (m)	± 0.04
DC Level (m)	± 0.03
GDCS Flow (l/m)	± 0.49
RPV Break Flow (l/m)	± 0.16

5.3.6.2 Test GS1

5.3.6.2.1 Test Phenomena

[

Redacted

]

[

Redacted

]

5.3.6.2.2 Comparison of TRACG Predictions with the Test

[

Redacted

]

[

Redacted

]

5.3.6.3 Test GS2

5.3.6.3.1 Test Phenomena

[

Redacted

]

[

Redacted

]

5.3.6.4.2 Comparisons of TRACG Predictions with the Test

[

Redacted

]

5.3.6.5 Test GS4

5.3.6.5.1 Test Phenomena

[

Redacted

]

[

Redacted

]

5.3.6.5.2 Comparison of TRACG Predictions with the Test

[

Redacted

]

5.3.6.6 Sensitivity Studies

[

Redacted

]

[

Redacted

]

5.3.7 Summary and Conclusions

5.3.7.1 General Conclusions

[

Redacted

]

5.3.7.2 Conclusions Related to Key PIRT Phenomena

[

Redacted

]

[

Redacted

]

5.3.7.3 Final Observations

[

Redacted

]

[

Redacted

]

5.3.8 References

- [5.3-1] J.D. Duncan, *GIRAFFE-SBWR Systems Interactions Test Report*, NEDC-32540P, June 1996.
- [5.3-2] *SBWR Test and Analysis Program Description*, NEDC-32391P, Revision C, Class 3, August 1995.
- [5.3-3] S. Sitaraman, *Pre-Test Analysis of the GIRAFFE System Interaction Tests: GSI-GS4*, Attachment to MFN 193-95, September 29, 1995.
- [5.3-4] R.E.Gamble et al., *Scaling of the SBWR Related Tests*, NEDC-32288P, Revision 1, Class 3, October 1995.
- [5.3-5] Shakedown Test Series, Toshiba, TOGE110-T18, May 1995.
- [5.3-6] P.F.Billig et al., *SBWR Testing Summary Report*, NEDC-32606P, Rev. 0, August 2002.

Table 5.3-1
List of 1-D Components

[

Redacted

]

Table 5.3-1
List of 1-D Components (cont'd)

[

Redacted

]

Table 5.3-2
TRACG GIRAFFE Nodalization vs. SBWR Nodalization

[

Redacted

]

Table 5.3-3
Initial Conditions for Test GS1
GDC Line Break, DPV Failure, IC/PCC off

Parameter	Value	Tolerance
RPV Pressure (kPa)	1026	±12 kPa
RPV Initial Water Level*(m)	-0.31	±5%
Initial Heater Power (kW)	134	±1 kW
Drywell Pressure (kPa)	271	±4 kPa
Drywell Air Pressure (kPa)	45	±4 kPa
Drywell Steam Pressure (kPa)	226	±4 kPa
Drywell Initial Water Level (m)	0.05	+20%-0%
Wetwell Pressure (kPa)	255	±4 kPa
Wetwell Air Pressure (kPa)	234	±4 kPa
GDCS Gas Space Pressure (kPa)	271	±4 kPa
GDCS Gas Space Air Pressure (kPa)	259	±4 kPa
Suppression Pool Temperature (K)	334	±2 K
Isolation Condenser Pool Temperature (K)	NA	NA
Isolation Condenser Pool Level* (m)	NA	NA
PCCS Pool Temperature (K)	NA	NA
GDCS Pool Temperature (K)	322	±2 K
GDCS Pool Level* (m)	16.3	±0.075 m
Suppression Pool Level* (m)	3.15	±0.075 m
PCC Pool Level* (m)	NA	NA

*Referenced to TAF

Table 5.3-4
Initial Conditions for GS2
GDC Line Break, DPV Failure, IC/PCC on

Parameter	Value	Tolerance
RPV Pressure (kPa)	1028	±12 kPa
RPV Initial Water Level* (m)	+ 0.04	±5%
Initial Heater Power (kW)	134	±1 kW
Drywell Pressure (kPa)	279	±4 kPa
Drywell Air Pressure (kPa)	37	±4 kPa
Drywell Steam Pressure (kPa)	242	±4 kPa
Drywell Initial Water Level (m)	0.05	+20%-0%
Wetwell Pressure (kPa)	263	±4 kPa
Wetwell Air Pressure (kPa)	245	±4 kPa
GDCS Gas Space Pressure (kPa)	279	±4 kPa
GDCS Gas Space Air Pressure (kPa)	267	±4 kPa
Suppression Pool Temperature (K)	331	±2 K
Isolation Condenser Pool Temperature (K)	373	±2 K
Isolation Condenser Pool Level* (m)	23.2	±0.075m
PCCS Pool Temperature (K)	373	±2 K
GDCS Pool Temperature (K)	322	±2 K
GDCS Pool Level* (m)	16.3	±0.075m
Suppression Pool Level* (m)	3.15	±0.075m
PCC Pool Level* (m)	23.2	±0.075m

*Referenced to TAF

Table 5.3-5
Initial Conditions for GS3
BDL Break, DPV Failure, IC/PCC on

Parameter	Value	Tolerance
RPV Pressure (kPa)	1027	±12 kPa
RPV Initial Water Level* (m)	+1.53	±5%
Initial Heater Power (kW)	113	±1 kW
Drywell Pressure (kPa)	310	±4 kPa
Drywell Air Pressure (kPa)	8	±4 kPa
Drywell Steam Pressure (kPa)	302	±4 kPa
Drywell Initial Water Level (m)	0.05	+20%--0%
Wetwell Pressure (kPa)	294	±4 kPa
Wetwell Air Pressure (kPa)	278	±4 kPa
GDCS Gas Space Pressure (kPa)	310	±4 kPa
GDCS Gas Space Air Pressure (kPa)	298	±4 kPa
Suppression Pool Temperature (K)	328	±2 K
Isolation Condenser Pool Temperature (K)	373	±2 K
Isolation Condenser Pool Level* (m)	23.2	±0.075m
PCCS Pool Temperature (K)	373	±2 K
GDCS Pool Temperature (K)	323	±2 K
GDCS Pool Level* (m)	16.3	±0.075m
Suppression Pool Level* (m)	3.15	±0.075m
PCC Pool Level* (m)	23.2	±0.075m

*Referenced to TAF

Table 5.3-6
Initial Conditions for GS4
GDC Line Break, GDC Valve Failure, IC/PCC on

Parameter	Value	Tolerance
RPV Pressure (kPa)	1037	±12 kPa
RPV Initial Water Level* (m)	-0.18	±5%
Initial Heater Power (kW)	134	±1 kW
Drywell Pressure (kPa)	274	±4 kPa
Drywell Air Pressure (kPa)	40	±4 kPa
Drywell Steam Pressure (kPa)	234	±4 kPa
Drywell Initial Water Level (m)	0.05	+20%-0%
Wetwell Pressure (kPa)	258	±4 kPa
Wetwell Air Pressure (kPa)	240	±4 kPa
GDCS Gas Space Pressure (kPa)	274	±4 kPa
GDCS Gas Space Air Pressure (kPa)	260	±4 kPa
Suppression Pool Temperature (K)	331	±2 K
Isolation Condenser Pool Temperature (K)	373	±2 K
Isolation Condenser Pool Level* (m)	23.2	±0.075m
PCCS Pool Temperature (K)	373	±2 K
GDCS Pool Temperature (K)	326	±2 K
GDCS Pool Level* (m)	16.3	±0.075m
Suppression Pool Level* (m)	3.15	±0.075m
PCC Pool Level* (m)	23.2	±0.075m

*Referenced to TAF

Table 5.3-7
Ratio of the Calculated Elevation Pressure Drop to the Total Pressure Drop
Results from Test GS1

[

Redacted

]

Table 5.3-8
Summary of Test and TRACG Comparisons

[

Redacted

]

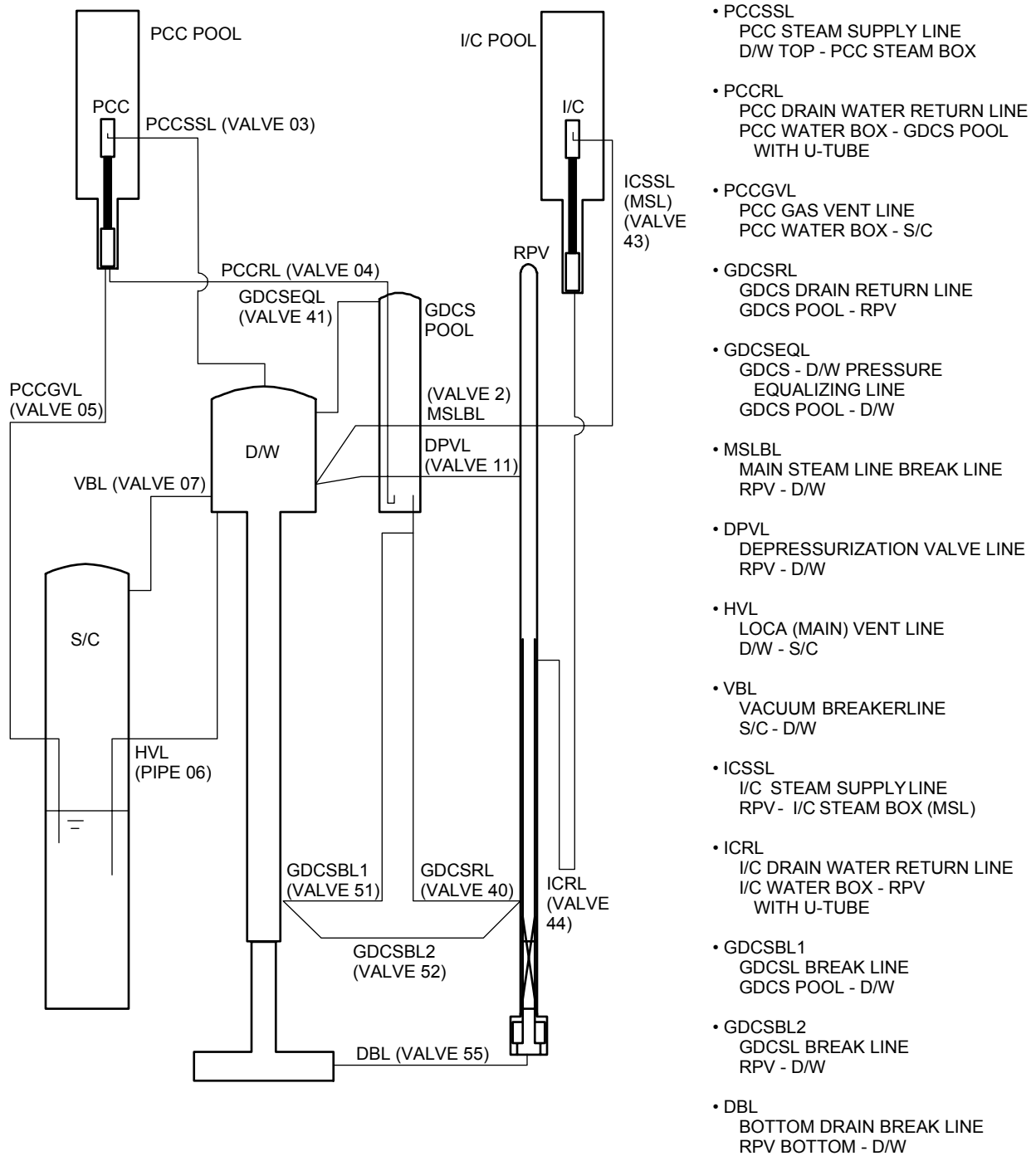


Figure 5.3-1 GIRAFFE Facility Layout

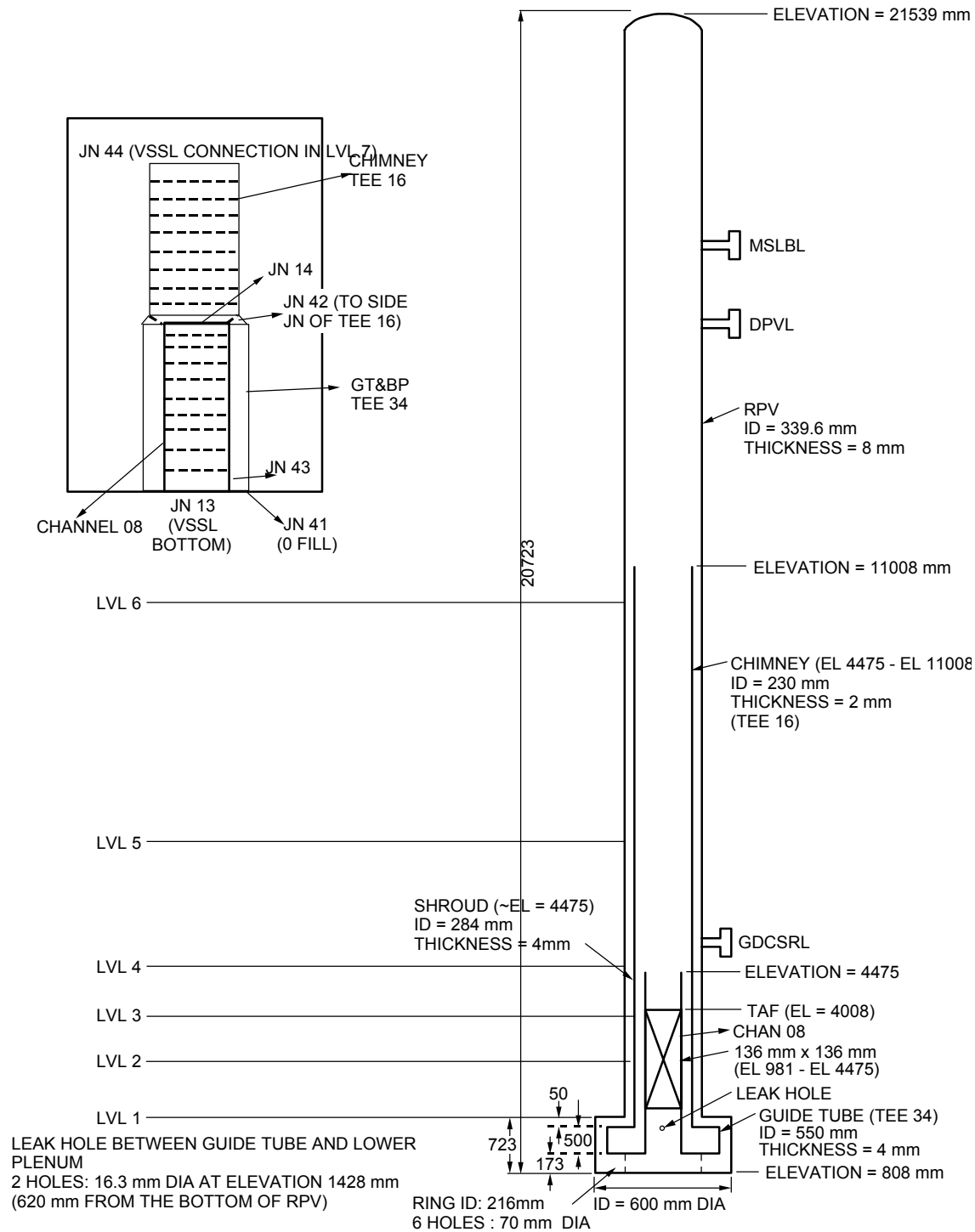


Figure 5.3-2 RPV Internals

Figures 5.3-3 through 5.3-118

Pages 53-36 through 5.3-99

Redacted

5.4 One-Sixth Scale Boron Mixing Tests

5.4.1 Introduction

The SBWR is equipped with a Standby Liquid Control System (SLCS) designed with the capability of shutting down the reactor from rated power to cold condition in a situation where the control rods cannot be inserted. This extremely unlikely event, referred to as the Anticipated Transient Without Scram (ATWS), can be controlled using a solution of sodium pentaborate salt injected through the SLCS. A key aspect of the success of this system is the ability of the boron solution to mix with coolant and carry it into the core and maintain it there to shut down the reactor.

In order to study this mixing phenomenon, a series of tests [5.4-1] was carried out in a facility that was a mockup of a BWR-5 to one-sixth scale in length (1/216 in volume). One test in this series, identified in Reference 5.4-1 as Test 342, was chosen as being representative of the conditions in a SBWR. This test had no forced circulation of the coolant in the system and the SLCS injection was in the upper plenum, conditions close to those in the SBWR. The objective of the study was to predict the transport of the salt solution through the bypass, core and lower plenum regions. However, the absence of a stratification model in TRACG necessitated the development of bounding models for the boron mixing phenomenon observed in the test rather than an actual simulation of all the test conditions. This section describes the test and the TRACG models developed based on the test. Finally, comparisons are made between the calculational results and the test data. All calculations were performed using TRACG04.

5.4.2 Test Facility

The test facility was located at the Vallecitos Nuclear Center of the General Electric Company in Pleasanton, California. A schematic of the reactor vessel is shown in Figure 5.4-1.

The lower plenum contained the control rod guide tubes, control rod drive housings and stub tubes, standby liquid control standpipe and core plate ΔP line. The control rods were not modeled.

The region inside the shroud consisted of the active fuel channels and bypass regions. The individual fuel rods were not explicitly represented in the test facility, but the flow resistance of the fuel channel as a whole was simulated by scaling the cross-sectional area of the open flow path. The ratio of the free flow area in the fuel bundles to the flow area in the leakage region was maintained between the prototype and the test facility within $\pm 10\%$. The flow entrance and exit regions from the fuel channels and bypass were modeled. The exit from bypass to upper plenum could be altered to simulate the different geometries of the BWR/5 and BWR/6 product lines. The flow connection between the core (active and bypass regions) and the lower plenum and the flow connection between the bypass and the inside of the control rod guide tubes were both present in the facility.

The core exit plenum contained the top guide, entrance to the separators and the separators. The separators were nonfunctional. A BWR/6 High Pressure Core Spray (HPCS) sparger and upper plenum were also modeled in the facility. The downcomer region contained jet pumps,

risers, suction and discharge ports. The test model provided for boron injection at one of three locations: HPCS sparger, Jet Pump Injection (JPI) lines in 16 of 20 jet pumps or SLCS injection line in the lower plenum.

The test facility was designed to include the following operating characteristics. The fluid in the simulation model was ambient temperature water at atmospheric pressure. Provisions were made to simulate reactor coolant flow either by forced circulation or by natural circulation. The void conditions inside the channels were simulated by air injection directly into the channels. Density differences between the reactor coolant inventory and the injected liquid were simulated by controlling the concentration of the injected solution. In the tests the injected solution had a temperature of approximately 350 K, while the reactor coolant inventory was at 296 K. The actual salt used in the tests was sodium thiosulfate to simulate the sodium pentaborate used in BWRs. The entire model was constructed using transparent material to allow for visual and photographic observation.

The main objective of the tests was to study the mixing process whereby the liquid borate solution is transported to and maintained in the core. The concentrations of the salt at various spatial locations in the system were either directly measured by obtaining the specific gravity of the solution or indirectly derived from temperature measurements. Since specific gravity measurements were not possible everywhere in the system, some results were obtained using the temperature measurements alone. Temperature sensors were provided at all locations where concentration measurements were required, both inside the shroud and in the downcomer. More complete details of instrumentation and test setup procedures can be found in Reference 5.4-1.

5.4.3 Applicability to SBWR

[

]

[

]

[

]

5.4.4 TRACG Model

5.4.4.1 Model Description

[

]

[

]

5.4.4.2 Test Initial Conditions

[

]

[

5.4.5 Test Simulation

[

]

]

[

]

5.4.5.1 Model 1

[

]

5.4.5.2 Model 2

[

]

5.4.6 TRACG Results

5.4.6.1 Model 1

[

]

[

]

5.4.6.2 Model 2

[

]

5.4.7 Conclusions

5.4.7.1 General Conclusions

[

]

5.4.7.2 Conclusions Related to Key PIRT Phenomena

[

]

[

]

5.4.8 References

- [5.4-1] J.M. Dotson, and B.H. Dillmann, *Test Report Three Dimensional Boron Mixing Model, Volumes I, II, and III*, NEDE-22267, Class III, GE Nuclear Energy, October 1982.
- [5.4-2] E.C. Eckert, *Summary of BWR Boron Remixing*, GE-NE-A00-05652-03, Class III, GE Nuclear Energy, February 1996.
- [5.4-3] F. Rahnema, *PANACEA, BWR Core Simulator*, NEDE-20884, Class III, August 1990.

Table 5.4-1
Dimensions and Grouping of the Channels

[

]

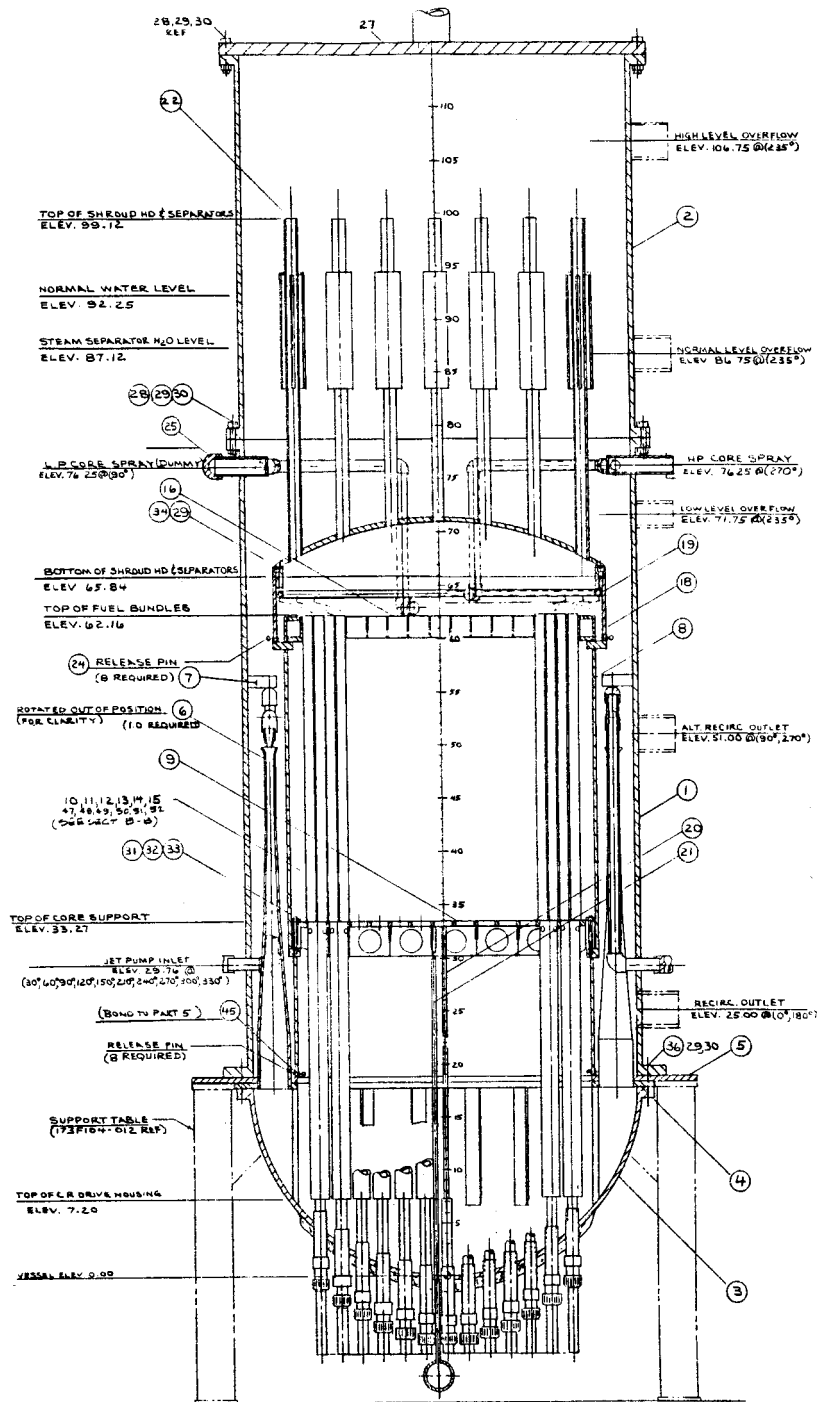


Figure 5.4-1 Schematic of the One-Sixth Scale BWR-5 Facility

Figures 5.4-2 through 5.4-19
Pages 5.4-12 through 5.4-21

Redacted

5.5 PSTF Mark III Containment Response

5.5.1 Introduction

General Electric carried out a multiphase Mark III Confirmatory Test Program in support of the Mark III pressure suppression containment concept using the horizontal vent system design. As a part of this confirmatory test program, three series of large-scale Demonstration Tests were conducted in the Pressure Suppression Test Facility (PSTF). This test facility is described in more detail in Reference 5.5-1. In these tests, emphasis was placed on investigation of vent clearing phenomena associated with the horizontal vent system during a pipe break accident. These three series of tests were designated the Test Series 5701 through 5703 and they were run in November 1973 through March 1974. Test Series 5701 represents single vent tests, Test Series 5702 represents two vent tests, and Test Series 5703 represents three vent tests.

Test Series 5703, which included a total of three tests, was selected to assess and demonstrate the adequacy of TRACG to simulate and calculate containment pressure response and the vent-clearing process for the horizontal vent pressure suppression system. The SBWR prototypical design uses the horizontal vent pressure suppression system with three rows of horizontal vents, similar to that tested in this test series.

5.5.2 Test Facility/Test Matrix

Figure 5.5-1 shows the PSTF test configuration as it was set up for Test Series 5703 [5.5-1]. An electrically heated pressure vessel simulated the reactor pressure vessel (RPV). The RPV was connected to another pressure vessel, which simulated the drywell (DW), by a blowdown line which included a critical flow venturi, rupture disc assembly, and a gate valve. The rupture disk in the blowdown pipe simulated the breaking of a main steamline, and the venturi upstream of the rupture disk set the size of the simulated break. The DW vessel was connected via a discharge duct to a set of three full-scale Mark III horizontal vents which discharged into a simulated 8-degree sector of a Mark III suppression pool. The wetwell (WW) air space was open to the atmosphere, and this was done to simulate the large enclosed WW air space of the Mark III containment configuration. During a pipe break accident, the DW starts pressurizing by the break blowdown flow and the liquid initially contained in the vents is expelled out into the suppression pool, ultimately opening a vapor flow path from the DW into the suppression pool.

The key measurements from Test Series 5703 which are compared to TRACG analysis results are the vent-clearing times and the drywell pressure. The vent-clearing times were measured within the time required for one scan of all data channels which was approximately 0.02 second for these tests. The drywell pressure measurement accuracy was less than 2% of the measured pressure. The 5703 test series simulated combinations of two break sizes of 63.5 mm and 92.0 mm and three top vent submergence values of 2.06m, 3.33m, and 3.37m. In all these three tests, the drywell was preheated to an average temperature in excess of 93°C before each run to minimize wall steam condensation effects during the transient. The key test initial conditions for this test series are shown in Table 5.5-1.

5.5.3 Applicability of Data to SBWR

5.5.3.1 General Data Applicability and Test Facility Scaling

[

Redacted

]

5.5.3.2 PIRT Phenomena and Coverage

[

Redacted

]

[

Redacted

]

5.5.3.3 Scaling Parameters Range

[

Redacted

]

5.5.4 TRACG Model and Nodalization

[

Redacted

]

5.5.5 Test Simulation

[

Redacted

]

5.5.6 Results of Post-Test Calculations

[

Redacted

]

[

Redacted

]

5.5.6.1 Results for Test 5703-01

[

Redacted

]

5.5.6.2 Results for Test 5703-02

[

Redacted

]

5.5.6.3 Results for Test 5703-03

[

Redacted

]

5.5.6.4 Accuracy of TRACG Calculations

[

Redacted

]

5.5.7 Summary and Conclusions

The TRACG calculation results and their comparison with the measured data show that TRACG adequately simulates and calculates the vent-clearing process of the horizontal vent system. [

Redacted

]

The results of the comparison of TRACG calculations and PSTF data discussed above demonstrate the adequacy of TRACG for calculating containment short-term response during and immediately following vent clearing with a horizontal vent system, similar to that used in the SBWR design. [

Redacted

]

5.5.8 References

- [5.5-1] *Mark III Confirmatory Test Program, Phase I - Large Scale Demonstration Tests, Test Series 5701 through 5703*, NEDM-13377, October 1974.
- [5.5-2] *Licensing Topical Report, TRACG Model Description*, NEDE-32176P, Revision 1, February 1996.

**Table 5.5-1
Test Initial Conditions**

Test Series	Run No.	Number Of Vents	Flow Restrictor Diameter	Top Vent Submergence
5703	01	3	63.5 mm	2.06m
5703	02	3	63.5 mm	3.33m
5703	03	3	92.0 mm	3.37m

**Table 5.5-2
Comparison of PSTF and SBWR Parameters**

[

Redacted

]

Table 5.5-3
Summary of TRACG Calculations vs Measured Data

[

Redacted

]

Table 5.5-4
Assessment of TRACG Accuracy for PSTF Mark III Tests

[

Redacted

]

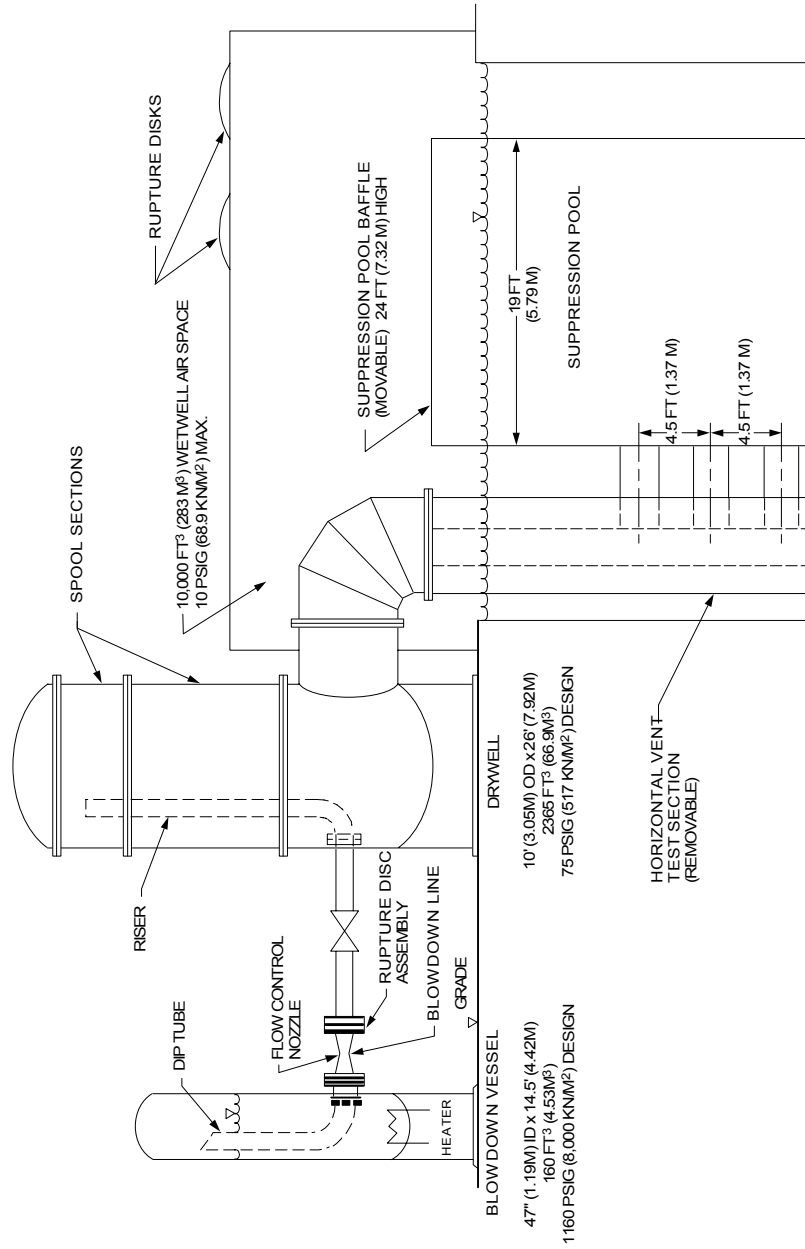


Figure 5.5-1 Pressure Suppression Test Facility (PSTF) Schematic

[

Redacted

]

Figure 5.5-1 PSTF TRACG Component Layout

[

Redacted

]

Figure 5.5-2 TRACG Model of PSTF Suppression Pool

[

Redacted

]

Figure 5.5-3 TRACG Vent System Model - PSTF and SBWR

[

Redacted

]

Figure 5.5-4 Drywell Pressure Response - TRACG vs Measured Data, Test 5703-01

[

Redacted

]

Figure 5.5-5 Drywell Pressure Response - TRACG vs Measured Data, Test 5703-02

[

Redacted

]

Figure 5.5-6 Drywell Pressure Response - TRACG vs Measured Data, Test 5703-03

5.6 4T/Mark II Containment Response

5.6.1 Introduction

In addition to the General Electric multiphase Mark III Confirmatory Test Program, a series of blowdown tests was performed to investigate suppression pool dynamic phenomena in the Mark II containment concept, and provide the necessary data for the vertical vent pressure suppression geometry used in the Mark II containment design.

In 1975, this Mark II test series, designated Series 5101, was performed at the Pressure Suppression Test Facility (PSTF). This test series utilized the steam generator and drywell of the PSTF and the Temporary Tall Test Tank (4T) to simulate the wetwell pool and air space. Tests with open tank (no backpressure effect) and closed tank (with backpressure effect) configurations were included in this test series. The vent geometry, connecting the drywell to the wetwell, was a single 590-mm I.D. vertical pipe. The Mark II and SBWR containment designs use a similar wetwell configuration (i.e., suppression pool with closed air space), but they use a different type of drywell-to-wetwell connecting vent system. The Mark II design uses a vertical vent system, whereas the SBWR design uses a horizontal vent system similar to that in Mark III design (Sections 4.4 and 5.5).

Although the 4T/Mark II tests focused on suppression pool dynamics with a vertical vent system, they were of particular interest in assessing TRACG capability for predicting short-term pressure response of a containment design with the closed wetwell configuration used in the SBWR. Seven tests with the closed wetwell configuration were chosen for TRACG analysis. Tests with the open pool configuration were not considered, since they are not representative of the SBWR wetwell design. The seven tests (and their initial conditions) chosen for TRACG qualification purpose are listed in Table 5.6-1. These tests cover the two break sizes and three vent submergence values which were tested in this test series. They provide a sufficiently broad database for determining the adequacy of TRACG for modeling and simulating containment short-term response with the closed wetwell configuration. Also included was a cold drywell test which was a special test characterized as an NRC demonstration run. Except for the initial drywell temperature, the cold drywell test (Test 5101-33) was a repeat of Test 5101-27.

5.6.2 Test Facility/Test Matrix

The Mark II Test Series 5101 used the same steam generator and drywell vessels as were used for the PSTF Mark III tests. The 4T vessel was used as a combination suppression pool and wetwell air space to represent the prototypical wetwell vessel configuration. A detailed description of the test facility is contained in Reference 5.6-1, and a schematic diagram of the facility is presented in Figure 5.6-1. The key measurements from the 5101 test series which are compared to TRACG analysis results are the vent-clearing times and the drywell pressure. The vent-clearing times were measured with an accuracy corresponding to the time required for one scan of all data channels, which was less than 0.02 second for these tests. The drywell pressure measurement accuracy was less than 2% of the measured pressure.

An electrically heated pressure vessel simulates the reactor pressure vessel (RPV). The RPV was connected by a blowdown pipe to another pressure vessel which simulated the drywell

(DW). The blowdown line is connected to a riser inside the steam generator to provide saturated vapor blowdown from the vessel. The DW was connected by a vertical vent pipe to the 4T vessel which simulates the wetwell (WW). A rupture disk in the blowdown pipe simulated the breaking of a main steam line, and a venturi located in the blowdown line set the size of the simulated break.

The test matrix of Series 5101 consisted of tests representing a combination of two break sizes - 63.5 and 76.2 mm - and three vent submergences - 2.74, 3.35 and 4.11m. The DW-to-WW vent was a 590 mm (inside diameter) pipe which terminated at an elevation of 3.66m above the suppression pool floor level. In all tests except one, a drywell heater was used to pre-heat the DW vessel to a minimum temperature of 105°C prior to test initiation to minimize steam condensation in the DW during the transient. The initial WW pool temperature ranged from 18°C to 21°C. The single unheated DW case (Test 5101-33) was run with the DW at an initial temperature of 15°C.

5.6.3 Applicability of Data to SBWR

5.6.3.1 General Data Applicability and Test Facility Scaling

[

Redacted

]

5.6.3.2 PIRT Phenomena and Coverage

[

Redacted

]

[

Redacted

]

5.6.3.3 Scaling Parameters Range

[

Redacted

]

5.6.4 TRACG Model

[

Redacted

]

[

Redacted

]

5.6.5 Test Simulation

[

Redacted

]

5.6.6 Results of Post-Test Calculations

[

Redacted

]

[Redacted]

5.6.6.1 Heated Drywell Tests

5.6.6.1.1 Drywell Pressure Response

5.6.6.1.2 Wetwell Airspace Pressure Response

[

Redacted

]

5.6.6.1.3 Drywell-to-Wetwell Pressure Differential

[

Redacted

]

5.6.6.1.4 Vent Clearing Time

[

Redacted

]

[

Redacted

]

5.6.6.2 Unheated Drywell Test

5.6.6.2.1 Measured Data

[

Redacted

]

5.6.6.2.2 TRACG Analyses

[

Redacted

]

5.6.6.3 Accuracy of TRACG Predictions

[

Redacted

]

[

Redacted

]

5.6.7 Summary and Conclusions

The TRACG calculation results and their comparison with the measured data show that TRACG adequately simulates interaction between the blowdown flow, drywell, wetwell and the vent system. TRACG predicts the drywell pressure responses which match well with the measured data and are on the conservative side. Also, TRACG adequately models and calculates steam condensation on the drywell walls.

The TRACG and 4T/Mark II data comparison results discussed above demonstrate the adequacy of TRACG for calculating containment short-term response with closed wetwell air space design, similar to that used in SBWR design. [

Redacted

]

5.6.8 References

[5.6-1] NEDE-13442P-01, *Mark II Pressure Suppression Test Program*, May 1976.

Table 5.6-1
Test Series 5101 Tests for TRACG Simulation

Test No.	Venturi Diameter (mm)	Drywell Temperature (°C)	Vent Submergence (m)	Pool Temperature (°C)	Remarks
5101-27	76.2	115.0	3.35	21.1	
5101-28	63.5	136.1	2.74	20.6	
5101-29	63.5	126.7	3.35	21.1	
5101-30	63.5	115.0	4.11	20.0	
5101-31	76.2	148.3	2.74	20.0	
5101-33	76.2	15.0	3.35	18.3	Unheated drywell test
5101-34	76.2	155.0	4.11	20.6	

Table 5.6-2
Comparison of 4T/Mark II PSTF and SBWR Parameters

[

Redacted

]

Table 5.6-3
Summary of TRACG Results vs Test Data

[

Redacted

]

Table 5.6-4
Drywell Wall Steam Condensation - TRACG vs Measured Data

[

Redacted

]

Table 5.6-5
Assessment of TRACG Accuracy for 4T Mark II Tests

[

Redacted

]

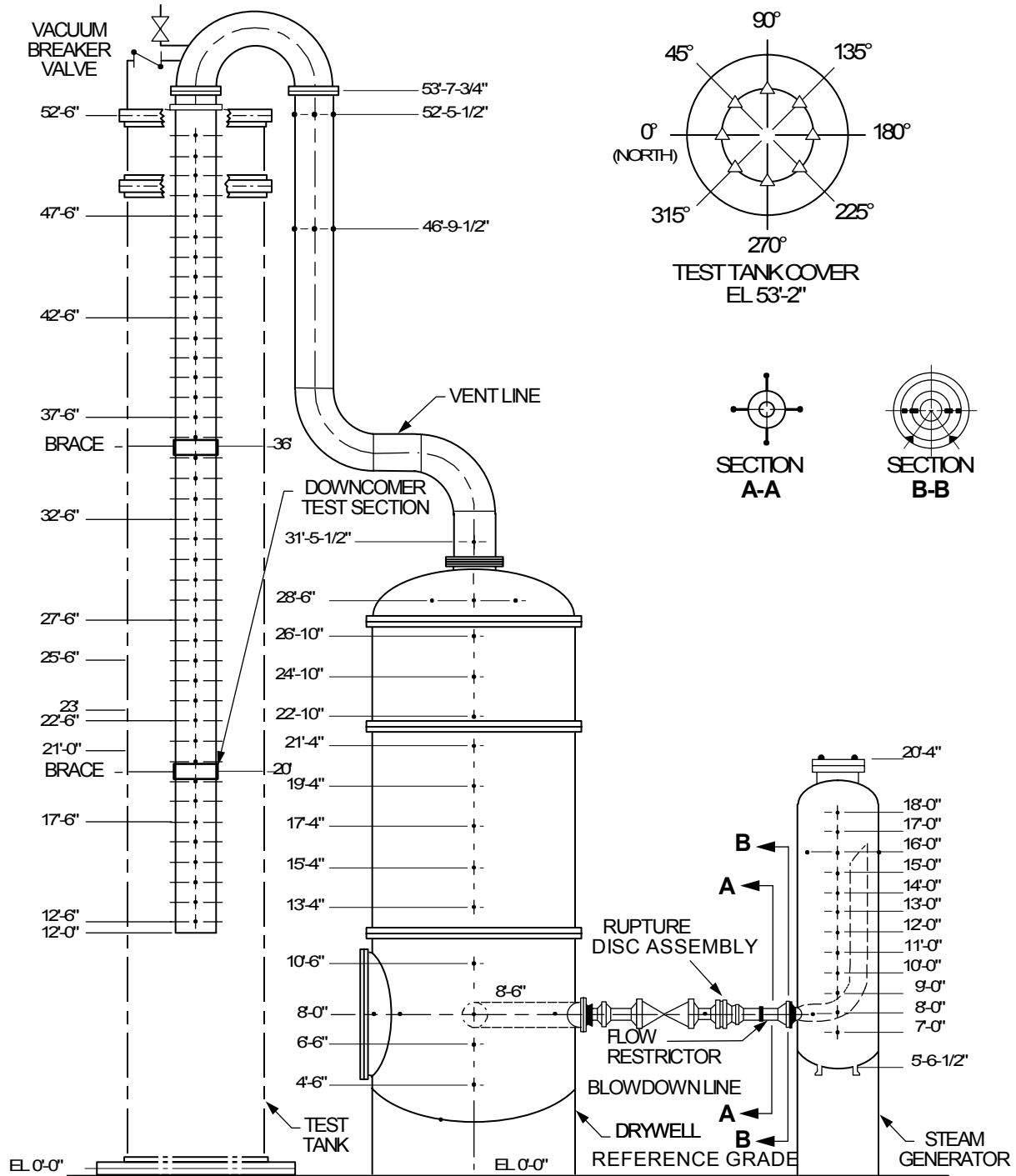


Figure 5.6-1 Pressure Suppression Test Facility Schematic

[

Redacted

]

Figure 5.6-2 TRACG Simulation of PSTF/Mark II

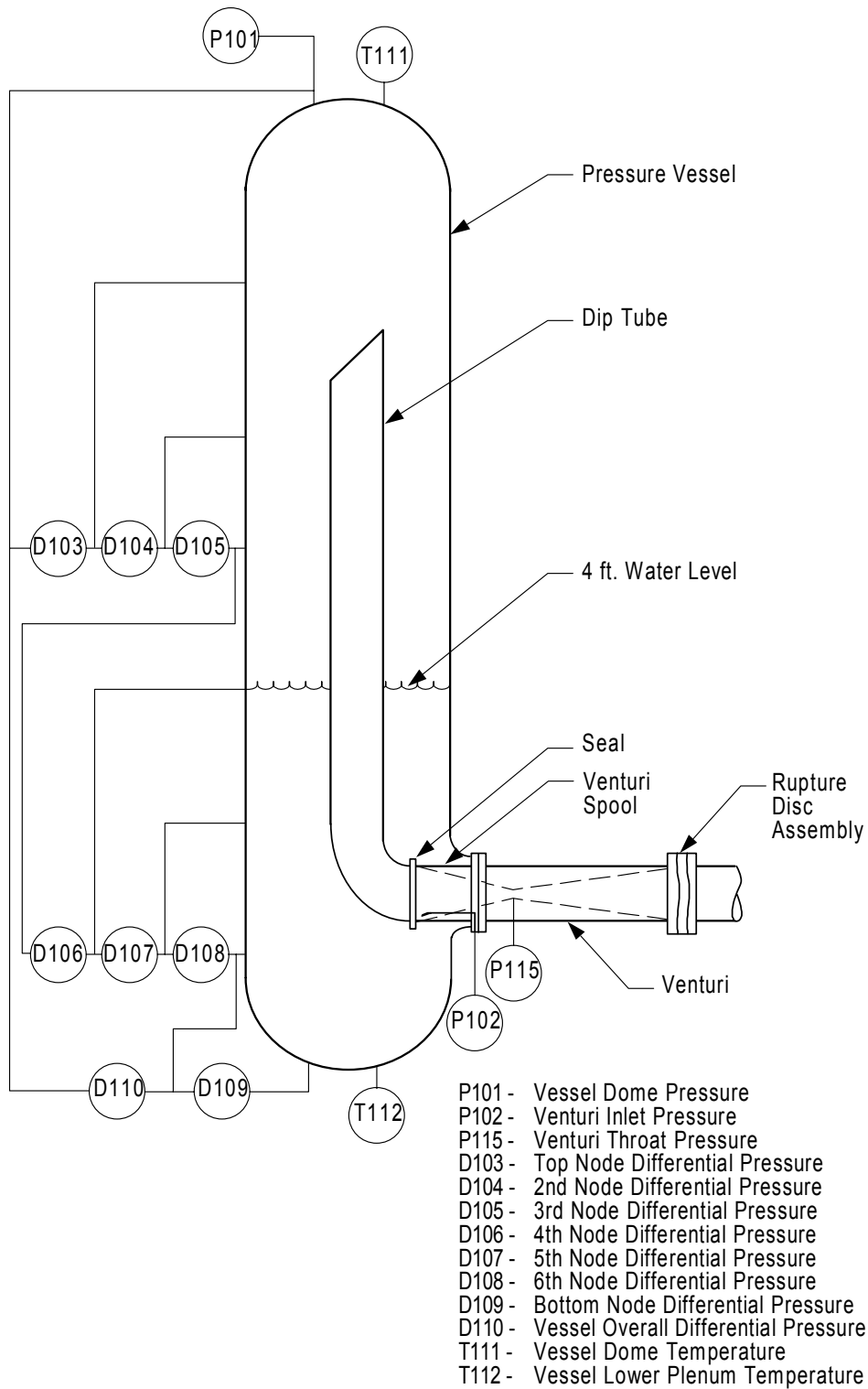


Figure 5.6-3 PSTF Steam Generator and Blowdown Line

[

Redacted

]

Figure 5.6-4 TRACG Nodalization of 4T/Mark II PSTF

[

Redacted

]

Figure 5.6-5 Drywell Pressure Response For Test 5101-34 - TRACG vs Measured Data

[

Redacted

]

Figure 5.6-6 Wetwell Airspace Pressure For Test 5101-34 - TRACG vs Measured Data

[

Redacted

]

Figure 5.6-7 Drywell-to-Wetwell Pressure Differential For Test 5101-34 - TRACG vs Measured Data

5.7 PANDA Transient Tests (M-Series)

5.7.1 Introduction

[

Redacted

]

This section describes the results of post-test analyses of all of the PANDA transient (M-series) tests (M2, M3, M3A, M3B, M6/8, M7, M9, M10A, and M10B). The post-test analyses of the transient tests were performed by an SBWR PANDA analysis team, with participation from the Paul Scherrer Institute (PSI) in Switzerland, where the tests were conducted, and the General Electric Company (GE) in the United States (U.S.). Pre- and post-test calculations of the PANDA test results were a shared responsibility of the team members with final documentation and quality assurance records maintained by GE.

The purpose of the PANDA post-test analysis activity was to demonstrate that TRACG is applicable for the calculation of long-term SBWR containment response to a postulated LOCA. The PANDA test facility includes all of the features of the SBWR containment required for an integrated system simulation of long-term LOCA response. Most notably, the PANDA facility includes a detailed representation of the Passive Containment Cooling System (PCCS) utilized for long-term decay heat removal. A satisfactory comparison between TRACG calculations of PANDA response to a simulated LOCA and the test data would provide strong evidence for the suitability of TRACG to calculate containment response to a postulated LOCA in the SBWR.

[

Redacted

]

The remainder of this section is organized as follows. Section 5.7.2 presents a brief description of the PANDA test facility and the transient (M-series) test matrix. Section 5.7.3

discusses the applicability of the PANDA transient data to the SBWR and includes a rationale for each of the M-series tests. Section 5.7.4 provides a description of the PANDA TRACG input model used for the post-test analyses and includes a section which describes the changes made relative to the input model used for the pre-test calculations [5.7-4 - 5.7-6]. The discussion in Section 5.7.4 is focused on that portion of the model which is independent of the particular test being simulated. Section 5.7.5 completes the TRACG input model description by describing those aspects of the simulation which are unique to a given test. For each test, there is a summary table of the measured thermodynamic conditions at the start of the test which were used for the initialization of the various components in the TRACG model. Section 5.7.6 presents the results of the post-test calculations on a test-by-test basis. Section 5.7.7 presents an overall evaluation of the TRACG simulation from the standpoint of the test results which are most significant for the modeling of the SBWR containment. Section 5.7.7.2 specifically references each of the PIRT phenomena addressed by the PANDA transient tests (as per Table 6.1.1 of Reference 5.7-1).

5.7.2 Test Facility and Test Matrix

The PANDA test facility and test matrix have been described in References 5.7-1, 5.7-9, and 5.7-10. A summary description is included here in the interest of keeping the present document reasonably self-contained. A schematic of the test facility is shown in Figure 5.7-1. The facility was designed to model the long-term cooling phase of the loss-of-coolant accident (LOCA) for the SBWR. It is a 1/25 volume-scaled, full-height simulation of the SBWR primary system and containment. Included in the facility are the major components necessary to model the SBWR system response during the long-term phase of the LOCA. These components include the containment drywell (DW), the wetwell (WW) or suppression chamber, the reactor pressure vessel (RPV) including the core, and those safety systems that would operate during the long-term phase of the LOCA. The RPV is represented by a single vessel in PANDA, while the DW and WW are represented by pairs of vessels, connected by large pipes. This double-vessel arrangement permits improved simulation of spatial distribution effects within the containment volumes.

Important passive safety systems modeled in PANDA include the Passive Containment Cooling System (PCCS), Isolation Condenser System (ICS) and the Gravity-Driven Cooling System (GDSCS). The PANDA PCCS is a direct representation of the SBWR PCCS with three separate loops, each containing a 1/25-scaled condenser unit. The PANDA ICS has one loop and condenser, scaled to represent two of the three ICS loops in the SBWR. The GDSCS pool is represented by a separate vessel in PANDA. The GDSCS airspace communicates with the DWs through pressure equalization lines. Other SBWR components represented in PANDA include the vacuum breakers (VBs) between the DW and the WW and the equalization line (EQL) between the suppression pool and the RPV. The piping interconnecting the PANDA vessels is scaled (primarily with the use of orifice plates) to produce the same pressure loss as the corresponding SBWR piping at 1/25th of the SBWR mass flow rate.

The PANDA test matrix included steady-state tests of the performance of one of the PCC units and a series of integrated system tests intended, primarily, to simulate the long-term cooling phase of the post-LOCA transient. As described in Reference 5.7-1, Test M3 was the base case for the transient series. Subsequent tests incorporated variations of key parameters and

addressed specific thermal-hydraulic phenomena which are considered to be of potential importance for calculation of long-term post-LOCA behavior in the SBWR. Tests M3A and M3B were repeats of Test M3, which also evaluated possible alternatives for configuring and refilling the PCC and IC pools. Tests M2, M10A, and M10B examined the influence of asymmetric distributions of steam and air in the DW on the startup and long-term performance of the PCCS.

Test M6/8 considered system interaction effects associated with parallel operation of the PCCS and ICS and the effect of a direct bypass of steam from the DW to the WW air space. Test M7 addressed the issue of PCCS startup and operation from a condition representing the upper limit of initial DW air inventory. Finally, Test M9 examined PCCS performance during the portion of the post-LOCA transient extending from the early GDCS injection phase into the long-term cooling phase. A detailed discussion of the relationship between each of these tests and the SBWR post-LOCA containment transient is presented in Section 5.7.3.

5.7.3 Applicability of Data to SBWR

[

Redacted

]

5.7.3.1 Overview of Data Applicability and Test Facility Scaling

As stated in Reference 5.7-1, the objectives of the PANDA Test Program were to: (1) provide additional data to qualify TRACG to calculate quasi-steady PCCS heat rejection rate and to identify the effects of scale on PCC performance; (2) provide a database to confirm the capability of TRACG to calculate SBWR containment system performance (including potential systems interaction effects); and (3) demonstrate startup and long-term operation of the PCCS. The testing philosophy adopted for the PANDA program was based on identification of a “Base-Case” test around which perturbations were made to assess the effects of specific systems, systems interactions, and phenomena of interest. The base case (Test M3) was a simulation of the long-term cooling phase following a LOCA caused by a guillotine rupture of one of the main steam lines. This LOCA scenario leads to the highest long-term containment pressure in the SBWR. A key identifying feature of Test M3 was equal steam flow from the RPV to each of the two PANDA DW vessels. Test M3 was followed by two similar tests (M3A and M3B) which demonstrated repeatability of the PANDA data while examining possible testing alternatives for interconnection and periodic refilling of the PCC and IC pools.

Tests M2, M10A, and M10B had the same initial conditions as the M3 series but were configured to examine the sensitivity of system behavior to asymmetric effects. Tests M2 and M10A forced all of the RPV steam flow to go to DW2, and Test M10B forced all of the steam flow to go to DW1. In addition, for Tests M10A and M10B, PCC1 (on DW1) was valved out, leaving only two PCC units to deal with the decay heat load. This modification introduced further system asymmetry and offered the PCCS a more severe challenge for startup and assumption of the decay heat load.

The final group of tests (M6/8, M7, and M9) each had a special purpose. Test M6/8 considered system interaction effects associated with parallel operation of the ICS and PCCS and the effect of a direct bypass of steam from the DW to the WW air space. Test M7 addressed the issue of PCCS startup and operation from a condition representing the upper limit of initial DW noncondensable gas inventory. Test M9 examined a range of system interaction effects associated with an earlier stage of the transient scenario (approximately 20 minutes from the instant of LOCA) and provided support for the concept of simulating a portion of a transient (e.g., long-term containment cooling) with initial conditions characterizing an appropriate intermediate stage of the transient scenario.

The following paragraphs discuss each of the three test groups in more detail with specific reference to their relationship to the response of the SBWR to a postulated design basis LOCA.

5.7.3.1.1 Tests M3, M3A, and M3B

The long-term cooling phase of the LOCA is defined as starting at one hour from the occurrence of the break. At this time, the effect of subcooling of RPV water by GDCS injection is just on the verge of being overcome by the decay power. When this occurs, the PCCS will be called upon to remove the energy added to the DW. To fulfill this role, the system must first purge residual noncondensable gases from the DW to the WW. The performance of the PCCS under these conditions represents the single most important element of the PANDA test program.

Conditions at this time in the LOCA transient were derived from SBWR TRACG calculations (see Table A.3-11 of Reference 5.7-1). The SBWR calculations show that thermodynamic conditions throughout the system are relatively stable at one hour from the initiation of the LOCA transient. The RPV blowdown is complete, the GDCS pools have drained their inventory to the RPV, the decay heat has just overcome the subcooling introduced by the injection of GDCS water, and steaming due to boiloff has resumed. The pressure difference between the RPV and DW is just sufficient to maintain flow of the boiloff steam through the break and the open depressurization valves. The pressure difference between the DW and WW is just sufficient to clear the PCC vents.

One of the compromises made in the design of the PANDA test facility was to not scale the volume of water available to replace boiloff in the SBWR PCCS. In the SBWR, this volume, which extends outside the individual PCC pools, is sufficient to maintain the water level above the top of the condenser tubes for approximately 72 hours. In PANDA, only the water in the four individual pools (three PCC pools and one IC pool) is available to replace boiloff. Capability was provided to either interconnect or isolate the individual pools and to provide replacement water through fittings in the pool bottoms. Starting from the prototypical SBWR

water level and without refill, the PANDA water volume was insufficient to prevent boildown below the top of the tubes for the maximum duration of 20 hours established for PANDA testing. In Test M3, which had the PCC pools interconnected, no refill, and the full 20-hour duration, the upper portion of the PCC tubes was uncovered.

Tests M3A and M3B were conceived to fulfill the dual purpose of establishing the basic repeatability of the PANDA data and evaluating possible alternatives for configuring and refilling the PCC and IC pools to prevent or minimize the non-prototypical uncovering of the condenser tubes. Both tests were run from the same nominal initial conditions as Test M3. In Test M3A, the four condenser pools were isolated and the individual PCC pools were periodically refilled to replace boiloff. The isolated IC pool played no role in this test. In Test M3B, all four pools were interconnected and periodically refilled via the pool connection line. It was expected that Tests M3A and M3B would demonstrate repeatability, even though the pool configurations varied, because the PCCS is substantially oversized relative to the long-term decay heat load.

At the completion of the M3 series of tests, which provided the necessary confirmation of repeatability, it was decided that the remaining tests in the M-series matrix would be run with the PCC and IC pools isolated from one another, no refill, and an initial water level 0.4m above the SBWR prototypical level of 4.4m. This choice simplified the test procedure, provided an independent means of performing individual heat balances on the PCC units, and minimized the uncovering of the condenser tubes. It should also be noted that, with the exception of Test M2, all the remaining tests were run for a duration of ten hours or less.

5.7.3.1.2 Tests M2, M10A, and M10B

The primary purpose of PANDA Tests M2, M10A, and M10B was to examine the influence of an asymmetric distribution of steam and air in the DW on the startup and long-term performance of the PCCS. Each of these tests started from the same nominal initial conditions as the M3 series. Test M2 was a perturbation of Test M3 in which all of the steam from the RPV was directed into DW2 (the DW vessel from which two of the PCCS loops take their inlet flow). This caused the concentration of steam in DW2 to increase relative to that in DW1. The resulting behavior simulates the effect of steam flowing preferentially to one side of the DW in the SBWR. A major design objective of the PCCS is that the performance of the system should be “robust” in the sense of being able to adjust to a widely varying range of inlet conditions, including those associated with nonuniform distributions of steam and noncondensable gas in the DW. Test M2 helped to confirm that this design objective has been achieved.

Tests M10A and M10B also directed all of the RPV steam to only one of the two PANDA DWs. For Test M10A, the steam went to DW2 (as for Test M2) and for Test M10B, it went to DW1. In addition to the asymmetry imposed by directing the steam flow to only one DW, M10A and M10B were run with PCC1 (the PCC unit on DW1) valved out. This modification changed the DW flow pattern. For Test M10A, DW1 was effectively isolated. The only steam entering DW1 was that required to maintain equality of pressure with DW2 through the large connecting pipe and, in the long term, a buoyancy-driven flow tending to reduce the temperature difference between the two DWs. For Test M10B, all the steam had to first sweep through DW1 and then back to DW2 via the connecting pipe to reach the active PCC inlets. In addition to the

asymmetry induced by the elimination of the DW1 PCC loop, Tests M10A and M10B demonstrate startup and operation of the PCCS in an overload condition with some steam bypassing the PCCS through the main vents.

It cannot be claimed that the geometry of the PANDA DW configuration or the asymmetric DW flow and mixing produced by these tests are direct simulations of the possible flow and mixing patterns which could occur in the SBWR DW. However, it can be reasonably claimed that satisfactory startup and operation of the PCCS for the range of conditions produced by the asymmetric test series provides strong evidence that the PCCS does have the inherent robustness to deal with the wide range of conditions to which it could be subjected in an SBWR post-LOCA environment. In this regard, it should be emphasized that the valving out of one of the PCCS loops is an extreme condition which has no credible counterpart in the SBWR. The SBWR PCCS is a totally passive system which is immune to such a failure.

5.7.3.1.3 Tests M6/8, M7, and M9

Test M6/8

Test M6/8 considered system interaction effects associated with parallel operation of the ICS and PCCS and the effect of a direct bypass of steam from the DW to the WW air space. Both of these features are directly applicable to design-basis evaluation of PCCS performance following a postulated LOCA in the SBWR. In the SBWR, the ICS would automatically come into operation on a low RPV water level signal and would immediately start condensing RPV steam, operating in parallel with the PCCS. The only uncertainty is whether the IC vents to the WW would be opened because this operation must be performed by the operator. As a result of this uncertainty, it was decided that Test M6/8 would be performed with the IC vent closed. This increased the likelihood of ICS shutdown resulting from accumulation of air. It was further decided that if the IC did not shut down from air accumulation, it would be intentionally valved out of service after a specified period of operation. This guaranteed that the test would address the situation in which, after an initial period of IC operation, the decay heat load must be shifted from the ICS to the PCCS.

Bypass leakage from the DW to the WW air space is a significant design consideration in the SBWR. In general, operation of the PCCS requires a sufficient pressure difference between the DW and WW to keep the PCCS vents open. If a leakage path between the DW and WW existed, this pressure difference would sustain a parallel bypass leakage flow. The SBWR design, particularly with regard to the VBs, has gone to great lengths to ensure that no DW-to-WW leakage path is possible. For design basis accident evaluations, however, a leakage path with an effective A/\sqrt{K} of 1 cm^2 is considered. Test M6/8 was performed with a scaled leakage path equivalent to 10 cm^2 in the SBWR. The inclusion of a leakage path with ten times the effective area of the SBWR design value provided confirmation that bypass leakage, in the unlikely event that it exists, will, at most, result in a gradual increase in system pressure which would allow adequate time for other remedial actions to be taken.

Test M7

Test M7 addressed the issue of PCCS startup and operation from a condition representing the upper limit of initial DW air inventory. Every known analysis of an RPV blowdown into a BWR

containment indicates that, within a matter of seconds, essentially all of the initial inventory of the DW inerting gas is forced into the WW, leaving the DW with a nearly pure-steam environment. Thus, when the SBWR PCCS is called upon to assume the decay heat load, it is expected that it will face a minimal challenge from residual noncondensable gas in the inlet mixture. It is certainly possible for gas to “hide out” in various dead-end regions of the DW and subsequently find its way to the PCCS inlet lines, but this is a long-term process which would not be expected to interfere with initial PCCS operation at high decay heat load. The best-estimate TRACG analysis of the SBWR main steam line break results in a PCCS inlet noncondensable mass fraction of about 8% at one hour from the instant of LOCA. This value was specified for the “base case” initial conditions which were used for most of the tests.

The above considerations notwithstanding, it is of interest to consider what would happen if the PCCS was confronted with the ultimate challenge of peak (one-hour) decay heat load and a DW essentially filled with noncondensable gas. The initial distribution of air for Test M7 was determined by postulating that the initial blowdown raised the temperature of the WW pool to 353 K (the standard one-hour condition) and that the DW was filled with dry air at approximately 303 K. The heatup of the WW pool, which increases the steam pressure in the WW air space, means that the DW air inventory is actually higher than it would be during normal operation and explains why the initial DW pressure (136 kPa) is above atmospheric pressure. The DW air inventory is further increased by the assumption (a practical necessity for PANDA) that the steam pressure in the DW is zero. As a final step toward making this a truly bounding case, the RPV power was held constant at the initial (one-hour) value of 1.13 MW, rather than allowing it to follow the decay heat curve. This was partly done to compensate for the fact that the DW walls are cold at the start of the test and that some power will be required to bring them up to temperature.

Test M9

The PANDA facility was originally designed to simulate the long-term cooling phase of the post-LOCA transient. All of the tests in the PANDA matrix, with the exception of Test M9, examine PCCS performance under various conditions following the initiation of the long-term cooling phase. As a result of detailed evaluation of the various elements of the overall SBWR test program, it was decided that one of the PANDA tests should simulate PCCS behavior and system interactions during the transitional period from the end of blowdown to the initiation of long-term cooling. With this objective in mind, conditions for Test M9 were developed to examine PCCS performance during the portion of the post-LOCA transient extending from the early GDSCS injection phase into the long-term cooling phase.

Based on analysis and understanding of SBWR post-LOCA performance, the following sequence of events is expected during the period simulated by PANDA Test M9. At the end of the blowdown (marked by the start of GDSCS injection and the cessation of flow through the main LOCA vents), the PCC units are operating at relatively high power in an essentially pure-steam environment. As GDSCS injection proceeds, steam flow from the RPV to the DW is reduced and the DW pressure begins to fall. The decreasing DW pressure, in turn, reduces the flow to the PCCS. Eventually, the decreasing DW pressure causes a series of VB openings, which allows the return of noncondensable gas to the DW. As the rate of GDSCS injection decreases and the RPV inventory heats up to saturation, the DW re-pressurizes and flow to the

PCCS resumes. This marks the initiation of the long-term cooling phase at about one hour from the instant of LOCA.

By simulating the portion of the post-LOCA transient described above, Test M9 addressed the behavior of the PCCS under conditions covering the range from high-power operation with pure-steam inlet conditions, flow reduction caused by decreasing DW pressure, resumption of flow caused by increasing DW pressure, degraded heat transfer with steam-air inlet conditions, and, finally, return to high-power operation. It further addressed systems interactions between the PCCS, GDCS, and the VBs.

[

Redacted

]

5.7.3.2 PIRT Phenomena and Coverage

[

Redacted

]

[

Redacted

]

[

Redacted

]

[

Redacted

]

[

Redacted

]

5.7.3.3 Conclusions on Data Applicability

[

Redacted

]

5.7.4 PANDA TRACG Input Model Description

[

Redacted

]

5.7.4.1 Wetwell, Drywell and GDCS Pool

[

Redacted

]

[

Redacted

]

5.7.4.2 RPV and Associated Piping

[

Redacted

]

5.7.4.3 PCC and IC Condensers and Their Pools

[

Redacted

]

[

Redacted

]

5.7.4.4 Main Vents and Vacuum Breakers

[

Redacted

]

5.7.4.5 System Line Flow Resistance

[

Redacted

]

[

Redacted

]

5.7.4.6 Component Heat Loss and Heat Capacity

[

Redacted

]

5.7.4.7 Decay Heat

[

Redacted

]

[

Redacted

]

5.7.4.8 Comparison with SBWR Containment Model

[

Redacted

]

[

Redacted

]

5.7.4.9 Model Changes for Post-Test Analyses

[

Redacted

]

5.7.4.9.1 Elimination of DW and WW Azimuthal Divisions

[

Redacted

]

5.7.4.9.2 Reduction in WW Level Divisions

[

Redacted

]

5.7.4.9.3 Heat Transfer Correlations for Condenser Tubes

[

Redacted

]

5.7.4.9.4 Modification of DW and WW Wall Thickness

[

Redacted

]

5.7.4.9.5 Nodalization of PCC and IC Condenser Tubes

[

Redacted

]

[
Redacted
]

5.7.4.9.6 Vacuum Breaker Bypass Line Model

[
Redacted
]

5.7.4.9.7 PCC and IC Pool Models

[

Redacted

]

5.7.4.9.8 Heat Transfer Between Main Vents and WW Airspace

[

Redacted

]

5.7.4.9.9 DW Flow Resistances

[

Redacted

]

[

Redacted

]

5.7.4.9.10 Use of Actual Test Conditions

[

Redacted

]

5.7.5 TRACG Simulation of PANDA Tests

[

Redacted

]

5.7.5.1 Initial Conditions

[

Redacted

]

[

Redacted

]

5.7.5.2 Test Control

[

Redacted

]

5.7.5.3 Tests M3, M3A, and M3B

[

Redacted

]

[

Redacted

]

5.7.5.4 Tests M2, M10A, and M10B

[

Redacted

]

[

Redacted

]

5.7.5.5 Tests M6/8, M7, and M9

[

Redacted

]

5.7.6 Results Of Post-Test Calculations

[

Redacted

]

[

Redacted

]

[

Redacted

]

5.7.6.1 Tests M3, M3A and M3B

[

Redacted

]

5.7.6.1.1 DW and WW Pressure

[

Redacted

]

[

Redacted

]

5.7.6.1.2 PCC Inlet Flow and Pool Levels

[

Redacted

]

[Redacted]

5.7.6.1.3 DW Gas Temperatures

5.7.6.1.4 WW Gas Temperatures

5.7.6.1.5 WW Liquid and Liquid Surface Temperatures

[Redacted]

[

Redacted

]

5.7.6.1.6 DW and WW Air Partial Pressures

[

Redacted

]

5.7.6.1.7 PCC Upper and Lower Header Temperatures

[

Redacted

]

5.7.6.1.8 PCC Tube Temperatures

[

Redacted

]

[

Redacted

]

5.7.6.1.9 Summary for Tests M3, M3A and M3B

[

Redacted

]

5.7.6.2 Tests M2, M10A and M10B

[

Redacted

\

]

5.7.6.2.1 DW and WW Pressures

[

Redacted

]

5.7.6.2.2 PCC Inlet Flows and Pool Levels

[

Redacted

]

5.7.6.2.3 DW Temperatures

[

Redacted

]

[

Redacted

]

5.7.6.2.4 WW Gas Temperatures

[

Redacted

]

[

Redacted

]

5.7.6.2.5 Main Vent Temperatures

[

Redacted

]

[

Redacted

]

5.7.6.2.6 WW Liquid Temperatures

[

Redacted

]

[

Redacted

]

5.7.6.2.7 DW and WW Air Partial Pressures

[

Redacted

]

[

Redacted

]

5.7.6.2.8 PCC Upper and Lower Header and Tube Temperatures

[

Redacted

]

[

Redacted

]

5.7.6.2.9 Summary for Test M2, M10A, and M10B

[

Redacted

]

5.7.6.3 Other Tests

[

Redacted

]

5.7.6.3.1 Test M7 (PCC Startup)

[

Redacted

]

[

Redacted

]

[

Redacted

]

[

Redacted

]

5.7.6.3.2 Summary of the M7 Predictions

[

Redacted

]

5.7.6.3.3 Test M6/8 (IC Operation and Bypass Leakage Test)

[

Redacted

]

[

Redacted

]

[

Redacted

]

5.7.6.3.4 Summary of the Test M6/8 Predictions

[

Redacted

]

5.7.6.3.5 Test M9 (Early Start Test)

[

Redacted

]

[

Redacted

]

5.7.6.3.6 Summary of the Test M9 Predictions

[

Redacted

]

[

Redacted

]

5.7.6.4 Accuracy of TRACG Predictions

[

Redacted

]

5.7.7 Summary and Conclusions

5.7.7.1 Purpose and Scope of Post-Test Evaluation

The major purpose of the post-test evaluation of the PANDA M-series tests was to provide support for the use of TRACG to model the post-LOCA behavior of the SBWR containment, including, specifically, the use of the PCCS to remove long-term decay heat. The post-test evaluation included all nine of the integrated systems tests performed in the PANDA facility as part of the SBWR Test and Analysis Program [5.7-1]. The nine M-series tests covered a wide range of PCCS startup and operating conditions. The M-series tests also addressed system interaction effects involving the various passive systems and components which play a role in the SBWR containment response to a LOCA. In addition to the PCCS, these systems and components included the ICS, GDCS and VBs. Finally, the M-series tests considered several extreme conditions, including PCCS startup with the DW filled with air, DW-to-WW bypass leakage equal to ten times the SBWR design value, and complete elimination of one PCC unit.

Each of the M-series tests was simulated in its entirety with a TRACG calculation using the PANDA input model described in Section 5.7.4. For convenience, the input model was divided into a “generic” section, common to all the tests, and nine “test-specific” sections which were, in turn, attached to the generic section for each specific test simulation. Thus, the measured initial conditions for each test were incorporated via the test-specific input file along with any unique inputs required to simulate the facility configuration or test procedures. The time spans for the TRACG simulations were set to equal or slightly exceed the durations of the corresponding tests.

The post-test evaluation considered a wide range of measurements from the regions of the test facility which represent the important volumes, components, and interconnecting lines in the SBWR containment. A standard set of comparisons between measured and calculated data was made for each test. These comparisons included DW and WW pressures, temperatures, and air partial pressures, WW liquid temperatures, PCC inlet flows, pool levels, upper and lower header temperatures, and PCC tube temperatures. Additional variables, including main vent temperatures, IC temperatures, and RPV and GDSC levels, were included for tests in which they contribute significantly to an understanding of system behavior. The results of these comparisons, which were discussed and interpreted in Section 5.7.6, are discussed below with reference to the TRACG “qualification needs” which provided the rationale and impetus for the PANDA test program.

5.7.7.2 Evaluation of TRACG Qualification Needs

[

Redacted

]

5.7.7.2.1 PCC Flow/Pressure Drop (PC1)

[

Redacted

]

[

Redacted

]

5.7.7.2.2 Condensation/Condensation-Degradation on Primary Side (PC2)

[

Redacted

]

5.7.7.2.3 Secondary-Side Heat Transfer (PC3)

[

Redacted

]

[

Redacted

]

5.7.7.2.4 Parallel PCC Tube Effects (PC4)

[

Redacted

]

5.7.7.2.5 Parallel PCC Unit Effects (PC5 and XC5)

[

Redacted

]

5.7.7.2.6 PCCS Startup (PC8)

[

Redacted

]

[

Redacted

]

5.7.7.2.7 DW Multi-Dimensional Effects (DW3)

[

Redacted

]

5.7.7.2.8 WW Free Surface Condensation/Evaporation (WW4)

[

Redacted

]

5.7.7.2.9 Pool Mixing and Stratification (WW6)

[

Redacted

]

5.7.7.2.10 WW Multi-Dimensional Effects (WW7)

[

Redacted

]

5.7.7.2.11 Leakage Between DW and WW (DWB1)

[

Redacted

]

5.7.7.2.12 System Interaction Effects (IC/DPV/GDCS/PCCS)

[

Redacted

]

5.7.7.3 Summary of Conclusions

Based on the model/data comparisons presented in Section 5.7.6 and the discussion with reference to the SBWR containment PIRT phenomena in Section 5.7.7.2, the following conclusions have been drawn relative to the ability of TRACG to calculate the post-LOCA transient behavior of the SBWR containment:

- TRACG accurately calculates the pressurization of the containment associated with the venting of residual noncondensable gases from the DW to the WW via the PCCS and subsequent mass/energy transfer to the WW by direct heating or bypass leakage.
- Comparison of the measured and calculated length of the PCC condensation zone at similar inlet conditions indicates that TRACG is slightly conservative in its calculation of PCC heat transfer rate. This result is consistent with the results of the PANTHERS PCC post-test evaluation (Section 4.1).

- TRACG is capable of calculating the onset of main vent opening when the PCCS is overloaded.

[

Redacted

]

- TRACG is well-suited to the calculation of post-LOCA containment transients involving interactions between the various passive systems which have a role in mitigating the effects of the LOCA.

5.7.8 References

- [5.7-1] NEDC-32391P, *SBWR Test and Analysis Program Description* (Rev. C), August 1995.
- [5.7-2] MFN 114-94, *Results of Pre-Test Calculations of PANDA PCC Steady- State Tests*, September 1994 (KEMA Letter Report 40315-NUC 94-7034, September 13, 1994).
- [5.7-3] MFN 006-96, *Post-Test Calculations of PANDA PCC Steady State Tests*, January 1996 (KEMA Report 40880-NUC 95-2516, October 1995).
- [5.7-4] MFN 161-95, *SBWR - Pre-Test Analysis for PANDA Test M3*, August 1995.
- [5.7-5] MFN 261-95, *SBWR - Pre-Test Analysis for PANDA Test M2*, November 1995.
- [5.7-6] MFN 270-95, *SBWR - Pre-Test Analysis for PANDA Test M9*, December 1995.
- [5.7-7] NEDE-32176P, *TRACG Model Description*, February 1996.
- [5.7-8] S.Z. Kuhn, V.E. Schrock, and P.F. Peterson, *Final Report on U.C. Berkeley Single Tube Condensation Studies*, UCB-NE-4201 (Rev. 2), August 1994.
- [5.7-9] GE Document 25A5587, *PANDA Test Specification* (Rev. 1), January 1995.
- [5.7-10] PSI Document ALPHA-606-0, *PANDA Facility, Test Program and Data Base General Description (DTR Umbrella Report)*, May 31, 1996.
- [5.7-11] NEDC-32288P, *Scaling of the SBWR Related Tests* (Rev. 1), October 1995.
- [5.7-12] NEDC-32606P, *SBWR Testing Summary Report* (Rev. 0), August 2002.
- [5.7-13] NEDC-32192, *TRACG02V User's Manual*, December 1993.

- [5.7-14] M. Huggenberger, *PANDA Experimental Facility Scaling of the System Lines*, PSI Report ALPHA-412, September 22, 1995.
- [5.7-15] GE Document 25A6938, *Decay Heat Requirements*, SBWR Design Specification (Rev. 1), June 1992.
- [5.7-16] PSI Document ALPHA-601-0, *M3 Integral System Test, Apparent Test Results*, March 1996.
- [5.7-17] PSI Document ALPHA-604-0, *M3A Integral System Test, Apparent Test Results*, March 1996.
- [5.7-18] PSI Document ALPHA-605-0, *M3B Integral System Test, Apparent Test Results*, April 1996.
- [5.7-19] PSI Document ALPHA-608-0, *M2 Integral System Test, Apparent Test Results*, April 1996.
- [5.7-20] PSI Document ALPHA-610-1, *M10A Integral System Test, Apparent Test Results*, June 1996.
- [5.7-21] PSI Document ALPHA-611-1, *M10B Integral System Test, Apparent Test Results*, June 1996.
- [5.7-22] PSI Document ALPHA-612-1, *M6/8 Integral System Test, Apparent Test Results*, June 1996.
- [5.7-23] PSI Document ALPHA-607-0, *M7 Integral System Test, Apparent Test Results*, April 1996.
- [5.7-24] SI Document ALPHA-614-0, *M9 Integral System Test, Apparent Test Results*, May 1996.
- [5.7-25] C. Aubert, *PANDA Instrumentation, System Line Instrumentation As-Built Drawings*, PSI Document ALPHA-515-A, September 6, 1995.
- [5.7-26] C. Aubert, and S. Lomperski, *PANDA Instrumentation, Vessel and Condenser/Pool Temperature and Gas Concentration Instrumentation As-Built Drawings*, PSI Document ALPHA-514-0, January 19, 1996.
- [5.7-27] M Siddique, *The Effects of Noncondensable Gases on Steam Condensation Under Forced Convection Conditions*, PhD Dissertation, MIT, January 1992.
- [5.7-28] W.R. Usry, *Single Tube Condensation Test Program*, NEDC-32301 (Rev. 0), March 1994.

Table 5.7-1
PANDA/TRACG VSSL01 Component Breakdown

[

Redacted

]

Table 5.7-2
PANDA/TRACG Components with Connections to VSSL01 Cells

[

Redacted

]

Table 5.7-3
PANDA/TRACG RPV Components

[

Redacted

]

Table 5.7-4
PANDA/TRACG PCCS Components

[

Redacted

]

Table 5.7-5
PANDA/TRACG ICS Components

[

Redacted

]

Table 5.7-6
Other PANDA/TRACG Components

[

Redacted

]

Table 5.7-7
PANDA Heater Power vs. Time for All Tests Except M7 and M9

Time (sec)	Heater Power (MW)
0	0.0
1	1.130
1	1.130
50	1.120
400	1.082
1400	1.007
2400	0.9392
3400	0.8911
3600	0.8817
3900	0.8709
4400	0.8527
5400	0.8238
6400	0.7971
8400	0.7721
10800	0.7550
11400	0.7480
14400	0.7134
16400	0.6941
21400	0.6602
25200	0.6350
26400	0.6292
32400	0.6020
36400	0.5864
46400	0.5275
56400	0.5050
66400	0.5013
76400	0.4872
82800	0.4768
86400	0.4712
96400	0.4576
116400	0.4336

Table 5.7-8
PANDA Heater Power vs. Time for Test M9

Time (sec)	Heater Power (MW)
0	0.0
1	1.400
543	1.400
560	1.395
610	1.381
660	1.366
960	1.280
1460	1.200
1900	1.130
1999	1.130
2000	1.130
2559	1.130
2560	1.130
2610	1.120
2960	1.082
3960	1.007
4960	0.9392
5960	0.8911
6160	0.8817
6460	0.8709
6960	0.8527
7960	0.8238
8960	0.7971
10960	0.7721
13360	0.7550
13960	0.7480
16960	0.7134
18960	0.6941
23960	0.6602
27760	0.6350
28960	0.6292
34960	0.6020
37960	0.5864
48960	0.5532
58960	0.5275
68960	0.5050
70960	0.5013
78960	0.4872
85360	0.4768
88960	0.4712
98960	0.4576
118960	0.4336

Table 5.7-9
Comparison of PANDA and SBWR Component Nodalizations

[

Redacted

]

Table 5.7-10
Initial Conditions for PANDA Test M3

	RPV	Drywell	Wetwell	GDCS	PCC/IC Pools
Total Pressure (kPa)	299	287	287	290	98
Air/Nit. Pressure (kPa)	0	20	244	270 (2)	N/A
Vapor Temperature (K)	406.6	402.1	350.4	333.7	N/A
Liquid Temperature (K)	406.6	402.1	351.2	333.7	369.4 (3)
Collapsed WL (m) (1)	12.63	0.13	3.89	0.07	4.51 (3)

Table 5.7-11
Initial Conditions for PANDA Test M3A

	RPV	Drywell	Wetwell	GDCS	PCC/IC Pools
Total Pressure (kPa)	301	284	288	287	99
Air/Nit. Pressure (kPa)	0.0	12	250	268 (2)	N/A
Vapor Temperature (K)	406.7	402.6	350.5	332.3	N/A
Liquid Temperature (K)	406.7	402.6	351.8	332.3	370.0 (4)
Collapsed WL (m) (1)	12.60	0.10	3.86	0.11	4.62

Table 5.7-12
Initial Conditions for PANDA Test M3B

	RPV	Drywell	Wetwell	GDCS	PCC/IC Pools
Total Pressure (kPa)	292	288	287	292	99
Air/Nit. Pressure (kPa)	0.0	18	246	273 (2)	N/A
Vapor Temperature (K)	405.8	402.5	351.6	332.0	N/A
Liquid Temperature (K)	405.8	402.5	353.3	332.0	369.8 (4)
Collapsed WL (m) (1)	12.73	0.02	3.87	0.06	4.59

(See Pg 5.7-69 for notes)

Table 5.7-13
Initial Conditions for PANDA Test M2

	RPV	Drywell	Wetwell	GDCS	PCC/IC Pools
Total Pressure (kPa)	297	287	289	290	99
Air/Nit. Pressure (kPa)	0.0	15	248	268 (2)	N/A
Vapor Temperature (K)	405.8	402.5	350.7	335.2	N/A
Liquid Temperature (K)	405.8	402.5	351.7	335.2	369.3
Collapsed WL (m) (1)	12.71	0.01	3.83	0.06	4.82

Table 5.7-14
Initial Conditions for PANDA Test M10A

	RPV	Drywell	Wetwell	GDCS	PCC/IC Pools
Total Pressure (kPa)	296	285	286	289	98
Air/Nit. Pressure (kPa)	0.0	15	242	268 (2)	N/A
Vapor Temperature (K)	405.6	402.5	351.9	334.2	N/A
Liquid Temperature (K)	405.6	402.5	352.3	334.2	369.9
Collapsed WL (m) (1)	12.72	0.04	3.84	0.06	4.85

Table 5.7-15
Initial Conditions for PANDA Test M10B

	RPV	Drywell	Wetwell	GDCS	PCC/IC Pools
Total Pressure (kPa)	293	292	289	295	97
Air/Nit. Pressure (kPa)	0.0	14	245	271 (2)	N/A
Vapor Temperature (K)	405.5	403.9	352.3	337.1	N/A
Liquid Temperature (K)	405.5	403.9	353.2	337.1	369.5
Collapsed WL (m) (1)	12.70	0.02	3.85	0.06	4.81

Table 5.7-16
Initial Conditions for PANDA Test M6/8

	RPV	Drywell	Wetwell	GDCS	PCC/IC Pools
Total Pressure (kPa)	300	283	286	286	98
Air/Nit. Pressure (kPa)	0.0	13	244	268	N/A
Vapor Temperature (K)	406.1	402.4	351.2	331.1	N/A
Liquid Temperature (K)	406.1	402.4	352.3	331.1	370.2
Collapsed WL (m) (1)	12.75	0.02	3.87	0.0	4.77

Table 5.7-17
Initial Conditions for PANDA Test M7

	RPV	Drywell	Wetwell	GDCS	PCC/IC Pools
Total Pressure (kPa)	134	136	135	139	98
Air/Nit. Pressure (kPa)	0.0	135	90	119 (2)	N/A
Vapor Temperature (K)	380.6	304.2	352.0	333.7	N/A
Liquid Temperature (K)	380.6	304.2	353.4	333.7	370.4
Collapsed WL (m) (1)	12.73	0.05	3.88	0.07	4.76

Table 5.7-18
Initial Conditions for PANDA Test M9

	RPV	Drywell	Wetwell	GDCS	PCC/IC Pools
Total Pressure (kPa)	310	291	304	295	98
Air/Nit. Pressure (kPa)	0.0	4 (5)	260 (5)	277 (2)	N/A
Vapor Temperature (K)	406.8	405.4	352.7	330.0	N/A
Liquid Temperature (K)	406.8	405.4	352.8	330.0	370.0
Collapsed WL (m) (1)	3.53	0.03	3.82	3.34	4.74

Notes for Tables 5.7-9 through 5.7-18:

- (1) Vessel water levels are specified relative to the inside bottom elevation.
- (2) GDCS air pressure based on saturated vapor at GDCS pool temperature.
- (3) IC pool empty for Test M3.
- (4) PCC pool makeup water at 289 K for Tests M3A and M3B.
- (5) DW and WW air pressures based on measurements from two oxygen probes, one near the top of DW1 and one near the top of WW1.

Table 5.7-19
PCC Instrumentation for PANDA Post-Test Evaluation

Figure No.	Instrument ID	Measurement
2	MV.P1F	PCC1 inlet flow
2	MV.P2F	PCC2 inlet flow
2	MV.P3F	PCC3 inlet flow
3	ML.U1	PCC1 pool level
3	ML.U2	PCC2 pool level
3	ML.U3	PCC3 pool level
16	MTG.P1.1	PCC1 upper header vapor temperature
16	MTG.P1.2	PCC1 lower header vapor temperature
17	MTG.P2.1	PCC2 upper header vapor temperature
17	MTG.P2.2	PCC2 lower header vapor temperature
18	MTG.P3.1	PCC3 upper header vapor temperature
18	MTG.P3.2	PCC3 lower header vapor temperature
19	MTG.P1.3	PCC1 tube vapor temperature, 0.81m above tube center
19	MTG.P1.4	PCC1 tube vapor temperature, 0.61m above tube center
19	MTG.P1.5	PCC1 tube vapor temperature, 0.41m above tube center
20	MTG.P2.3	PCC2 tube vapor temperature, 0.81m above tube center
20	MTG.P2.4	PCC2 tube vapor temperature, 0.61m above tube center
20	MTG.P2.5	PCC2 tube vapor temperature, 0.41m above tube center
21	MTG.P3.3	PCC3 tube vapor temperature, 0.81m above tube center
21	MTG.P3.4	PCC3 tube vapor temperature, 0.61m above tube center
21	MTG.P3.5	PCC3 tube vapor temperature, 0.41m above tube center
22	MTG.P1.6	PCC1 tube vapor temperature, 0.20m above tube center
22	MTG.P1.7	PCC1 tube vapor temperature at tube center
22	MTG.P1.8	PCC1 tube vapor temperature, 0.41m below tube center
22	MTG.P1.9	PCC1 tube vapor temperature, 0.81m below tube center
23	MTG.P2.6	PCC2 tube vapor temperature, 0.20m above tube center
23	MTG.P2.7	PCC2 tube vapor temperature at tube center
23	MTG.P2.8	PCC2 tube vapor temperature, 0.41m below tube center
23	MTG.P2.9	PCC2 tube vapor temperature, 0.81m below tube center
24	MTG.P3.6	PCC3 tube vapor temperature, 0.20m above tube center
24	MTG.P3.7	PCC3 tube vapor temperature at tube center
24	MTG.P3.8	PCC3 tube vapor temperature, 0.41m below tube center
24	MTG.P3.9	PCC3 tube vapor temperature, 0.81m below tube center

Table 5.7-20
DW Instrumentation for PANDA Post-Test Evaluation

Figure No.	Instrument ID	Measurement
4	MTG.D1.1	DW1 vapor temperature, 7.11m from tank bottom
4	MTG.D1.2	DW1 vapor temperature, 5.78m from tank bottom
4	MTG.D1.3	DW1 vapor temperature, 4.46m from tank bottom
4	MTG.D1.4	DW1 vapor temperature, 3.13m from tank bottom
4	MTG.D1.5	DW1 vapor temperature, 1.81m from tank bottom
4	MTG.D1.6	DW1 vapor temperature, 0.48m from tank bottom
5	MTG.D2.1	DW2 vapor temperature, 7.11m from tank bottom
5	MTG.D2.2	DW2 vapor temperature, 5.78m from tank bottom
5	MTG.D2.3	DW2 vapor temperature, 4.46m from tank bottom
5	MTG.D2.4	DW2 vapor temperature, 3.13m from tank bottom
5	MTG.D2.5	DW2 vapor temperature, 1.81m from tank bottom
5	MTG.D2.6	DW2 vapor temperature, 0.48m from tank bottom

Table 5.7-21
WW Instrumentation for PANDA Post-Test Evaluation

Figure No.	Instrument ID	Measurement
6	MTG.S1.1	WW1 vapor temperature, 9.5m from tank bottom
6	MTG.S1.2	WW1 vapor temperature, 8.8m from tank bottom
6	MTG.S1.3	WW1 vapor temperature, 7.6m from tank bottom
6	MTG.S1.4	WW1 vapor temperature, 6.4m from tank bottom
6	MTG.S1.5	WW1 vapor temperature, 5.2m from tank bottom
6	MTG.S1.6	WW1 vapor temperature, 4.0m from tank bottom
7	MTG.S2.1	WW2 vapor temperature, 9.5m from tank bottom
7	MTG.S2.2	WW2 vapor temperature, 8.8 m from tank bottom
7	MTG.S2.3	WW2 vapor temperature, 7.6m from tank bottom
7	MTG.S2.4	WW2 vapor temperature, 6.4m from tank bottom
7	MTG.S2.5	WW2 vapor temperature, 5.2m from tank bottom
7	MTG.S2.6	WW2 vapor temperature, 4.0m from tank bottom
8	MTL.S1.1	WW1 liquid temperature, 3.50m from tank bottom
8	MTL.S1.2	WW1 liquid temperature, 3.20m from tank bottom
8	MTL.S1.3	WW1 liquid temperature, 2.95m from tank bottom
8	MTL.S1.4	WW1 liquid temperature, 2.74m from tank bottom
9	MTL.S2.1	WW2 liquid temperature, 3.50m from tank bottom
9	MTL.S2.2	WW2 liquid temperature, 3.20m from tank bottom
9	MTL.S2.3	WW2 liquid temperature, 2.95m from tank bottom
9	MTL.S2.4	WW2 liquid temperature, 2.74m from tank bottom
10	MTS.S1.1	WW1 liquid temperature just below pool surface
10	MTS.S1.2	WW1 liquid temperature at pool surface
10	MTS.S1.3	WW1 liquid temperature just above pool surface
11	MTS.S2.1	WW2 liquid temperature just below pool surface
11	MTS.S2.2	WW2 liquid temperature at pool surface
11	MTS.S2.3	WW2 liquid temperature just above pool surface

Table 5.7-22
Oxygen Probe Instrumentation for PANDA Post-Test Evaluation

Figure No.	Instrument ID	Measurement
12	MPG.D1.1	DW1 air partial pressure, 6.8m from tank bottom
12	MPG.D1.2	DW1 air partial pressure, 3.1m from tank bottom
13	MPG.D2.1	DW2 air partial pressure, 6.8m from tank bottom
13	MPG.D2.2	DW2 air partial pressure, 3.1m from tank bottom
14	MPG.S1	WW1 air partial pressure, 9.2m from tank bottom
15	MPG.S2	WW2 air partial pressure, 9.2m from tank bottom

Table 5.7-23
IC Instrumentation for Post-Test Evaluation of PANDA Test M6/8

Figure No.	Instrument ID	Measurement
2	MV.I1F	IC inlet flow
3	ML.U0	IC pool level
25	MTG.I1.1	IC upper header vapor temperature
25	MTG.I1.2	IC lower header vapor temperature
26	MTG.I1.3	IC tube vapor temperature, 0.81m above tube center
26	MTG.I1.4	IC tube vapor temperature, 0.61m above tube center
26	MTG.I1.5	IC tube vapor temperature, 0.41m above tube center
27	MTG.I1.6	IC tube vapor temperature, 0.20m above tube center
27	MTG.I1.7	IC tube vapor temperature at tube center
27	MTG.I1.8	IC tube vapor temperature, 0.41m below tube center
27	MTG.I1.9	IC tube vapor temperature, 0.81m below tube center

Table 5.7-24
Main Vent Instrumentation for Post-Test
Evaluation of PANDA Tests M10A, M10B, and M7

Figure No.	Instrument ID	Measurement
25	MTG.MV1.1	Main vent 1 inlet temperature
25	MTG.MV1.3	Main vent 1 temperature, 2.82m above vent exit
25	MTG.MV1.4	Main vent 1 temperature, 0.03m above vent exit
26	MTG.MV2.1	Main vent 2 inlet temperature
26	MTG.MV2.3	Main vent 2 temperature, 2.82m above vent exit
26	MTG.MV2.4	Main vent 2 temperature, 0.03m above vent exit

Table 5.7-25
RPV and GDCS Level Instrumentation for
Post-Test Evaluation of PANDA Tests M7 and M9

Figure No.	Instrument ID	Measurement
27/M7	ML.RP.1	RPV collapsed level
25/M9	ML.RP.1	RPV collapsed level
25/M9	ML.GD	GDCS level

Table 5.7-26
PANDA Measurement Uncertainties

Measurement	Maximum Uncertainty
Temperature	$\pm 0.8^{\circ}\text{C}$
Pressure	$\pm 2.3 \text{ kPa}$
Flow	$\pm 2\%$
Air Partial Pressure	$\pm 4\%$
PCC/IC Pool Level	$\pm 0.156\text{m}$

Table 5.7-27
Assessment of TRACG Accuracy for PANDA Transient (M-Series) Tests

[

Redacted

]

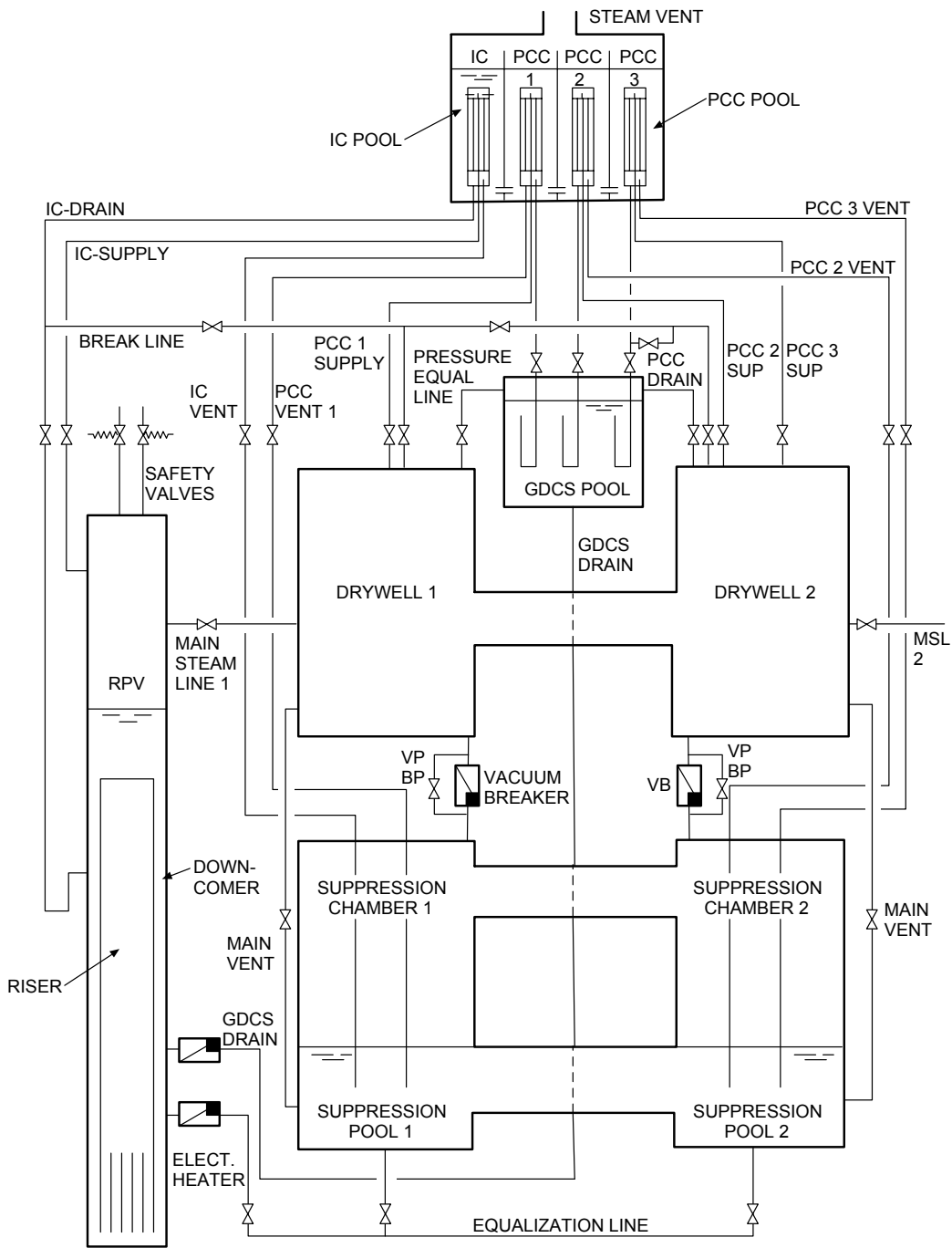


Figure 5.7-1 PANDA Test Facility Schematic

[

Redacted

]

Figure 5.7-2 PANDA Vessel Component Nodalization Diagram

[

Redacted

]

Figure 5.7-3 RPV, IC, and Connected Piping Nodalization Diagram

[

Redacted

]

Figure 5.7-4 PCCS (PCC1) Nodalization Diagram

[

Redacted

]

Figure 5.7-5 PCCS and ICS Pools Nodalization Diagram

[

Redacted

]

Figure 5.7-6 Main Vent (DW2 to WW2) Nodalization Diagram

[

Redacted

]

Figure 5.7-7 Vacuum Breaker (DW2 to WW2) Nodalization Diagram

Attachment A to Section 5.7

This attachment contains the figures comparing TRACG calculations to test measurements for the nine PANDA transient (M-series) tests. The figures have been given a special numbering system which utilizes the test number.

Attachment A Figures
Pages 5.7A-1 through 5.7A-233/5.7A-234

Redacted

6. Natural Circulation and Flow Oscillation Tests

This section documents comparisons of TRACG calculations with data on natural circulation and manometric type oscillations that could occur during plant startup. Comparisons for steady-state natural circulation tests were shown in the generic TRACG qualification report for the FRIGG test loop [6.0-1, Section 3.7]. Natural circulation flow was also important in the prediction of the TLTA Boiloff Test [6.0-1, Section 5.1.1] and the FIST Small Break Test [6.0-1, Section 5.2.3]. Simulations of SBWR LOCAs with the gravity-driven GDCS flow and natural circulation between the downcomer and core are shown in Section 5.3 for the GIRAFFE/SIT and in Section 5.1 for the GIST tests. Predictions of the natural circulation flow in operating BWRs (LaSalle, Leibstadt, Forsmark and Cofrentes), made as precursors to stability calculations, have shown excellent agreement with data [6.0-1, Sections 7.4 - 7.7]. The core flow following a two-pump trip at Hatch [6.0-1, Section 7.2] agrees with measurements to about 10%. These comparisons are supplemented in Section 6.1 with process computer measurements at the Dodewaard reactor for steady operating conditions.

[

Redacted

]. Section 6.2 shows TRACG analysis of a natural circulation plant startup at Dodewaard. No oscillations were observed during the plant startup. Comparisons with tests performed at the CRIEPI facility [6.0-6], where oscillatory behavior was observed and predicted, are described in Section 6.3. The phenomenon observed was not condensation-induced oscillations, but adiabatic flashing in the chimney, causing manometric oscillations between the core/chimney and the downcomer. These oscillations were initiated by propagation of enthalpy perturbations up the core and chimney, corresponding to changes in the circulation flow, leading to periodic flashing in the upper part of the chimney. The mechanism is similar to the traditional density wave oscillations, except that changes in enthalpy are propagated rather than changes in void fraction. Finally, oscillations observed during exploratory tests at the PANDA facility are also analyzed in Section 6.4. The oscillation mechanism appears to be similar to that in the CRIEPI tests. A summary of the results and the implications for the SBWR is presented in Section 6.5.

References

[6.0-1] J.G.M.Andersen, et al., *TRACG Qualification*, NEDE-32177P, Revision 2, January 2000.

- [6.0-2] M. Aritomi, T. Nakahashi, J.H. Chiang, M. Wataru, M. Mori, *Transient Behavior of Natural Circulation for Boiling Two-Phase Flow (Experimental Results)*, Transactions of the ANS meeting, November 11-15, 1990, Washington DC, Vol. 62, pp. 504-507.
- [6.0-3] M. Aritomi, T. Nakahashi, J.H. Chiang, M. Mori, (1991). *Transient Behavior of Natural Circulation for Boiling Two-Phase Flow (2nd Report: Mechanism of Geysering)* Transactions of the First JSME/ASME Joint International Conference on Nuclear Engineering (ICONE-1), Tokyo, Japan, November 4-7, 1991, pp. 87-94.
- [6.0-4] M. Aritomi, J.H. Chiang, M. Mori (1992), *Fundamental Studies on Safety-Related Thermal-Hydraulics of Natural Circulation Boiling Parallel Channel Flow Systems Under Startup Conditions (Mechanism of Geysering in Parallel Channels)*, Nuclear Safety, Vol. 33, No. 2, 1992, pp. 170-182.
- [6.0-5] F. Inada, Y. Yasuo, *The Boiling Flow Instability of a Natural Circulation BWR with a Chimney at Low Pressure Startup*, Proceedings of the International Conference on the Design and Safety of Advanced Nuclear Power Plants (ANP '92), Tokyo, Japan, Paper 25.3, October 25-29, 1992.

6.1 Dodewaard Steady-State Operation

6.1.1 Introduction

The purpose of this section is to demonstrate the capability of the TRACG thermal hydraulic and neutronic models to predict the steady-state operating characteristics of a natural circulation BWR. The LWRSIM computer code, which is used at Dodewaard in conjunction with the plant process computer [6.1-1], is used as the basis for comparison. This semi-steady-state code was especially adapted for the natural-circulation situation in Dodewaard, and is used for detailed core behavior predictions. LWRSIM has been extensively validated against measurement data from the plant [6.1-4] for core flow and power distribution. The results of the LWRSIM code supplement plant measurements by providing derived parameters that are not or cannot be directly measured.

Data and LWRSIM calculations were available for comparison only at rated conditions. This comparison is supplemented by comparisons at several state points at low power during startup of the Dodewaard reactor, reported in Section 6.2. Additionally, TRACG has been qualified against natural circulation data from thermal hydraulic test facilities such as FRIGG and operating BWRs in the generic TRACG qualification report.

6.1.2 Description of Dodewaard

The Dodewaard reactor is a natural circulation BWR with internal free surface steam separation. The reactor, with a maximum thermal power capability of 183 MWt, is connected to a turbine generator capable of producing 60 MWe. Initial startup of the Dodewaard reactor was in 1969, and it operated continuously until its planned shutdown in 1997. Figure 6.1-1 shows the overall configuration of the reactor vessel and the key internal components. The Dodewaard RPV has a diameter of 2.8m and is 12.1m high. The core consists of 164 fuel bundles with a 6x6

lattice. The fuel length is 1.79m. The reactor is controlled with 37 control rods consisting of sheathed cruciform arrays of stainless steel tubes filled with boron carbide.

The core shroud assembly is a stainless steel cylinder which encloses the reactor core and forms the interior wall of the downcomer annulus. The lower portion of the shroud has numerous large cutouts to allow the reactor water to enter the bottom of the core. This portion extends from the bottom of the reactor vessel to the bottom of the active core zone. The core shroud is 3.7m long with a diameter of 2.1m. Natural circulation is achieved with the help of a 3.06m high chimney above the core. The chimney assembly is divided into 45 cells by vertical partitions, of which 37 are square and are located over the fuel assemblies surrounding control rod positions. The remaining 8 cells are rectangular and cover the fuel assemblies outside the control rod pattern.

The primary separation of steam and water occurs at the water surface, which is typically about 0.55m above the top of the chimney in the hot standby mode and 0.8m during full power operation (Figure 6.1-1). The plant has an annular dryer assembly with the main steam line coming off the top head. The plant operates with an estimated carryunder fraction of 1.5 - 2.0%.

Figure 6.1-1 also shows the instrumentation used to measure the downcomer flow, subcooling, downcomer level and the locations of the in-core flux monitors. The downcomer flow was derived from cross correlation of thermocouple signals. A more detailed discussion of how the parameters of interest are obtained from the plant instrumentation is provided in Section 6.2.2.5. Many of the parameters used in the TRACG steady-state comparisons are derived from plant data using the LWRSIM code.

6.1.3 Applicability of Data to SBWR

[

Redacted

]

[

Redacted

]

[

Redacted

]

6.1.4 TRACG Model

[

Redacted

]

[

Redacted

]

6.1.5 TRACG Simulation

[

Redacted

]

[

Redacted

]

6.1.6 Results of Calculations

[

Redacted

]

[

Redacted

]

6.1.7 Summary and Conclusions

[

Redacted

]

6.1.8 References

- [6.1-1] *Steady-State Thermal Hydraulic Analysis Report for the GKN Upgrade Project*, GEGKN-93-0103, NEDC-32299P, May 1994.

- [6.1-2] *Description of the TRACG Analysis of the February 1992 Startup of the Dodewaard Natural Circulation BWR*, KEMA Report 41180-NUC 96-2043, May 1996.
- [6.1-3] *Steady- State Nuclear Methods*, GE Licensing Topical Report NEDE-30130-P-A, April 1985.
- [6.1-4] J.A.A. Wouters and F.C.M. Verhagen, *Validation of LWRSIM 3.10 for Dodewaard*, KEMA Report 13705-NUC-92-2247, June 1993.

Table 6.1-1
Comparison of Dodewaard and SBWR Geometry and Steady-State Parameters

[

Redacted

]

Table 6.1-2
Dodewaard Nodalization vs. SBWR Nodalization

[

Redacted

]

Table 6.1-3
Comparison of TRACG Steady-State Calculations to Plant Parameters

[

Redacted

]

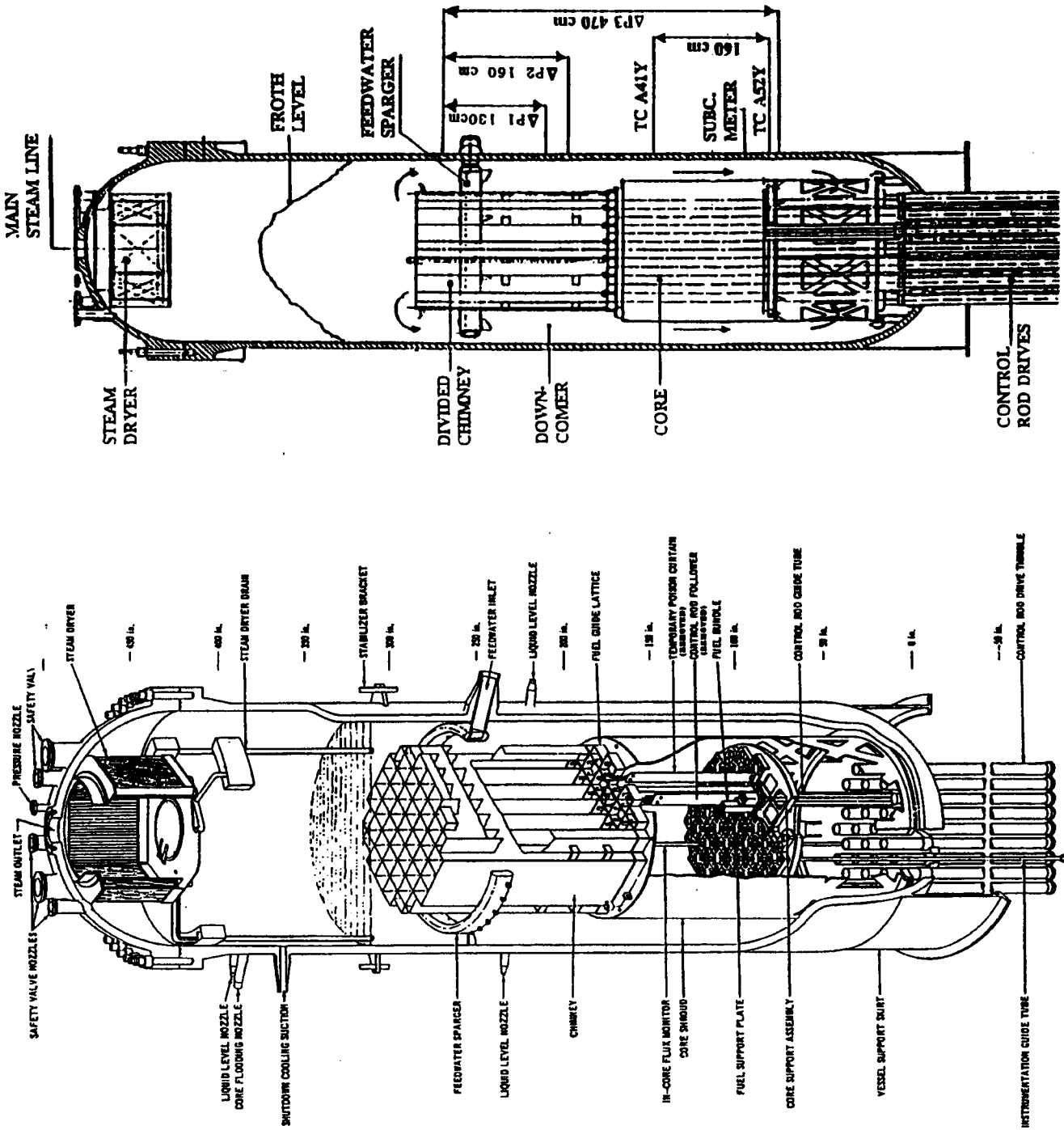


Figure 6.1-1 Dodewaard RPV with Internals (Left) and with Measurement Equipment (Right)

[

Redacted

]

Figure 6.1-2 TRACG Model for Dodewaard Steady-State and Transient Analysis

[

Redacted

]

Figure 6.1-3 Axial Power Distribution at End of Cycle 23

6.2 Analysis of February 1992 Startup of Dodewaard Natural Circulation BWR

6.2.1 Introduction

Startup data are available for the Dodewaard natural circulation BWR in the Netherlands, the only operating BWR in the world that uses natural circulation. The Dodewaard natural circulation power plant in the Netherlands is similar to the SBWR in many respects. Measurements were performed during various stages of the February 15 and 16, 1992 startup process. No instabilities were observed during this or any of the earlier startups in Dodewaard. This section describes the TRACG simulation of that particular startup.

Nissen et al. [6.2-1] and Van der Hagen et al. [6.2-2] measured various plant parameters during the startup following the refueling outage for Cycle 23 (February 1992). The results of the measurements show early establishment of recirculation flow during low power operation. No indication of reactor instability of any kind was observed. However, during the next startup in February 1993 [6.2-3], small oscillations were observed in the ex-vessel neutron noise signals, although under slightly different pressure-power conditions. Since the detailed data from this 1993 startup were not yet available, GE decided to use the data of the 1992 startup to assess the capability of TRACG to predict the thermal hydraulic conditions during the startup of a natural circulation plant.

The Dodewaard plant and its normal startup procedure are described in Section 6.2.2. A detailed description of the steps during the February 1992 startup is given, as well as an overview of the measured data available for the simulation. The applicability of the Dodewaard data to the SBWR is discussed in Section 6.2.3, Section 6.2.4 describes how the TRACG model was set up, and Section 6.2.5 explains how the initial and boundary conditions were determined. The simulation results (comparison with measured data) are analyzed in Section 6.2.6, and the conclusions and recommendations are summarized in Section 6.2.7. No LWRSIM calculations were available at startup conditions, and all TRACG comparisons are with the measured data as discussed later in this section.

6.2.2 Dodewaard Plant and Startup Procedure

6.2.2.1 Brief Description of Dodewaard

The Dodewaard reactor is a natural circulation BWR with internal free surface steam separation (Figure 6.1-1). The reactor, with a maximum thermal power output of 183 MWt, is connected to a turbine generator capable of producing 60 MWe. Initial startup of the Dodewaard reactor was in 1969, and it operated continuously until its planned shutdown in 1997. In January 1992, the reactor was shut down for regular (annual) maintenance and refueling after the successful completion of Cycle 22. On February 15 and 16, 1992 the reactor startup was performed in accordance with the normal startup procedure.

6.2.2.2 Normal Startup Procedure

The reactor becomes critical approximately 6 hours after heating up of the water in the vessel starts. The Shutdown Cooling (SDC) System is switched into heatup mode, supplying water at about 95°C to the vessel. The Control Rod Drive (RSA) purge flow (10°C) is temporarily switched off in order to prevent accumulation of cold water at the vessel bottom. The dome pressure is approximately 0.1 MPa, and the water level is located just below the flange, about 2m above nominal. When all water in the vessel has reached 95°C, the RSA purge flow is put back into operation and withdrawal of control rods begins. The reactor becomes critical and withdrawal of rods continues. The turbine and bypass valves are closed, and only a small vent at the main steamline is available to release steam. In this way pressure is built up. When a dome pressure of 0.4 MPa is reached, the bypass valve is opened and the pressure controller is put into operation. At the same time, the Reactor Water Cleanup (RZS) System is put into operation and the SDC System is switched off. The RZS return flow is set lower than the drain flow, and thus the water level is gradually lowered to its nominal elevation. Withdrawal of control rods continues until operating pressure and power are reached. A summary of the normal startup procedure is given in Table 6.2-1.

6.2.2.3 Sequence of Steps During February 1992 Startup

During the February 1992 startup, an extensive set of measurements was performed [6.2-2]. The normal startup procedure was followed, except that measurements were made (generally over one hour) at nine test conditions. At each test condition, the system pressure was maintained constant and the reactor power increase was halted. Figure 6.2-1 shows the power-pressure path of this startup compared to the power pressure path of a regular startup [6.2-1]. For both trajectories in Figure 6.2-1, time zero corresponds to the time at which the reactor became critical. Comparison of the plots shows that the February 1992 startup lasted much longer due to the measurement waiting periods. In February it took almost 20 hours to reach a pressure of 7.0 MPa and a thermal power of 45 MWt, whereas in the June startup it took only 7 hours.

Table 6.2-2 contains the steps that are important for the thermal hydraulic simulation of the startup (partially taken from Reference 6.2-2, partially based on plant recordings).

6.2.2.4 General Discussion of First Phase of Startup

During the very first phase of the startup (between pressures of 0.1 and 0.5 MPa), the reactor power and pressure are very closely coupled. In this phase, the turbine valves are closed, and only a little vent at the main steamline is available to release steam from the vessel. When the operators withdraw control rods, the power that becomes available first is used to heat the water up to the local saturation temperature. Once saturation is reached and boiling starts, the steam flow increases and, thus, the pressure increases.

There are, however, two different feedback mechanisms that feed back negatively into this process:

- When the pressure increases, the saturation temperature increases *sharply*, thus delaying the boiling process.

- When the temperature increases, the moderator reactivity coefficient is decreased, thus reducing the reactivity and thus slowing down the boiling process.

6.2.2.5 Discussion of the Measurements

Table 6.2-3 contains a general overview of the quantities that were measured during the 1992 startup.

There are a few general aspects about the measured data that should be noted:

- The measurements were not performed in a test facility but in an operating plant, where the measurements are subordinate to the prescribed startup procedure. This leaves little flexibility for the experiment coordinator to choose the measurement conditions.
- Most of the data are only available at discrete time intervals, some of them only as average of semi-equilibrium one-hour measurements.
- Not all parameters have been measured at all data points. Some parameters could not be measured because they fell outside the instrument range.
- Many parameters had to be measured in the lower/upper end of the instrument range and therefore do not have optimal accuracy.
- In References 6.2-2 and 6.2-3 no quantitative uncertainty estimation was made for most of the measured data. The accuracy estimations in this report are based mainly on the judgment of the experimenters.

Several of the measured data [6.2-2] had to be converted, combined or re-calibrated before they could be used for further analysis (this process is described in Reference 6.2-3). The remainder of this section includes a brief description of the most important variables: the method of measurement, the conversion from the raw data and the expected uncertainties.

Thermal Power

In Reference 6.2-2, two different methods were used to calculate thermal power from measured data:

- One method is based on mass and heat balance using measured flows and temperatures. The heat balance method uses readings from flow instruments that are at the low end of their scale, thus yielding a rather large uncertainty. In Reference 6.2-3, the heat balance is recalculated, taking into account several special startup conditions. These recalculated thermal power data are slightly higher than the ones reported in Reference 6.2-3.
- The other method uses the neutron flux-data from ex-vessel neutron detectors. Here again, the instruments were at the low end of their scale, yielding a rather large uncertainty. For the conversion from flux to thermal power in Reference 6.2-2, there was no pressure correction for the water density in the downcomer (varying from 1000 to 740 kg/m³ for the pressure range from 0.1 to 7.0 MPa), which significantly increases the uncertainty for the

measurements at low pressure. In Reference 6.2-3, an empirical method (using the power calculated from the heat balance for calibration) was used to include the density dependence in the conversion. The thermal power data from Reference 6.2-3 were used as boundary conditions for the TRACG simulation.

The uncertainty in the thermal power is large at the low end of the scale. At very low power (<10 MW), the measurement uncertainty is on the order of 50 to 100%, decreasing to approximately 3% at rated conditions.

Pressure

The system pressure is obtained from a differential pressure measurement connected to the main steamline. The accuracy is expected to be within 50 kPa.

Main Steamline Flow

This variable is measured at a flow limiter located in the steamline. For startup conditions, the steam flow is at the low end of its scale, and has a rather large uncertainty. The automatic conversion of the measured pressure difference to a mass flow, as used in Reference 6.2-2, is based on the density of steam that corresponds to the nominal pressure of 7.55 MPa. In Reference 6.2-3, the reported steam flow values from Reference 6.2-2 were recalculated, using the actual steam density data. The uncertainty is estimated to be between 50 and 100% at low flows, decreasing to an estimated 10% at nominal conditions.

Collapsed Water Level

Several pressure differential transmitters are used in the plant to obtain an indication of the collapsed water level. They indicate water level in percent of full scale and have different readings, depending on pressure and water temperature in the measuring legs. In Reference 6.2-3, the water level readings were converted to actual meters. They may be expected to have an uncertainty of less than 0.15m during the simulation.

Downcomer Subcooling

This quantity is directly measured by a differential thermocouple, installed in the lower part of the downcomer, with the hot junction boiling at *local* pressure (a detailed description of this subcooling measurement device can be found in Reference 6.2-4; in Figure 6.2-1 the location of the subcooling meter is indicated). The accuracy of these measurements is expected to be within 0.5 °C and it is one of the most reliable values during the initial phase of the startup.

Downcomer Pressure Differences

Three pressure differentials are measured at different elevations in the downcomer. Each pressure transmitter has one pressure measuring leg connected to a nozzle located 0.4m below the top of the chimney (Figure 6.1-1). The other legs of the pressure transmitters are connected to nozzles located at 1.7, 2.0 and 5.1m below the top of chimney. Corrections are made to account for the hydrostatic pressure of the cold legs, using measured temperatures in the drywell. The measurements are considered accurate, with errors smaller than 1 kPa.

Downcomer Coolant Velocity

This velocity is estimated from noise analysis of two downcomer thermocouples, TC A41Y and TC A52Y located 1.60 m apart at the elevations of the top and bottom of the core (Figure 6.1-1). The transient time of the maximum of the cross-correlated signals is determined by fitting the linear phase of the cross power spectral density [6.2-5]. This velocity has a larger uncertainty in the initial phase of the startup (9%), but this decreases (to 1%) when coolant velocity increases [6.2-2].

Bypass Temperatures

These temperatures are measured at six different elevations by a thermocouple string located in the bypass close to the center of the core. The accuracy of this temperature data is expected to be within 3°C.

Bypass Velocity

This quantity is determined from noise analysis of the thermocouple signals in the bypass. The uncertainty in this estimated velocity is similar to the downcomer coolant velocity.

6.2.3 Applicability of the Dodewaard Startup Data to the SBWR

[

Redacted

]

[

Redacted

]

[

Redacted

]

6.2.4 TRACG Model of Dodewaard for Startup Simulation

[

Redacted

]

6.2.4.1 Model Description

[Redacted]

6.2.4.2 Vessel

[Redacted]

Redacted

6.2.4.2.1 Power Control

[Redacted]

Redacted

]

6.2.4.2.2 Water Level Controller

[

Redacted

]

6.2.4.2.3 Pressure Control

[

Redacted

]

6.2.5 Simulation of the February 1992 Startup

6.2.5.1 Initial Conditions

[

Redacted

]

[

Redacted

]

6.2.5.2 Boundary Conditions

[

Redacted

]

6.2.5.2.1 First Phase

[

Redacted

]

6.2.5.2.2 Second Phase

[

Redacted

]

6.2.5.2.3 Overview of Boundary Conditions

[

Redacted

]

6.2.6 Qualification Results

[

Redacted

]

6.2.6.1 Comparison of TRACG Results with Measured Data

[

Redacted

]

[

Redacted

]

[

Redacted

]

[

Redacted

]

6.2.6.2 Analysis of Other TRACG Results

[

Redacted

]

[

Redacted

]

6.2.6.3 General Analysis of TRACG Results

[

Redacted

]

[

Redacted

]

[

Redacted

]

[

Redacted

]

6.2.6.4 Discussion of the Results

[

Redacted

]

[

Redacted

]

6.2.6.5 Accuracy of TRACG Predictions

[

Redacted

]

6.2.7 Conclusions/Results of the Assessment

The major conclusion of the study described in this section is that the thermal hydraulic models in TRACG are capable of simulating the startup of a full-scale natural-circulation system at low-power low-flow low-pressure conditions.

6.2.7.1 General Conclusions

[

Redacted

]

[

Redacted

]

6.2.7.2 Adequacy of TRACG Models

[

Redacted

]

6.2.8 References

- [6.2-1] W.H.M. Nissen, J. van der Voet, J. Karuza, *The Startup of the Dodewaard Natural Circulation BWR - Experiences*, Nuclear Technology, Vol. 107, pp. 93-102, July 1994.
- [6.2-2] T.H.J.J. van der Hagen, F.J. van der Kaa, J. Karuza, W.H.M. Nissen, A.J.C. Stekelenburg, J.A.A. Wouters, *Startup of the Dodewaard Natural Circulation Boiling Water Reactor*, GKN-report 92-017/FY/R (1992).
- [6.2-3] J.A.A. Wouters, *Evaluation of the February 1992 Startup Data of the Dodewaard Natural Circulation BWR*, KEMA-Report 41180-NUC 96-2335 (1996).
- [6.2-4] J.A.A. Wouters, F.J. van der Kaa, W.H.M. Nissen, (1991), *Measurements on the Thermal Hydraulics and Reactor Physics of the Dodewaard Natural Circulation BWR*. Proceedings of the Specialists meeting on incore instrumentation and reactor core assessment, Pittsburgh, PA, USA, October 1-4, 1991, pp. 99-106.
- [6.2-5] A.J.C. Stekelenburg, *Statics and Dynamics of a Natural Circulation Cooled Boiling Water Reactor*, Thesis, Interfaculty Reactor Institute, Delft University of Technology (1994).
- [6.2-6] J.A.A. Wouters, F.C.M. Verhagen, *Validation of LWRSIM3.10 for Dodewaard*, KEMA-report 13705-NUC 92-2247 (1993).

- [6.2-7] F. Inada, Y. Yasuo, *The Boiling Flow Instability of a Natural Circulation BWR with a Chimney at Low Pressure Startup*, Proceedings of the International Conference on the Design and Safety of Advanced Nuclear Power Plants (ANP'92), Tokyo, Japan, October 25-29, 1992, paper 25.3 (1992).
- [6.2-8] T.H.J.J. van der Hagen, , A.J.C. Stekelenburg (1995), *The Low-Power Low-Pressure Flow Resonance in a Natural Circulation Cooled Boiling Water Reactor*, Proceedings of the 7th International Meeting on Nuclear Reactor Thermal Hydraulics NURETH-7, Saratoga Springs, NY, USA, September 10-15, 1995, Vol. 4, pp. 2785-2795.
- [6.2-9] J.A.A. Wouters, J.B. Morales and H.T. Kim, *Description of the TRACG Analysis of the February 1992 Startup of the Dodewaard Natural Circulation BWR*, KEMA Report 41180-NUC 96-2043, May 1996.

Table 6.2-1
Sequence of Steps of a Regular Startup

1. Heat reactor coolant to 100°C at atmospheric pressure:
 - Place the Reactor Shutdown Cooling (SDC) System heaters in operation if needed.
 - Terminate *temporarily* RSA cooling flow to reduce thermal stratification in lower plenum.
 - Due to the hydrostatic head, the local pressure and saturation temperature are higher at the bottom of the vessel. Thus, the subcooling increases from almost zero at the water level surface, up to about 20°C at the bottom of the vessel (assuming the liquid temperature is 100°C over the whole RPV).
2. Deaerate reactor coolant.
 - Draw vacuum at main condenser.
 - Open isolation condenser vent line and main steam drain line to establish a partial vacuum at the reactor dome (turbine bypass valves and control valves closed).
3. Withdraw control rods to establish reactor criticality.
4. Increase power at a heatup rate less than 55 K/hr:
 - Control reactor power with control rod motion.
 - Pressure is determined by the amount of produced steam (turbine valves are closed, only a small main steam vent line is used for venting steam).
5. As pressure increases, open turbine bypass valve to control pressure.
6. Place Reactor Water Cleanup System (RZS) in operation to:
 - Reduce thermal stratification.
 - Control reactor water level.
 - Maintain water chemistry.
7. Switch off Shutdown Cooling System.
8. Startup the turbine at pressures round 3.0 MPa.
9. Turbine is synchronized at rated pressure of 7.0 MPa.
10. Continue power ascension.

Table 6.2-2
Sequence of Steps During the February 1992 Startup

Time (hh.mm)	Elapsed Time(s)	Step
16:00	-21,900	RSA System switched OFF to allow heatup of vessel bottom. SDC System switched into heatup mode, supplying 95°C water to the vessel.
20:45	-4800	RSA system switched ON.
21:02	-3900	Start withdrawal of control rods.
22:04	0	<i>Reactor critical</i>
22:19	840	Start further withdrawal of control rods. The turbine bypass valve is closed: only a little vent line is available (15 mm diam.).
23:04	3540	End withdrawal of control rods.
23:15	4200	Start 1st physics measurements at p=0.31 MPa.
01:30	12,300	End 1st physics measurements at p=0.31 MPa
02:53	17,280	Start of further withdrawal of control rods. Result: reactor pressure increase from ~0.3 to ~0.4 MPa. The pressure increase is the result of pulling rods (power increase). The bypass valve is still kept closed.
03:56	21,060	End of further withdrawal of control rods.
04:30	23,100	RZS switched ON for both drains (bottom tap and side tap).
05:00	24,900	SDC switched OFF. At this time the turbine bypass valve has been opened, and the pressure control system has been put into operation.
05:15	25,800	Start of further withdrawal of control rods. Result: reactor pressure increase from ~0.4 to ~0.6 MPa. According to the operating procedures, the opening of the bypass valve is supposed to be somewhere between 10 and 15%.
05:31	26,760	End of further withdrawal of control rods.
06:00	28,500	Start of lowering of the water level. This is done by temporarily reducing the RZS return flow.
06:00	28,500	Start of 2nd physics measurement at p=0.6 MPa.
06:50	31,500	End of 2nd physics measurement at p=0.6 MPa.
06:56	31,860	Start of further withdrawal of control rods.
07:20	33,300	End of further withdrawal of control rods.
07:24	33,540	Start of 3rd physics measurement at p=1.1 MPa.
07:45	34,800	Reactor vessel level has reached 50%. The RZS return flow is now set approximately equal to the drain flow again, to keep the water level constant.
08:20	36,900	End of 3rd physics measurement at p=1.1 MPa
08:39	38,040	Start of further withdrawal of control rods.
09:10	39,900	End of further withdrawal of control rods.

Table 6.2-2 (continued)
Sequence of Steps During the February 1992 Startup

Time (hh.mm)	Elapsed Time(s)	Step
09:34	41,340	Start of 4th physics measurement at p=2.0 MPa
10:31	44,760	End of 4th physics measurement at p=2.0 MPa
10:38	45,180	Start of further withdrawal of control rods.
11:06	46,860	End of further withdrawal of control rods.
11:10	47,100	Start of 5th physics measurement at p=3.0 MPa
12:14	50,940	End of 5th physics measurement at p=3.0 MPa
13:16	54,660	Start of 6th physics measurement at p=4.0 MPa
14:21	58,560	End of 6th physics measurement at p=4.0 MPa
15:02	61,020	Start of 7th physics measurement at p=5.0 MPa
15:52	64,020	End of 7th physics measurement at p=5.0 MPa
17:03	68,280	Start of 8th physics measurement at p=6.0 MPa
17:31	69,960	End of 8th physics measurement at p=6.0 MPa
18:04	71,940	Start of 9th physics measurement at p=7.0 MPa
18:57	75,120	End of 9th physics measurement at p=7.0 MPa

Table 6.2-3
Overview of All Available Measurement Data

Parameters set by the operators:

- System pressure*
- Water level*
- Control rod pattern

Measured quantities:

- Flows and temperatures of :
 - Feedwater (FW)
 - Steam flow*
 - Reactor water cleanup (RZS)
 - Control rod drive (RSA)
- Downcomer temperature noise
- Downcomer subcooling**
- Downcomer pressure differences**
- Bypass temperatures
- Bypass temperature noise
- Ex-vessel neutron flux*

Parameters calculated from measured quantities:

- Thermal power: calculated from (a) heat balance and (b) ex-vessel neutron flux
- Downcomer velocity: from cross-correlation of downcomer temperature noise
- Bypass velocity: calculated from cross-correlation of bypass temperature noise**
- Decay ratio: calculated from ex-vessel neutron flux**

* Time-dependent pen-writer recordings available

** Only one-hour average values available

Table 6.2-4
Comparison of Key Features of Dodewaard and SBWR

[

Redacted

]

Table 6.2-5
Vessel Axial and Radial Nodalization

[

Redacted

]

Table 6.2-6
Channel Initial Conditions

[

Redacted

]

Table 6.2-7
Measurement Data Used for Initial and Boundary Conditions

Converted data Dodewaard startup 15/16 February 1992

Nr	Time hh:mm	Elapsed time sec	Pres- sure bar	Steam flow kg/s	Feedw. flow kg/s	CRD flow kg/s	RWCU drain kg/s	RWCU return kg/s	SDC flow kg/s	Sparger flow kg/s	CRGT flow kg/s	Water level m.TOC	Water level m.TOC	Water level m.TOC	Equilibr. power MWth
1	23:45	6000	3,1	1,0	0,0	1,6	0,0	0,0	8,6	9,4	0,82	o.i.r.	o.i.r.	2,60	3,7
2	05:59	28440	6,4	2,9	0,0	1,7	2,7	1,4	0,0	0,9	0,87	1,81	o.i.r.	1,96	9,3
3	06:14	29340	6,4	2,3	0,0	1,6	2,7	1,4	0,0	0,8	0,81	1,66	1,63	1,71	7,9
4	06:38	30780	6,4	2,3	0,4	1,7	3,0	1,3	0,0	1,3	0,85	1,35	1,45	1,52	7,9
5	07:24	33540	10,8	4,1	0,5	n.m.	n.m.	n.m.	0,0	n.m.	n.m.	0,75	n.m.	n.m.	n.m.
6	07:40	34500	10,8	3,7	0,5	n.m.	n.m.	n.m.	0,0	n.m.	n.m.	0,17	n.m.	n.m.	n.m.
7	08:20	36900	10,8	3,1	0,9	n.m.	n.m.	n.m.	0,0	n.m.	n.m.	0,21	n.m.	n.m.	n.m.
8	09:34	41340	20,6	5,2	1,9	n.m.	n.m.	n.m.	0,0	n.m.	n.m.	0,28	n.m.	n.m.	n.m.
9	09:59	42840	20,5	5,2	1,8	n.m.	n.m.	n.m.	0,0	n.m.	n.m.	0,37	n.m.	n.m.	n.m.
10	10:31	44760	20,5	5,1	1,6	n.m.	n.m.	n.m.	0,0	n.m.	n.m.	0,37	n.m.	n.m.	n.m.
11	11:10	47100	30,5	7,3	4,0	n.m.	n.m.	n.m.	0,0	n.m.	n.m.	0,33	n.m.	n.m.	n.m.
12	11:43	49080	30,5	7,5	3,2	n.m.	n.m.	n.m.	0,0	n.m.	n.m.	0,39	n.m.	n.m.	n.m.
13	12:14	50940	30,5	7,2	3,1	n.m.	n.m.	n.m.	0,0	n.m.	n.m.	0,36	n.m.	n.m.	n.m.
14	13:16	54660	40,4	9,7	5,7	1,7	4,3	4,2	0,0	6,6	0,84	0,44	0,44	0,48	29,7
15	13:51	56760	40,4	9,7	5,7	1,7	4,3	4,2	0,0	6,5	0,84	0,43	0,43	0,47	29,7
16	14:21	58560	40,4	9,4	5,4	1,7	4,3	4,2	0,0	6,2	0,84	0,44	0,44	0,48	29,0
17	15:02	61020	50,2	12,0	9,1	1,7	4,3	4,2	0,0	9,9	0,84	0,46	0,47	0,52	35,2
18	15:52	64020	50,2	11,7	9,3	1,7	4,3	4,3	0,0	10,1	0,84	0,47	0,49	0,54	34,5
19	17:03	68280	59,9	14,6	12,9	1,7	4,3	4,3	0,0	13,7	0,84	0,52	0,54	0,59	41,8
20	17:31	69960	59,9	13,6	14,0	1,7	4,3	4,3	0,0	14,9	0,84	0,52	0,55	0,58	38,5
21	18:04	71940	69,7	15,4	15,5	1,7	4,2	4,3	0,0	16,3	0,84	0,57	0,61	0,63	42,9
22	18:32	73620	69,8	15,5	15,1	1,7	4,2	4,3	0,0	15,9	0,84	0,57	0,61	0,65	43,5
23	18:57	75120	69,8	14,9	15,0	1,7	4,2	4,3	0,0	15,8	0,84	0,56	0,61	0,63	41,8

n.m. = not measured

n.i.o. = not in operation

Table 6.2-7 (cont'd)
Measurement Data Used for Initial and Boundary Conditions

Converted data Dodewaard startup 15/16 February 1992

Nr	Time hh:mm	Elapsed time sec	Feedw. temp dgr.C	Sparger temp. dgr.C	CRD temp. dgr.C	RWCU drain dgr.C	RWCU return dgr.C	SDC drain dgr.C	SDC return dgr.C
1	23:45	6000	87,3	99,2	13,0	n.i.o.	n.i.o.	126,5	94,4
2	05:59	28440	74,1	107,0	13,1	154,9	144,7	n.i.o.	n.i.o.
3	06:14	29340	70,8	81,5	13,1	154,0	146,0	n.i.o.	n.i.o.
4	06:38	30780	70,1	88,8	13,3	154,8	145,4	n.i.o.	n.i.o.
5	07:24	33540	n.m.	n.m.	n.m.	n.m.	n.m.	n.i.o.	n.i.o.
6	07:40	34500	n.m.	n.m.	n.m.	n.m.	n.m.	n.i.o.	n.i.o.
7	08:20	36900	n.m.	n.m.	n.m.	n.m.	n.m.	n.i.o.	n.i.o.
8	09:34	41340	n.m.	n.m.	n.m.	n.m.	n.m.	n.i.o.	n.i.o.
9	09:59	42840	n.m.	n.m.	n.m.	n.m.	n.m.	n.i.o.	n.i.o.
10	10:31	44760	n.m.	n.m.	n.m.	n.m.	n.m.	n.i.o.	n.i.o.
11	11:10	47100	n.m.	n.m.	n.m.	n.m.	n.m.	n.i.o.	n.i.o.
12	11:43	49080	n.m.	n.m.	n.m.	n.m.	n.m.	n.i.o.	n.i.o.
13	12:14	50940	n.m.	n.m.	n.m.	n.m.	n.m.	n.i.o.	n.i.o.
14	13:16	54660	40,5	75,6	10,8	247,6	199,9	n.i.o.	n.i.o.
15	13:51	56760	41,8	77,3	9,1	246,8	199,0	n.i.o.	n.i.o.
16	14:21	58560	42,1	78,1	9,1	247,1	198,8	n.i.o.	n.i.o.
17	15:02	61020	40,4	74,7	9,6	259,5	209,3	n.i.o.	n.i.o.
18	15:52	64020	41,3	75,1	9,5	260,0	209,1	n.i.o.	n.i.o.
19	17:03	68280	33,5	71,5	9,6	271,0	218,8	n.i.o.	n.i.o.
20	17:31	69960	33,5	71,3	9,7	270,9	218,6	n.i.o.	n.i.o.
21	18:04	71940	34,8	72,9	9,9	280,6	226,2	n.i.o.	n.i.o.
22	18:32	73620	32,3	71,2	9,8	280,9	226,5	n.i.o.	n.i.o.
23	18:57	75120	32,6	71,7	9,8	281,1	226,4	n.i.o.	n.i.o.

n.m. = not measured

n.i.o. = not in operation

Table 6.2-8
Calculation of Subcooling Number and Phase Change Number

[

Redacted

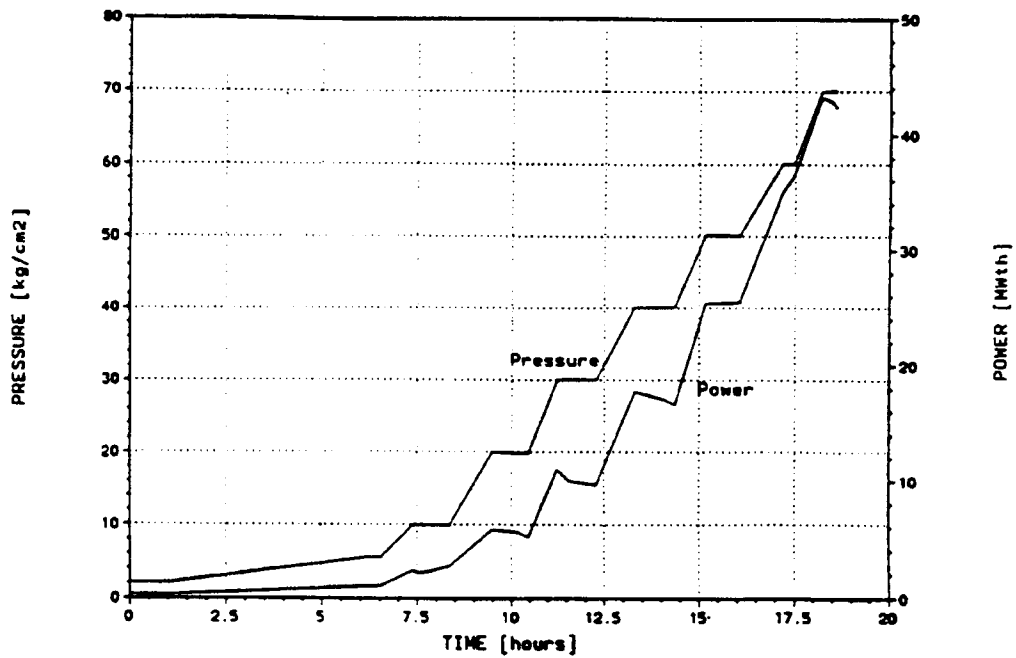
]

Table 6.2-9
Assessment of TRACG Accuracy for Dodewaard Startup Tests

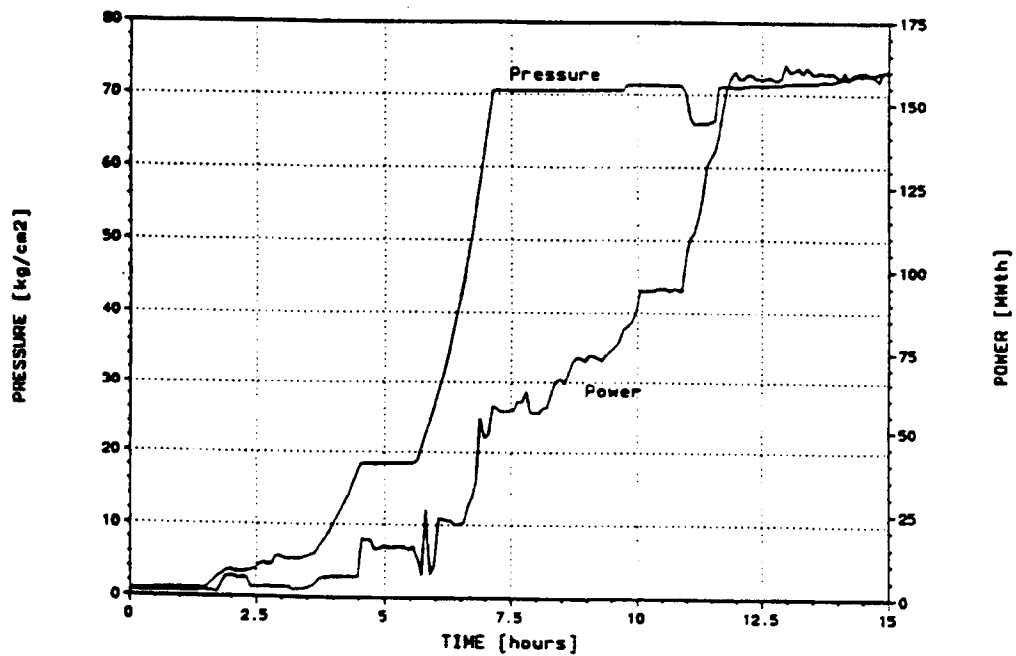
[

Redacted

]



Reactor vessel pressure and reactor power during the startup on February 15 and 16, 1992.



Reactor vessel pressure and reactor power during the startup on June 11 and 12, 1992.

Figure 6.2-1. Comparison of the Power-Pressure Path of the February 1992 Startup with a Regular Startup (From [6.2-9]).

Figures 6.2-2 through 6.2-21
Pages 6.2-34 through 6.2-53

Redacted

6.3 CRIEPI Low Pressure Oscillation Tests

6.3.1 Introduction

Thermal-hydraulic oscillations that can occur in boiling two-phase flow have been investigated for a long time and detailed reviews and classifications have been published [6.3-1 - 6.3-2]. In most of the published results (experimental and theoretical), density wave oscillations were considered, and the mechanism of these oscillations is well understood. Traditionally, density wave oscillations have been analyzed using frequency domain methods, which consist of a first order perturbation of a given frequency to the steady-state solution. These methods generally calculate the onset of density wave oscillations well. However, because of linear considerations, frequency domain methods cannot calculate the amplitude of limit cycle oscillations. To capture nonlinear effects of the density wave oscillations, time domain codes have to be used. TRACG has been successfully qualified against test data in the FRIGG facility (Section 3.3.8) and plant data (LaSalle Stability Event, Leibstadt Stability Tests) [6.3-4, 6.3-5]. It has been suggested that oscillations caused by flashing in a SBWR chimney region could be a potential problem during SBWR startup at low pressure and natural circulation conditions. Detailed data for different system pressures, power and temperature conditions were obtained at the CRIEPI test facility [6.3-6, 6.3-7]. The design of the CRIEPI test facility, applicability of the test data to the SBWR, the TRACG model and comparison of the experimental and analytical results are discussed in the following sections.

6.3.2 Test Facility/Test Matrix

A schematic diagram of the CRIEPI test facility is shown in Figure 6.3-1. The test loop consisted of two electrically heated channels ($\approx 1.8\text{m}$ in height), a chimney ($\approx 5.5\text{m}$ in height), a separator (upper plenum), downcomer, preheater and subcooler. (The condenser and pressure relief line are not shown.) The total length of the downcomer section was $\approx 30\text{m}$. The maximum channel power capability was 64 kW, but power in this test series was limited to 10 kW. The water temperature at the channel inlet was measured by thermocouples and the flow rate was measured by an orifice flow meter [6.3-6]. The tests were conducted at three different pressure levels: 0.2 MPa, 0.35 MPa and 0.5 MPa.

Detailed measurements of the pressure drop across different sections of the test loop under forced liquid flow conditions were used to obtain local loss coefficients. A schematic diagram showing the eight segments over which the pressure drop measurements were made is presented in Figure 6.3-2. The pressure drops were measured at nine different flow rates (Table 6.3-1). On the basis of these data, local loss coefficients were defined by the CRIEPI experimenters for the channel inlet, chimney exit and the flow convergence region between the top of the channels and the chimney inlet (Segments 5 and 6 in Figure 6.3-2).

The transient data for a fixed pressure level were obtained by maintaining constant channel power and adjusting channel inlet subcooling. Channel inlet subcooling was defined relative to the saturation temperature at system (separator) pressure. Thus, the subcooling can be negative even though the channel inlet temperature is less than local saturation temperature. For high inlet subcooling ($\approx 20\text{ K}$), a constant circulation flow was established. By adjusting the electrical power to the preheater, a new channel inlet subcooling was established and transient

data for pressure drop, flow and temperature were collected. This procedure was repeated at different channel power levels to generate a Power-Inlet Subcooling stability map.

The test matrix for a system pressure of 0.2 MPa and channel power of 2.5 kW/chan (heat flux $\approx 40 \text{ kW/m}^2$) is shown in Table 6.3-2. Stable circulation flow was observed at an inlet subcooling of 20.7 K (Figure 6.3-3, Curve 1). An increase in the channel inlet temperature led to a higher circulation flow. At this pressure and power level, no flow or void fraction oscillations were observed when the channel inlet subcooling was within the range of 20.7 K to 8.7 K. Starting at an inlet subcooling of 7.5 K, periodic large flow increases were observed (Curve 2 in Figure 6.3-3). The time interval between two consecutive flow peaks was on the order of 100s. This time interval, as well as the amplitude of the flow peak, varied with system pressure, channel power and channel inlet subcooling. The experimenters called the observed phenomena “intermittent” oscillations [6.3-6]. When the channel inlet subcooling approached 0 K, sinusoidal flow oscillations with a smaller period (on the order of 50s) were observed (Curve 3 in Figure 6.3-3). Eventually, as inlet subcooling was further reduced, stable circulation flow was restored (Curve 4 in Figure 6.3-3). For all four cases shown in Figure 6.3-3, the heat flux was not large enough to produce significant vapor generation in the heated channel section. However, there was flashing in the chimney for all except the case with the high (20.7 K) inlet subcooling. In summary, an oscillatory region with two boundaries (at high and low inlet subcooling) and encompassing two different types of oscillations was observed at the CRIEPI test facility.

6.3.3 Applicability of Data to SBWR

[

Redacted

]

[

Redacted

]

6.3.4 TRACG Model

[

Redacted

]

6.3.5 Test Simulation

[

Redacted

]

6.3.6 Results of Post-Test Calculations

[

Redacted

]

[

Redacted

]

[

Redacted

]

[

Redacted

]

6.3.6.1 Accuracy of TRACG Calculations

[

Redacted

]

6.3.7 Summary and Conclusion

Results of TRACG computer simulation were compared with CRIEPI experimental data for the steady-state and oscillatory regimes. Good agreement between TRACG results and experimental data was shown. Two modes of oscillation and their mechanism were analyzed. The Power-Inlet Subcooling stability map obtained with TRACG (system pressure 0.2 MPa) is in good agreement with the experimental stability map. Based on TRACG-CRIEPI test data comparisons, it can be concluded that TRACG can accurately calculate the oscillations observed at the CRIEPI test facility. Thus, TRACG can be used to analyze the potential for oscillations during SBWR startup.

6.3.8 References

- [6.3-1] J.A. Boure, et al., *Review of Two-Phase Flow Instability*, Nuc. Eng. and Design, 25, pp. 165-192 (1973).
- [6.3-2] A.E. Bergles, *Instabilities in Two-Phase Systems*, in A.E. Bergles. et al., *Two-Phase Flow in Power and Process Industries* (1981).
- [6.3-3] R.T. Lahey, Jr. and F.J. Moody, *The Thermal-Hydraulics of a Boiling Water Reactor* (1984).
- [6.3-4] J.G.M. Andersen et al, *Time-Domain Analysis of Thermal-Hydraulic Stability with TRACG - Sensitivity to Numerical Methods and Qualification to Data*, BWR Stability Symposium, Idaho (1989).
- [6.3-5] J.G.M Andersen,. et al., *TRACG Analysis of BWR Plant Stability Data*, Proc. of Int. Workshop on Boiling Water Reactor Stability, OECD, New York (1990).

- [6.3-6] F. Inada, et al., *Thermo-Hydraulic Instability of Natural Circulation BWR at Low Pressure Startup; Experimental Estimation of Instability Region with Test Facility Considering Scaling Law*”, Third Int. Conf. on Nuc. Eng., 1995, Kyoto, Japan (1995).
- [6.3-7] F. Inada, and A. Yasuo, *The Boiling Flow Instability of a Natural Circulation BWR with a Chimney at Low Pressure Startup*, Int. Conf. Des. Safety of Adv. Nuc. Power Plants, AESJ, 25,3 (1992).
- [6.3-8] J.G.M. Andersen, et al, *TRACG Qualification*, NEDE-32177P Revision 2 (2000).

Table 6.3-1
Forced Flow Data Points

No	1	2	3	4	5	6	7	8	9
Velocity (m/s)	0.0398	0.0676	0.0844	0.105	0.13	0.152	0.172	0.195	0.215

Table 6.3-2
Test Matrix (System Pressure = 0.2 MPa , Channel Power = 2.5 kW/chan)

Run No.	1	2	3	4	5	6	7	8	9
Inlet Subcooling (K)	20.7	18.5	16.6	14.6	12.2	10.6	9.7	8.7	7.5
Run No.	10	11	12	13	14	15	16	17	18
Inlet Subcooling (K)	6.2	5.1	4.3	3.5	2.8	2.1	0	-1.5	-2.1

Table 6.3-3
Comparison of Nondimensional Parameters Between the Test Loop and SBWR

Nondimensional Parameter	Physical Meaning	Rated Power Condition at 7.2 MPa		Startup Condition at 0.1 MPa	
		SBWR	CRIEPI	SBWR	CRIEPI
Froude Number	Gravity-to-fluid momentum ratio	0.058	0.053	0.00105	0.00078
Channel Inlet Loss Factor	Pressure loss coefficient	10 - 50	30	10-50	30
Chimney Exit Loss Factor		20 - 40	21	20 - 40	21
Nondimensional Downcomer Flow Area	Parameters depending on test facility shape	1.05	1.11	1.05	1.11
Nondimensional Chimney Flow Area		2.59	2.47	2.59	2.47
Nondimensional Chimney Length		3.34	3.38	3.34	3.38
Ratio of Vapor to Liquid Density	Density ratio	0.052	0.052	0.00062	0.00062
Subcooling Number	Inlet subcooling	0.58	0.58	9.0	9.0

Table 6.3-4
Assessment of TRACG Accuracy for CRIEPI Low Pressure Oscillation Tests

[

Redacted

]

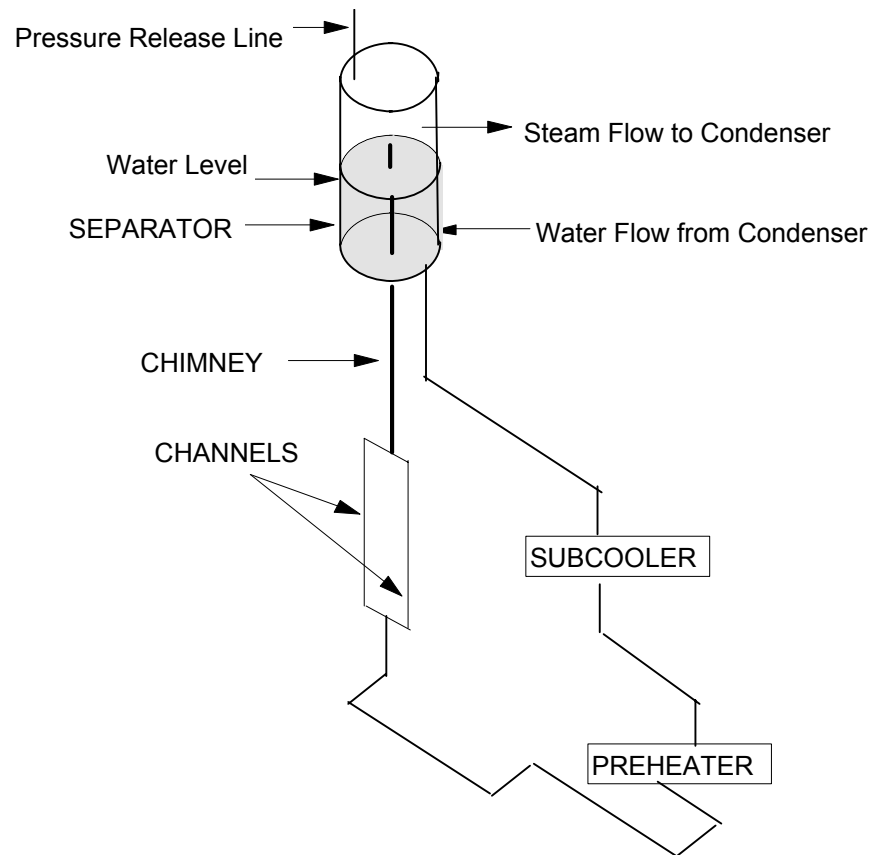


Figure 6.3-1 Schematic Diagram of the CRIEPI Thermal Hydraulic Test Facility

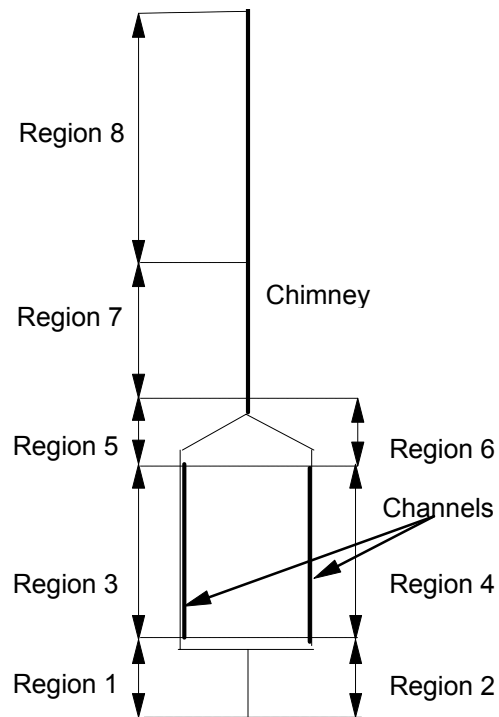


Figure 6.3-2 Schematic Diagram of the Pressure Drop Measurement Location

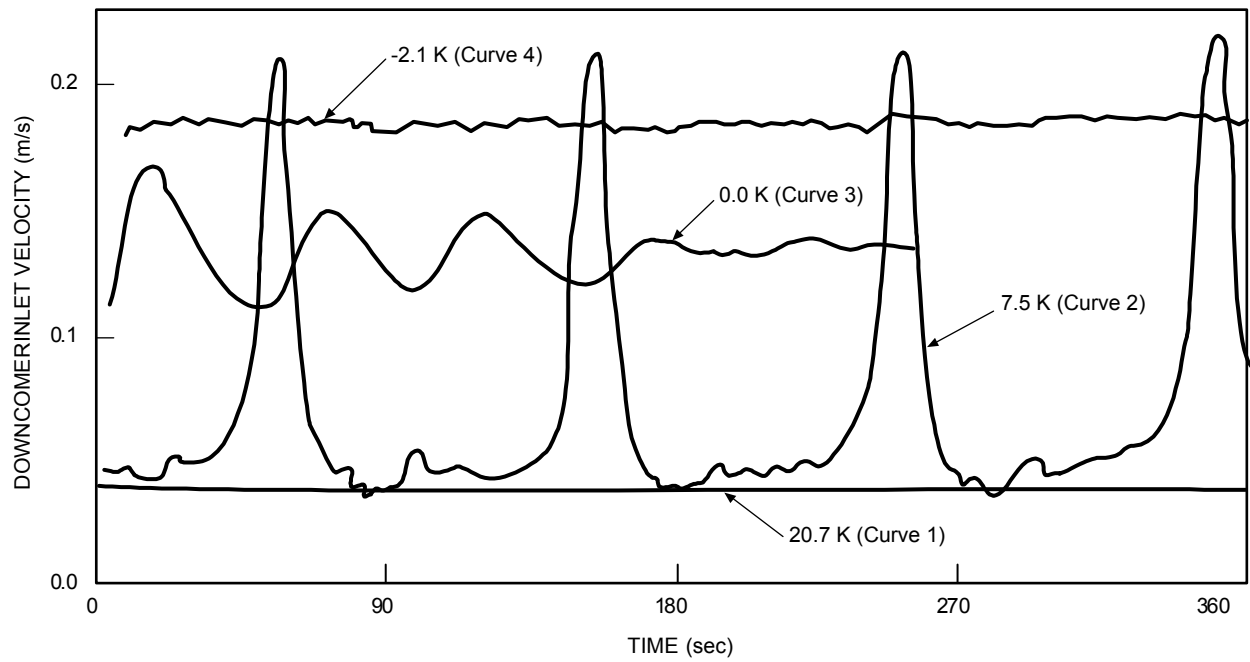


Figure 6.3-3 Sketch of CRIEPI Circulation Flow for Various Values of Inlet Subcooling

Figures 6.3-4 through 6.3-23
Pages 6.3-14 through 6.2-24

Redacted

6.4 PANDA Exploratory Tests

6.4.1 Introduction

Section 4.3 presented a post-test evaluation of data from the PANDA steady-state PCCS performance tests (the “S-series”). Pressure and steam flow oscillations were observed at PANDA during some of the steady-state shakedown tests. To further investigate and clarify the nature of these oscillations, five additional exploratory (“E-series”) tests were performed. The objective of these tests was to evaluate the sensitivity of the oscillations to the RPV power, RPV water level and air fraction in the PCCS inlet flow. This section presents the results of TRACG post-test evaluation of the E-series tests. The purpose of this evaluation is to identify the mechanism responsible for the observed oscillations and determine its sensitivity to system parameters. The TRACG02 version of TRACG was used for all simulations presented in this section.

6.4.2 Test Facility/Test Matrix

A summary description of the PANDA test facility was given in Section 5.7 and the configuration of the facility for the PCCS steady-state performance (“S-series”) tests was described in Section 4.3. The S-series matrix included both steam-air and pure-steam tests. The test facility configuration and instrumentation were the same during the E-series tests as they were during the S-series. The valve alignments for the E-series air/steam tests and steam only tests were also the same as they were during the S-series tests, except that the valves in lines connected to the RPV were opened to add or drain water from the RPV in order to investigate the effect of RPV level on the oscillations. The principal hardware modification for the S-series tests was to install a pipe to deliver steam directly from the RPV to the inlet of PCC3, the PCC unit tested in the S-series tests. Air was injected into the inlet line to provide specified steam-air mixtures to PCC3. The drywell vessels, from which the PCC units normally draw their inlet flow, were isolated from the system. The PCC3 drain line was open to the GDCS tank and the GDCS drain line was open to the RPV. The PCC3 vent line to the wetwell vessel was not submerged. For the steam-air tests, the wetwell pressure was controlled to keep the condenser pressure near 0.3 MPa. For the pure-steam tests, the valve on the vent line was closed and the condenser pressure was allowed to seek the level required to condense all of the inlet steam.

For all the data from the E-series tests, the amplitude of the pressure perturbations in the PCC line was smaller than the amplitude of the pressure perturbations in the RPV. Based on this observation, it was concluded that the RPV was the key component for the E-series oscillatory behavior. A schematic of the PANDA RPV is shown in Figure 6.4-1. The RPV total height is approximately 19m and the inner diameter is approximately 1.2m. Power input is provided by electrical heaters over an axial distance of 1.3m, extending from 0.2m above the bottom of the RPV. The chimney region is located above the heated region, and the total chimney height is 9.5m.

The test matrix for the exploratory tests is shown in Table 6.4-1. Initial conditions for all tests were similar except for the initial RPV water level. The tests can be divided into tests with initial water level below the top of the chimney (Tests E1A and E1B) and tests with initial water level above the top of the chimney (Tests E1C, E2 and E3). For Test E3, water was initially

added to the RPV and then slowly drained to reduce the level. For Test E2, the power level was reduced by 50% during the test. All the exploratory tests had an air injection rate of 6 g/s except for Test E3, which was run with pure-steam inlet conditions.

Figures 6.4-2 through 6.4-12 show key measurements from each of the E-Series tests. A summary of key observations from these measurements is given in Tables 6.4-2 and 6.4-3. For Tests E1A (Figures 6.4-2 and 6.4-3) and E1B (Figures 6.4-4 and 6.4-5), the pressure and flow are very noisy, without any dominant frequency. These two tests were performed with the RPV collapsed level below the top of the chimney (Table 6.4-1). In contrast, Tests E1C and E2 were performed with the RPV collapsed level above the top of the chimney. The measurements from Test E1C (Figures 6.4-6 and 6.4-7) show a well-defined oscillation with a period of approximately 240s. Similar behavior is observed in Test E2 (Figures 6.4-8 and 6.4-9) up to the time when the power was reduced by 50%, at approximately 600s after the beginning of data recording, at which point the oscillation stopped. Tests E1C and E2 were characterized by relatively small temperature variations at the channel inlet (about 0.5 K) and larger temperature variations at the chimney inlet (about 4 K). This indicates that significant oscillations in circulation flow were occurring. The collapsed level variation in Tests E1A, E1B, E1C and E2 was small (Table 6.4-1).

Based on the available data it can be concluded that Test E1C and E2 are almost identical (before the power reduction in Test E2): initial power, collapsed level position and system pressure are the same. The amplitude of the flow and pressure oscillations in Test E1C may have decreased because the test conditions were at the stability threshold and drifted slightly. Based on the available data, it also can be concluded that at the beginning of data recording in Test E2 the oscillatory behavior was not fully developed. It could be that if Test E2 were run for a longer time at the initial power level, the observed oscillations would have also died out, as was observed in Test E1C.

The conditions for Test E3 differed from those for the other tests in two respects. First, the test was run without air injection and with the vent line from the PCC lower header to the wetwell closed. Second, the RPV collapsed water level changed significantly over the course of the test. At the beginning of the test, the collapsed level was slightly below the chimney exit. During the first 500s of the test, saturated water was added to the RPV to raise the level to approximately 11.4m (0.4m above the chimney exit). The initial collapsed level given in Table 6.4-1 is the level at 500s from test initiation. Water was then slowly drained from the RPV until, at the end of the test, the collapsed level was again below the chimney exit. Relatively large pressure and chimney inlet temperature oscillations, similar to those in Tests E1C and E2, occurred at low collapsed levels (i.e., near the beginning and end of the test). The pressure oscillations, which were actually larger than those observed in Tests E1C and E2, did not produce oscillations in the RPV steam flow. The absence of steam flow oscillations in Test E3 can be attributed to the close coupling between the PCC3 condenser unit and the RPV, enabled by closure of the PCC3 vent. Pressure changes in the RPV were matched by corresponding changes in the RPV-to-PCC3 steamline with essentially zero time delay. As a result, the steam flow remained nearly constant.

6.4.3 Applicability of Data to SBWR

[

Redacted

]

[

Redacted

]

6.4.4 TRACG Models

[

Redacted

]

[

Redacted

]

6.4.5 Test Simulation

[

Redacted

]

6.4.6 Results of Post-Test Calculations

[

Redacted

]

[

Redacted

]

6.4.7 Summary and Conclusion

Results of TRACG simulations were compared with PANDA E-series test data for the two E-series tests (E1C and E2) which exhibited well-defined oscillations. From these comparisons, it was concluded that the instabilities observed in these tests were primarily associated with flashing phenomena in the chimney region and mixing in the upper plenum. The period of oscillation is governed by channel heatup time and propagation time around the RPV circulation path. Good agreement between TRACG results and experimental data was shown and, accordingly, it was concluded that TRACG is qualified for the evaluation of flashing instabilities during SBWR startup. When the two-phase level approached the chimney exit in the PANDA tests, as was the case for Tests E1A and E1B, some void propagation in the downcomer region (carryunder flow) and flashing in the downcomer due to system pressure oscillations are predicted. These phenomena introduce additional feedback effects which may explain the noisy behavior exhibited by these tests.

6.4.8 Reference

[6.4-1] NEDC-32288P, *Scaling of the SBWR Related Tests*, October 1995.

Table 6.4-1
Test Matrix for PANDA E-series Tests

Test	Initial Power (kW)	Final Power (kW)	Initial Collapsed Level Position (m)	Final Collapsed Level Position (m)	Air Injection Rate (g/s)	Comments
E1A	460	460	10.75	10.7	6	
E1B	460	460	10.85	10.8	6	
E1C	460	460	11.12	11.08	6	
E2	460	230	11.2	11.15	6	Power Reduction Test
E3	460	460	11.4	10.8	0	Water Drained from the RPV

Table 6.4-2
Major Observations from PANDA E-series Tests (Pressure)

[

Redacted

]

Table 6.4-3
Major Observation from PANDA E-series Tests (Flow)

[

Redacted

]

Table 6.4-4
Comparison of the Key Features of PANDA Facility and SBWR

[

Redacted

]

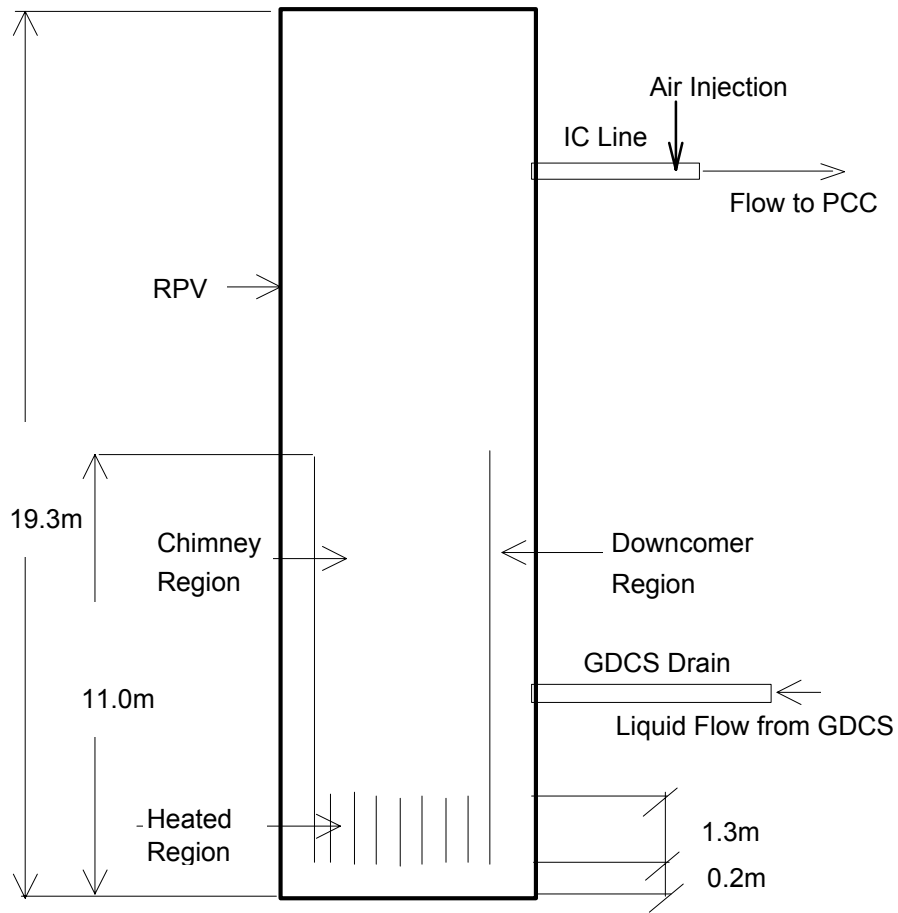


Figure 6.4-1 PANDA RPV Schematic

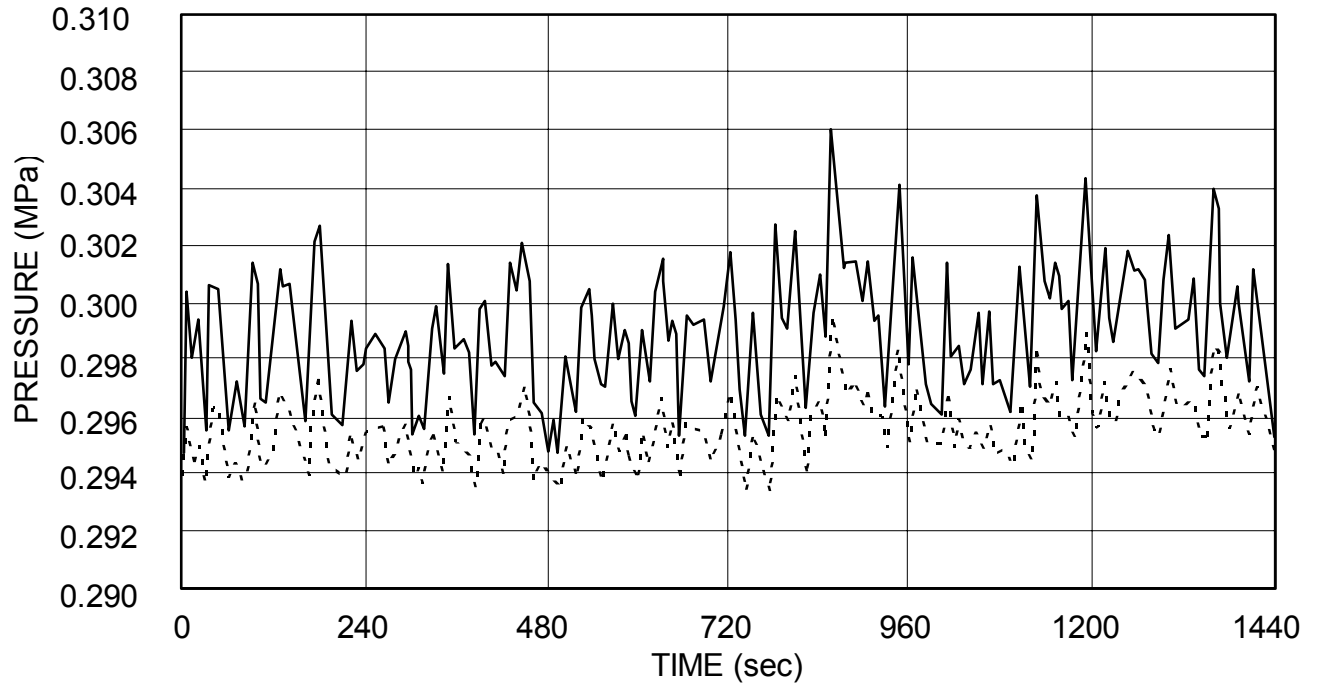


Figure 6.4-2 Test E1A: Pressure at the Top of the RPV (solid) and in the PCC3 Inlet Line (dash)

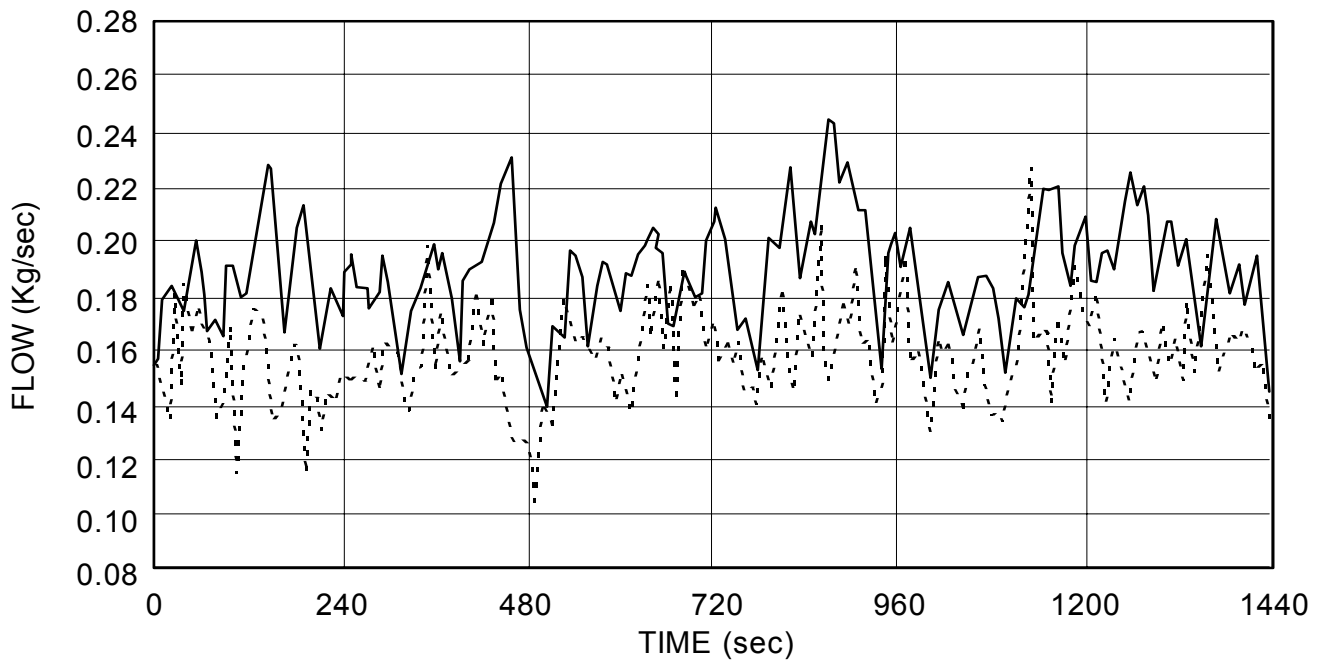


Figure 6.4-3 Test E1A: Flow from the RPV to PCC3 (solid) and from PCC3 to the GDCS Pool (dash)

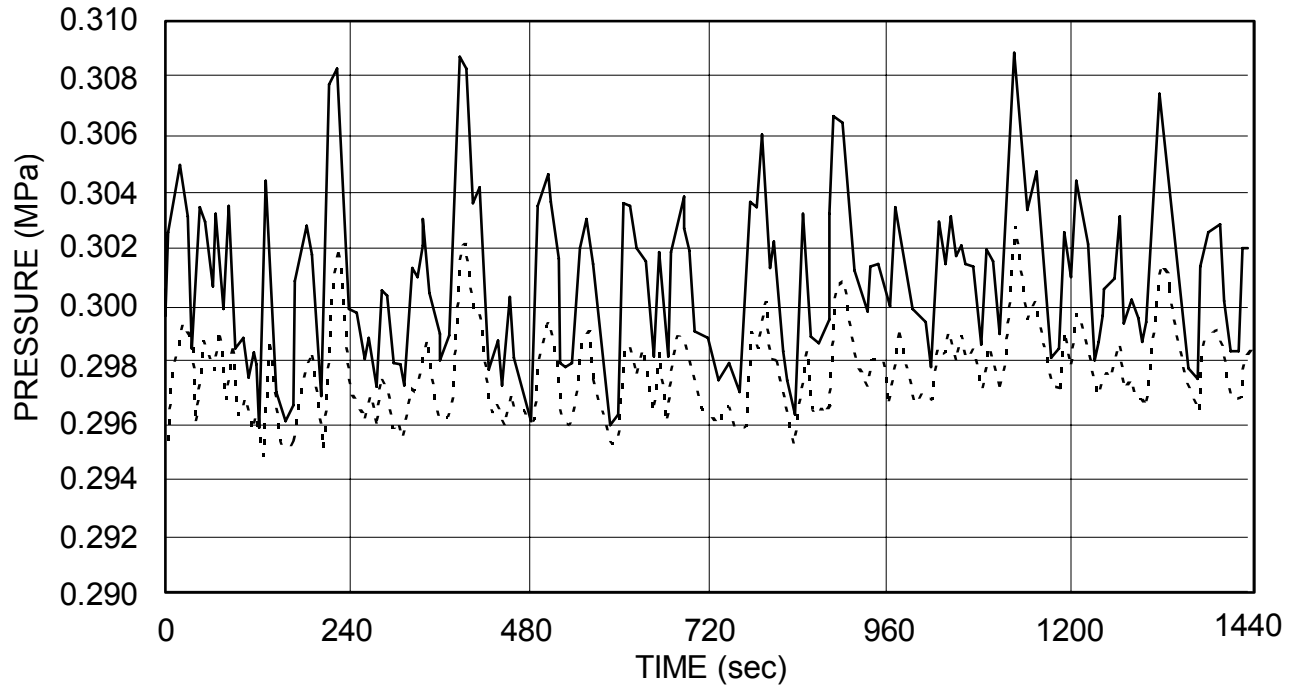


Figure 6.4-4 Test E1B: Pressure at the Top of the RPV (solid) and in the PCC3 Inlet Line (dash)

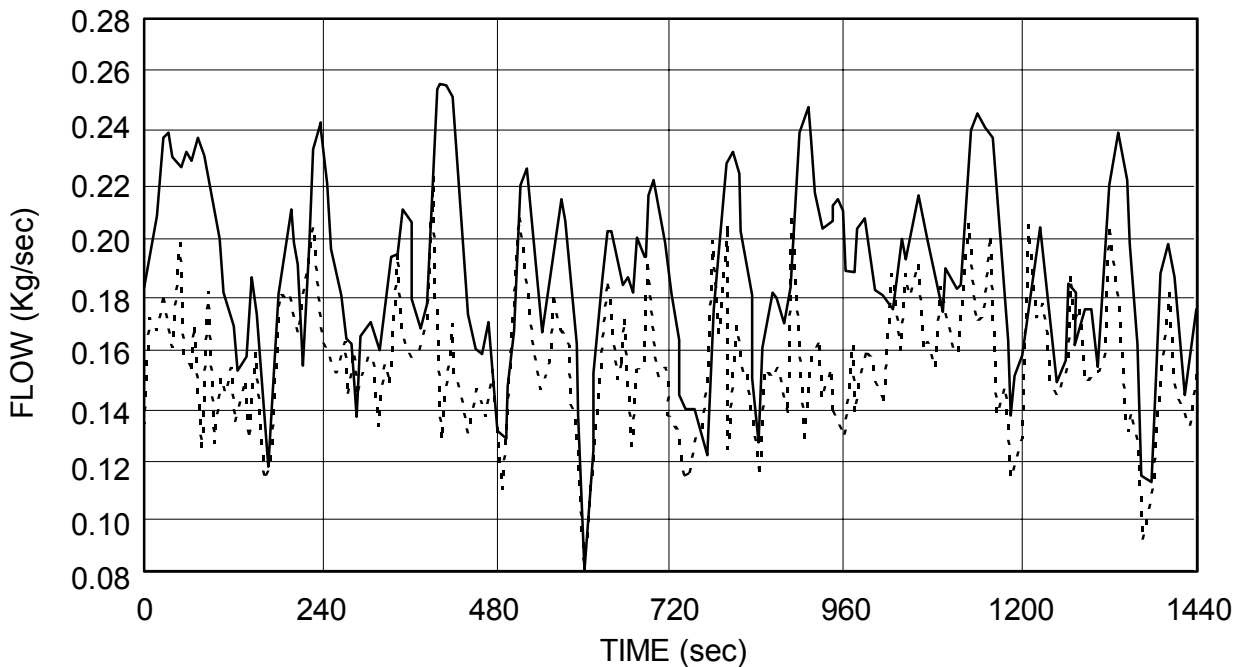


Figure 6.4-5 Test E1B: Flow from the RPV to PCC3 (solid) and from PCC3 to the GDCS Pool (dash)

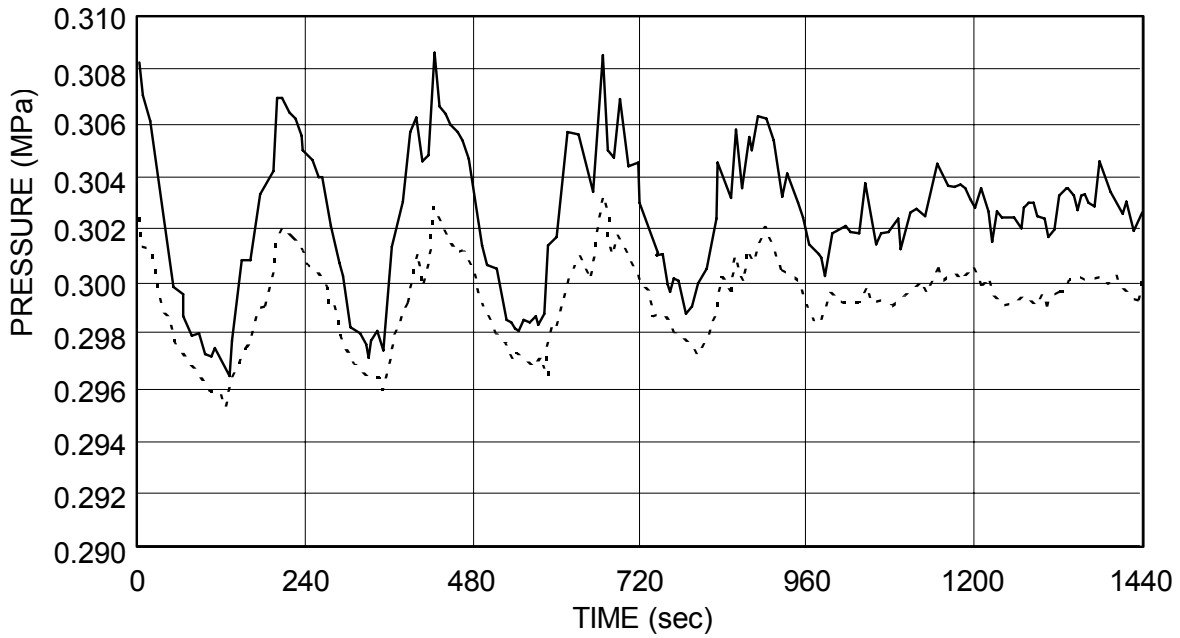


Figure 6.4-6 Test E1C: Pressure at the Top of the RPV (solid) and in the PCC3 Inlet Line (dash)

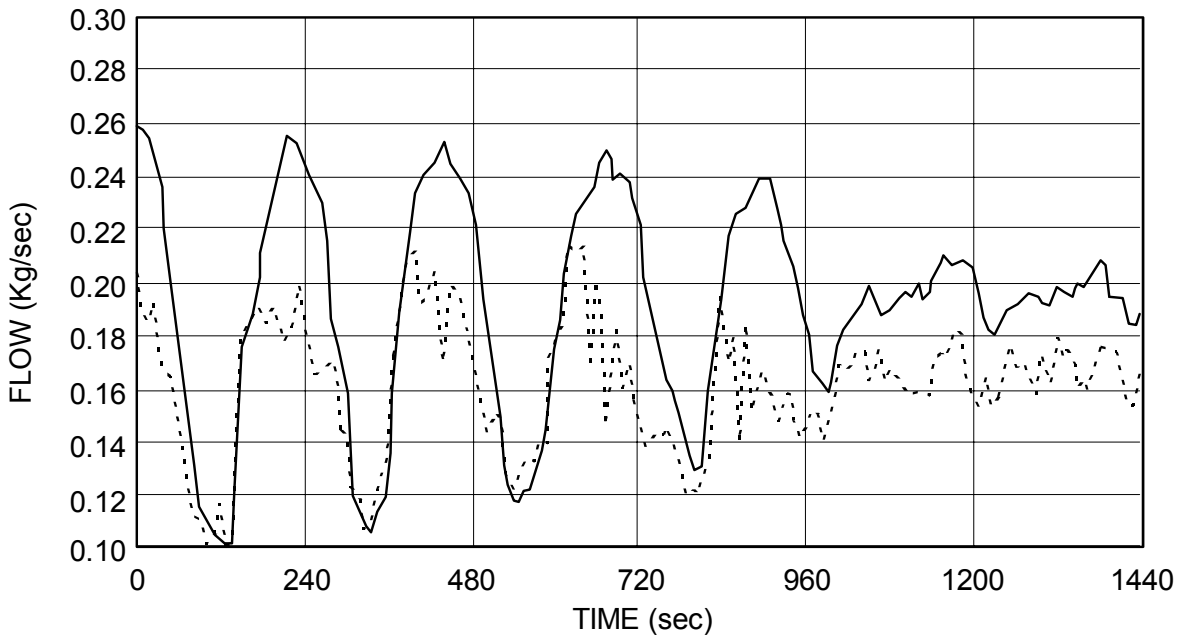


Figure 6.4-7 Test E1C: Flow from the RPV to PCC3 (solid) and from PCC3 to the GDCS Pool (dash)

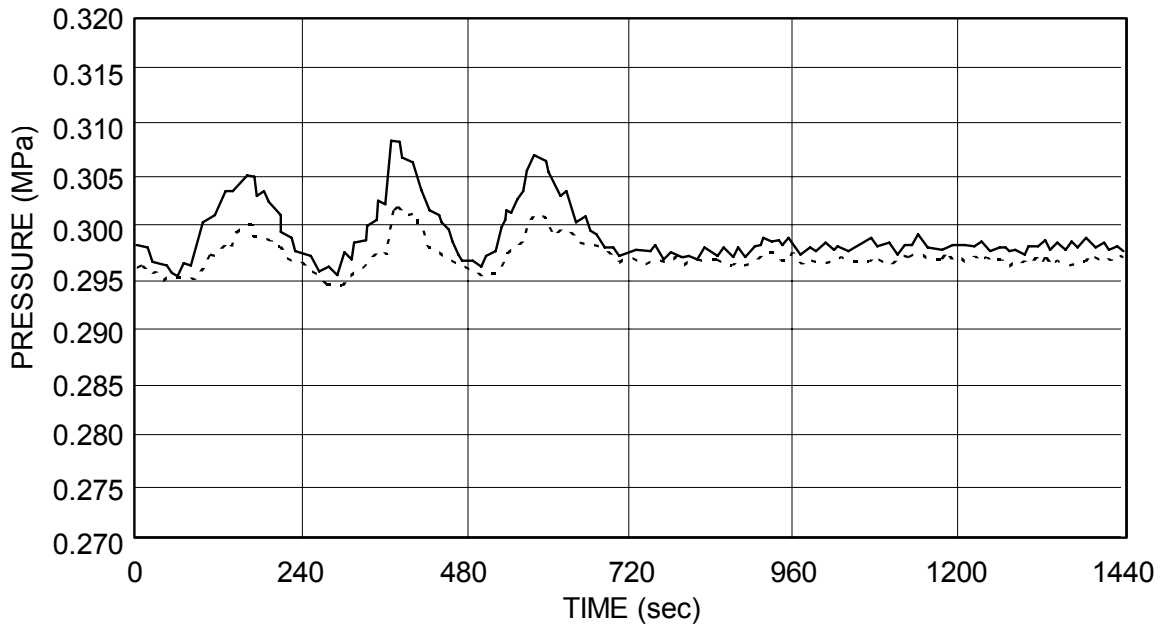


Figure 6.4-8 Test E2: Pressure at the Top of the RPV (solid) and in the PCC3 Inlet Line (dash)

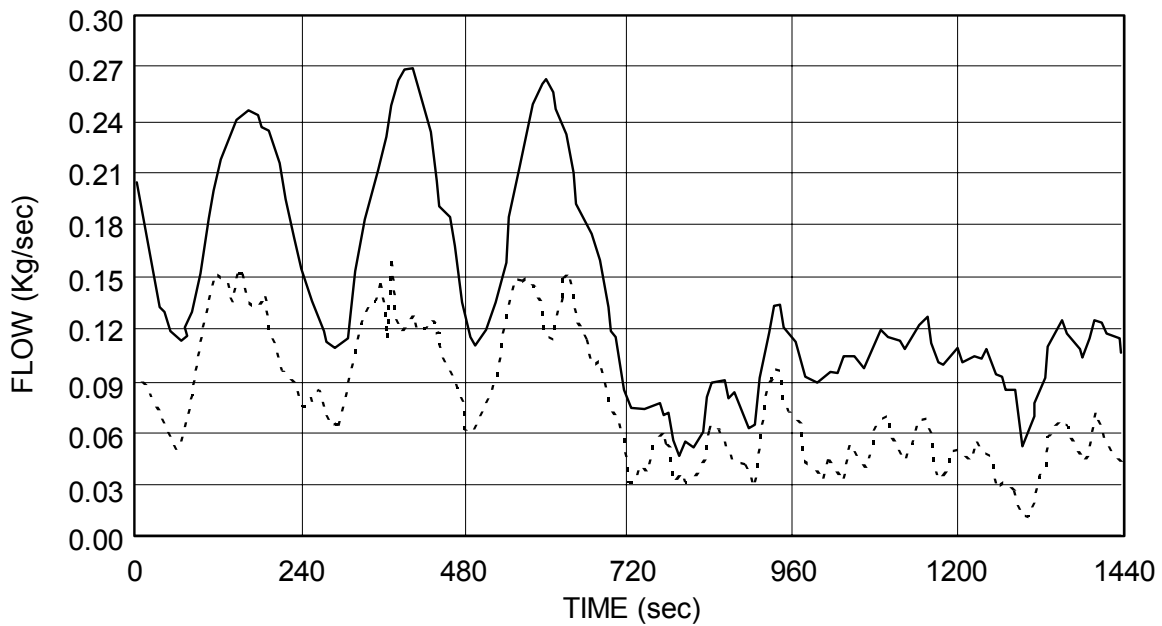


Figure 6.4-9 Test E2: Flow from the RPV to PCC3 (solid) and from PCC3 to the GDCS Pool (dash)

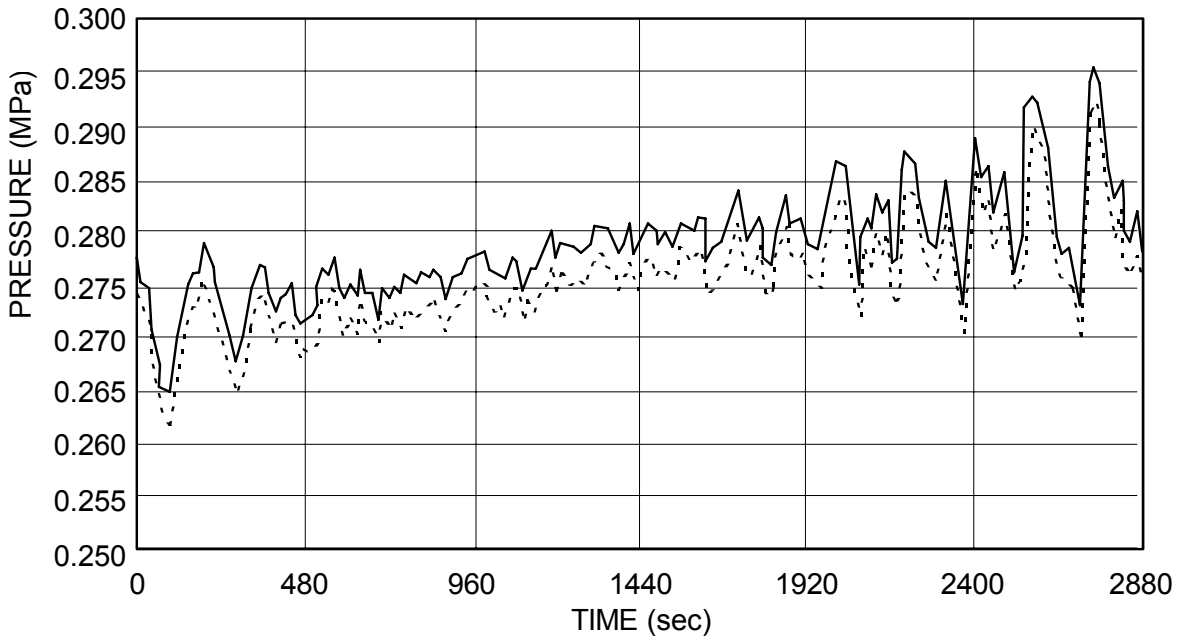


Figure 6.4-10 Test E3: Pressure at the Top of the RPV (solid) and in the PCC3 Inlet Line (dash)

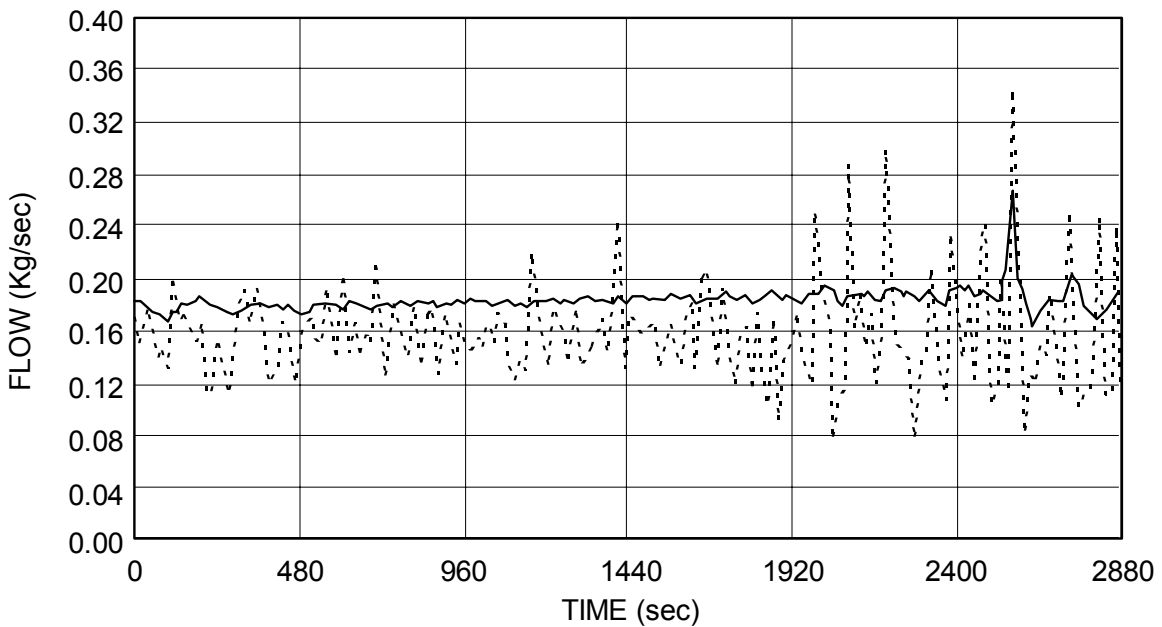


Figure 6.4-11 Test E3: Flow from the RPV to PCC3 (solid) and from PCC3 to the GDCS Pool (dash)

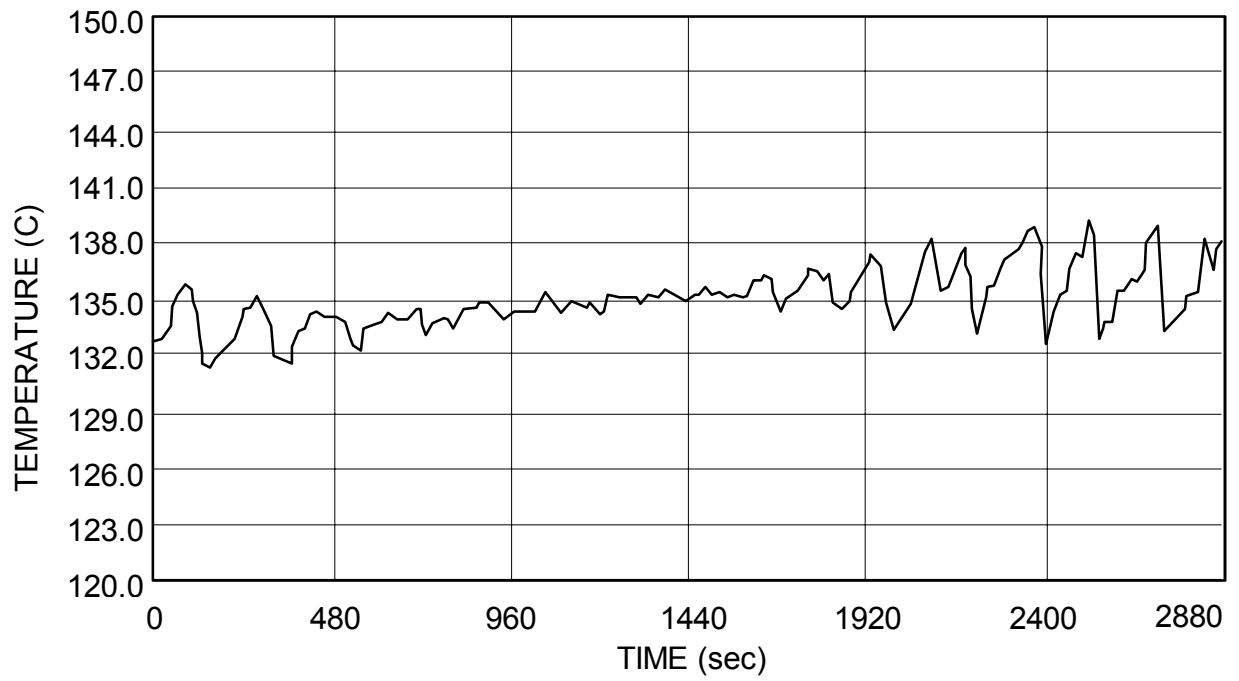


Figure 6.4-12 Test E3: Liquid Temperature at the Chimney Inlet

[

Redacted

]

Figure 6.4-13 Base TRACG Model of PANDA RPV

[

Redacted

]

Figure 6.4-14 Simplified TRACG Model of PANDA RPV

[

Redacted

]

**Figure 6.4-15 TRACG Simulation of Test E1C:
1) PCC3 Flow (solid); 2) Steam Flow into the Steam Dome (dash)**

[

Redacted

]

**Figure 6.4-16 TRACG Simulation of the Test E1C:
RPV Pressure at 1) Top; 2) Bottom**

[

Redacted

]

**Figure 6.4-17 TRACG Simulation of the Test E1C:
Liquid temperature at 1) Channel Inlet; 2) Chimney Inlet**

[

Redacted

]

**Figure 6.4-18 TRACG Simulation of the Test E2:
1) PCC3 Flow (solid); 2) Steam Flow into the Steam Dome (dash)**

[

Redacted

]

**Figure 6.4-19 TRACG Simulation of the Test E2:
RPV Pressure at 1) Top; 2) Bottom**

[

Redacted

]

**Figure 6.4-20 Flow Dependency on Inlet Subcooling (K) for Test E1C:
1) 0.6; 2) 0.4; 3) 0.15; 4) -0.6; 5) -1.35; 6) -1.4**

[

Redacted

]

Figure 6.4-21 Circulation Flow for Test E2

[

Redacted

]

6.5 Summary of Low-Power Stability Analyses

6.5.1 Introduction

Post-test evaluations of the CRIEPI Oscillation Tests and the PANDA Exploratory Tests were presented in Sections 6.3 and 6.4, respectively. In both cases, it was shown that the oscillations observed at these test facilities were primarily the result of flashing phenomena in the chimney region of the simulated RPV. The mechanism of the circulation flow oscillations due to flashing in the chimney region was examined in detail in Section 6.3. TRACG calculation of the Dodewaard startup (Section 6.2), characterized by natural circulation at low power and pressure, also predicted low-amplitude oscillations due to flashing in the chimney region. Oscillations were not apparent in the Dodewaard data but, under single-phase conditions in the core, it is possible that there was increased flow noise which was not sensed by the available instrumentation.

The objectives of Section 6.5 are to (1) demonstrate the similarity of the oscillations observed at the CRIEPI and PANDA test facilities, (2) analyze the dependence of the oscillatory regimes on key system parameters (inlet subcooling, power, pressure and geometry), and (3) develop appropriate stability criteria. The applicability and implications of the stability criteria for the Dodewaard startup test and the SBWR at startup conditions are addressed. The evaluation will be performed by direct use of the available data in conjunction with TRACG simulations of the test facilities and the Dodewaard and SBWR RPVs. The good agreement between TRACG calculations and the observed behavior at CRIEPI and PANDA, demonstrated in Sections 6.3 and 6.4, has established the credibility of the code for analysis of flow oscillations driven by intermittent flashing in the chimney region of the RPV.

6.5.2 Review of Data from CRIEPI and PANDA Test Facilities

The prominent features of the measurements at the CRIEPI test facility are large circulation flow oscillations, chimney inlet (channel exit) temperature oscillations and periodic flashing in the chimney region (Figures 6.5-1 - 6.5-3). It can also be deduced from the CRIEPI data that no oscillations occurred when there were no voids formed in the chimney region. Results from a typical TRACG simulation of an oscillatory test at CRIEPI are shown for comparison in Figure 6.5-4. TRACG calculates that circulation flow oscillates in-phase with void fraction and out-of-phase with chimney inlet temperature. These results are consistent with the measured data. The power level for all the oscillatory regimes analyzed with TRACG was low enough to essentially preclude vapor generation in the channel region. The term “channel region” is used for the heater region in the test facilities. Later in this section this term is used either for heater or core region. It was concluded that the chimney inlet temperature oscillations and the flow oscillations are strongly coupled: hence, temperature oscillations can be used as an indicator of flow oscillations.

The use of temperature data to infer flow behavior was useful in the evaluation of the PANDA exploratory tests, where there were no direct circulation flow measurements. The time dependence of the chimney inlet temperature for the PANDA exploratory test E1C is shown in Figure 6.5-5. The chimney inlet temperature oscillated while the channel inlet temperature was almost constant. The amplitude of the oscillations in the chimney inlet temperature was approximately 4 K, with a minimum and maximum, respectively, of 408 K (135°C) and 412 K

(139°C). The saturation temperatures at the chimney inlet and chimney exit, obtained from pressure measurements, were approximately 416 K (143°C) and 407.4 K (134.4°C), respectively. It can be concluded that there was no vapor generation in the channel region because the maximum chimney inlet liquid temperature is substantially less than saturation temperature at the chimney inlet. This reinforces the conclusion that the temperature oscillations at the chimney inlet indicate circulation flow oscillations.

The minimum chimney inlet temperature is slightly greater than the chimney exit saturation temperature but not by enough to provide the necessary superheat to initiate vapor generation (i.e., there would be no vapor generation in the chimney region if the chimney was filled with water at 408 K (135°C). The fact that the maximum chimney inlet temperature exceeded saturation temperature at the chimney exit by 4 to 5 K indicates that there was periodic flashing in the chimney region. Thus, it can be concluded that instabilities observed at both the CRIEPI and PANDA test facilities were driven by intermittent flashing in the chimney region.

6.5.2.1 Sensitivity to Inlet Subcooling

[

Redacted

]

6.5.2.2 Sensitivity to System Power

[

Redacted

]

6.5.2.3 Sensitivity to System Pressure

[

Redacted

]

6.5.2.4 Sensitivity to Static Head and Hydraulic Losses

[

Redacted

]

6.5.3 Development of a Stability Map for Startup Oscillations

[

Redacted

]

6.5.3.1 Criteria for the Upper Boundary

[

Redacted

]

[

Redacted

]

6.5.3.2 Criteria for the Lower Boundary

[

Redacted

]

6.5.3.3 Effect of the Flashing Number

[

Redacted

]

[

Redacted

]

6.5.4 Implications for Dodewaard Startup

[

Redacted

]

[
 Redacted
]

Pressure (MPa)	Subcooling (K)	N_{sub}	N_{PCH}	N_n
0.31	9.0	9.7	2.7	7.6
0.64	3.5	2.0	2.3	1.4

[
 Redacted
]

6.5.5 Implications for the SBWR Startup

[
 Redacted
]

[

Redacted

6.5.6 Conclusions

[

Redacted

]

]

[

Redacted

]

6.5.7 References

- [6.5-1] F. Inada, et al., *Thermo-Hydraulic Instability of Natural Circulation BWR at Low Pressure Startup: Experimental Estimation of Instability Region with Test Facility Considering Scaling Law*, Third Int. Conf. on Nucl. Eng., Kyoto, Japan, 1995.
- [6.5-2] M. Furuya, et al., *Two-Phase Flow in a Boiling Natural Circulation Loop at Relatively High System Pressure* (to be presented at NURETH-8, Kyoto, Japan, September 30-October 4, 1997).

Table 6.5-1
Dependence of the Period and Amplitude of CRIEPI Oscillations on Inlet Subcooling

[

Redacted

]

Table 6.5-2
Dependence of the Upper and Lower CRIEPI Oscillatory Boundary on Channel Power
(System Pressure = 0.2 MPa)

[

Redacted

]

Table 6.5-3
Calculated Subcooling and Phase Change Numbers at Upper Boundary of Oscillatory Region

[

Redacted

]

Table 6.5-4
Calculated Channel Inlet Subcooling at Lower Boundary of Oscillatory Region

[

Redacted

]

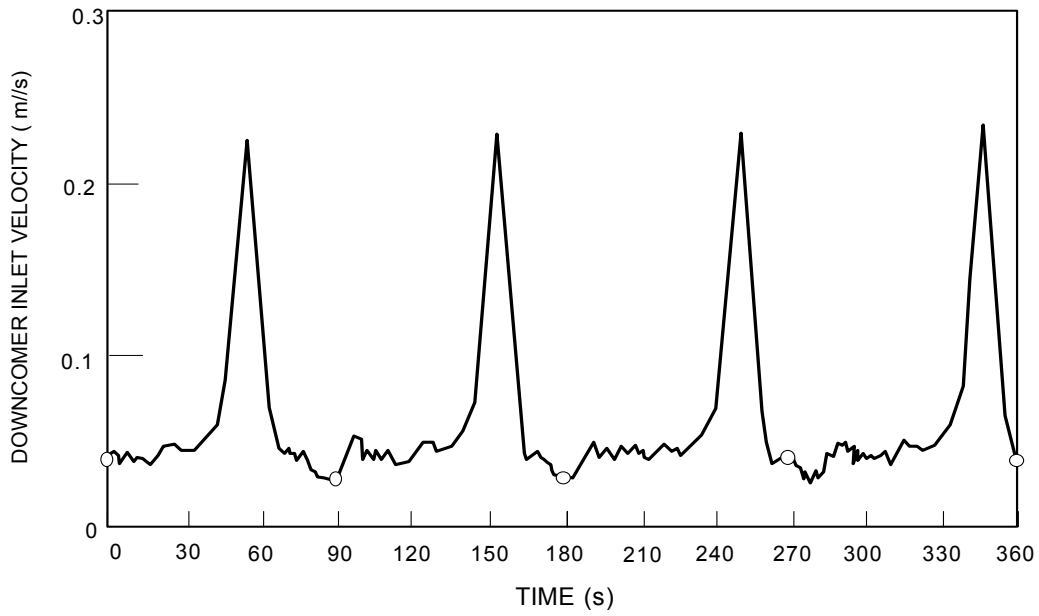


Figure 6.5-1 Measured CRIEPI Circulation Flow
(P = 0.2 MPa, q = 2.5 kW/chan , Inlet subcooling = 5.1 K)

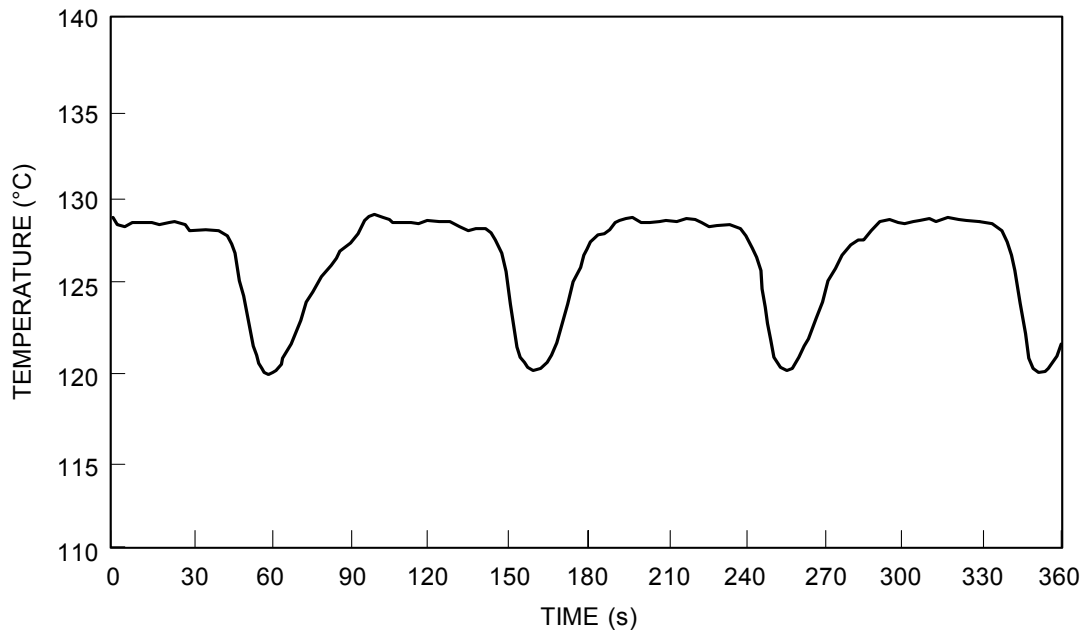
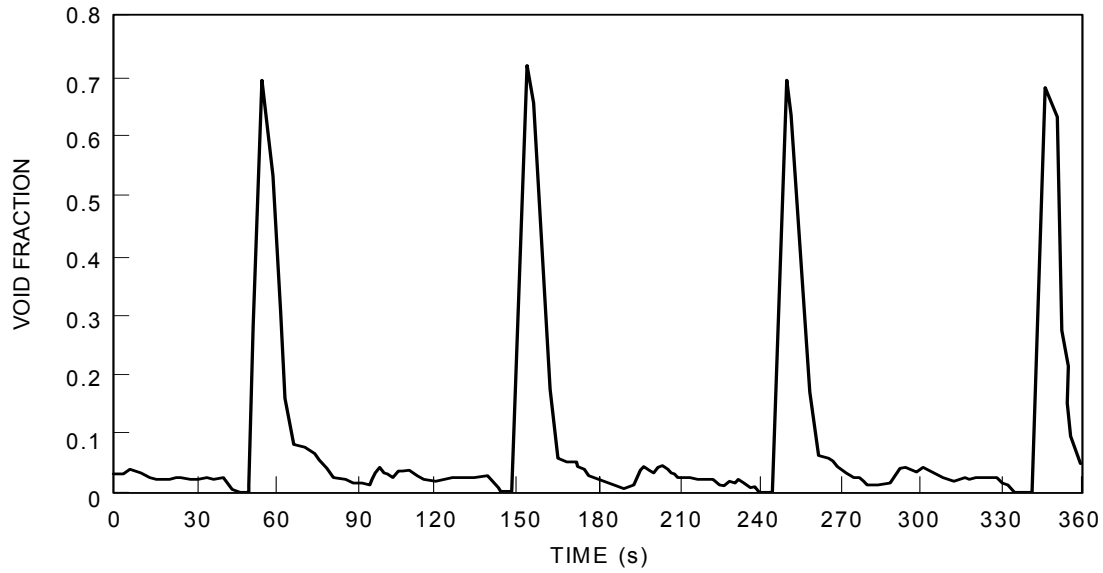


Figure 6.5-2 Measured CRIEPI Chimney Inlet Temperature
(P = 0.2 MPa, q = 2.5 kW/chan , Inlet subcooling = 5.1 K)



**Figure 6.5-3 Measured CRIEPI Upper Chimney Void Fraction
(P = 0.2 MPa, q = 2.5 kW/chan , Inlet subcooling = 5.1 K)**

[

Redacted

]

**Figure 6.5-4 TRACG Simulation: 1 - Nondimensional Circulation Flow;
2 - Nondimensional Chimney Inlet Temperature; 3 - Chimney Exit Void Fraction**

[

Redacted

]

Figure 6.5-5 Measured Chimney Inlet Temperature for PANDA Exploratory Test E1C

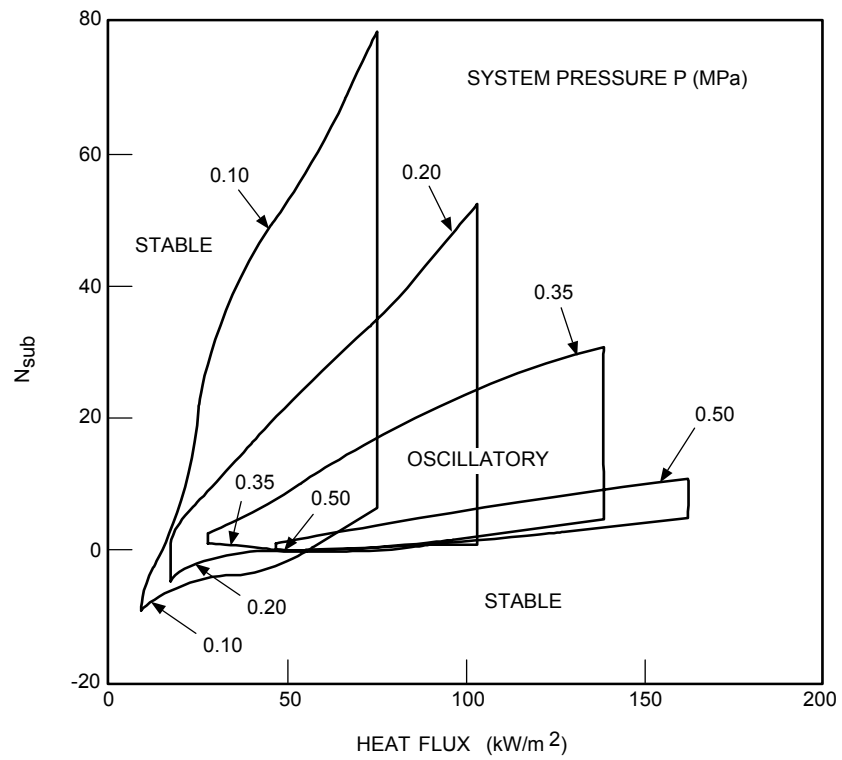


Figure 6.5-6 CRIEPI Data: Stability Maps at Various System Pressures

[

Redacted

]

Figure 6.5-7 TRACG Simulation: Dependence of Subcooling Number on Phase Change Number at the Upper Boundary of the Oscillatory Region

[

Redacted

]

Figure 6.5-8 CRIEPI Data: Dependence of Subcooling Number on Phase Change Number at the Upper Boundary of the Oscillatory Region

[

Redacted

]

Figure 6.5-9 TRACG Simulation: Sensitivity of Circulation Flow to Chimney Height at Zero Inlet Subcooling

[

Redacted

]

Figure 6.5-10 TRACG Simulation: Dependence of the Flow Oscillation Period on Flashing Number

[

Redacted

]

Figure 6.5-11 TRACG Simulation: Sensitivity of Circulation Flow to System Pressure at Zero Inlet Subcooling

[

Redacted

]

Figure 6.5-12 TRACG Model with Five Channel-Chimney Regions

[

Redacted

]

Figure 6.5-13 Core Flow Calculated with Multiple Channel TRACG Model

7. Modeling Techniques to address TRACG Model Limitations

[

Redacted

]

7.1 Phenomena Requiring More Modeling Detail

[

Redacted

]

7.1.1 Passive Containment Condenser Modeling

[

Redacted

]

[

Redacted

]

7.1.2 Parallel PCC Operation

[

Redacted

]

7.2 Phenomena Treated with Bounding Models

[

Redacted

]

7.2.1 Operation of the Standby Liquid Control System (SLCS)

[

Redacted

]

[

Redacted

]

7.2.2 Suppression Pool Stratification

[

Redacted

]

[

Redacted

]

7.2.3 Stratification of Leakage Flow in the Wetwell Gas Space

[

Redacted

]

[

Redacted

]

7.2.4 Mixing of Drywell Noncondensable Gases

[

Redacted

]

[

Redacted

]

[

Redacted

]

Figure 7.2-1 SBWR Boron Concentrations Estimated Using TRACG Models

[

Redacted

]

Figure 7.2-2 TRACG SBWR Drywell Model

7.3 Conclusions

[

Redacted

]

7.4 References

- 7-1. F. Rahnema, *PANACEA - BWR Core Simulator*, NEDE-20884, August 1990.
- 7-2. NEDE-32178P, *Application of TRACG Model to SBWR Licensing Safety Analysis* (Rev. 1), January 1998.

8. SBWR Plant Nodalization

8.1 SBWR Reactor Vessel

8.1.1 Introduction

This section describes two TRACG system input definition models for the SBWR, one for LOCA/ECCS and the other for transient analysis. The LOCA/ECCS nodalization is described in Section 8.1.5, which describes the major components of the SBWR vessel and internals. The transient nodalization is described in Section 8.1.6.

The reactor vessel, internals and main steamlines, and the isolation condenser (IC) systems are described for both the LOCA/ECCS and the transient models. The coverage includes discussion of nodalization rationale and adequacy with respect to relevant thermal-hydraulic phenomena, and reference to prior qualification comparisons. The level of nodalization detail is chosen to capture the important local phenomena and regional interactions without unduly burdening computational time. Nodalization rationale is discussed in Section 8.1.3.

The LOCA/ECCS model contains a description of the GDCS lines, the containment, and piping to simulate broken portions of the GDCS drain line, bottom drain line or the steamlines, depending on the break location. For short-term LOCA/ECCS calculations, a relatively simple containment nodalization is used and includes the drywell, wetwell and suppression pool, GDCS pool, and the drywell-to-wetwell vents. Section 8.2 includes a more detailed model of the containment used for analysis of long-term containment behavior.

8.1.2 Evolution of SBWR Nodalization

This section briefly describes the evolution of the current SBWR models. Nodalization features required to accurately capture local, regional, and global thermal-hydraulic phenomena have steadily evolved since the early 1980s and good summaries are provided in References [8.1-1]. TRACG input modeling and nodalization lessons learned from these prior calculations have been factored into the present SBWR models as described in Section 8.1-4, and Tables 8.1-1a, 8.1-1b, and 8.1-1c.

[

Redacted

]

[

Redacted

]

8.1.3 Nodalization Rationale

[

Redacted

]

8.1.4 Nodalization Feedback from Test Facility and BWR Plant Qualification

[

Redacted

]

8.1.5 Nodalization for LOCA/ECCS

[

Redacted

]

[

Redacted

]

8.1.5.1 Reactor Vessel for LOCA/ECCS

[

Redacted

]

[

Redacted

]

8.1.5.2 Fuel Channels for LOCA/ECCS

[

Redacted

]

[

Redacted

]

8.1.5.3 Guide Tubes

[

Redacted

]

8.1.5.4 Downcomer

[

Redacted

]

8.1.5.5 GDCS Line

[

Redacted

]

[

Redacted

]

8.1.5.6 Chimney

[

Redacted

]

8.1.5.7 Separators

[

Redacted

]

[

Redacted

]

8.1.5.10 Feedwater System

[

Redacted

]

8.1.5.11 Isolation Condensers

[

Redacted

]

8.1.5.12 PCCS for LOCA/ECCS

[

Redacted

]

[

Redacted

]

8.1.5.13 Control System for LOCA/ECCS

[

Redacted

]

8.1.5.14 Containment Model for LOCA/ECCS

[

Redacted

]

8.1.6 Nodalization for Transients

[

Redacted

]

[

Redacted

]

8.1.6.1 Fuel Channels Grouping for Transients

[

Redacted

]

8.1.6.2 Main Steamlines for Transients

[

Redacted

]

8.1.6.3 Control System for Transients

[

Redacted

]

8.1.7 References

[8.1-1] J.G.M Andersen et al., *TRACG Qualification*, NEDE-32177P, Rev. 2, January 2000.

[8.1-2] J. G. M. Andersen, et al, *TRACG Application for Anticipated Operational Occurrences Transient Analysis*, NEDE-32906P, January 2000.

Table 8.1-1a
Major Findings from Test Facility Nodalization Factored into the SBWR TRACG Model

[

Redacted

]

Table 8.1.1-1b
SBWR Nodalization vs. TRACG Facility Nodalization for LOCA/ECCS and Transients

[

Redacted

]

Table 8.1-1b (continued)

[

Redacted

]

Table 8.1-1b (continued)

[

Redacted

]

Table 8.1-1c
Justification of SBWR TRACG RPV Input Model Approach for LOCA/ECCS

[

Redacted

]

Table 8.1-1c (continued)
Justification of SBWR TRACG RPV Input Model Approach for LOCA/ECCS

[

Redacted

]

Table 8.1-2
TRACG Components Used for LOCA/ECCS and Transient Decks

[

Redacted

]

Table 8.1-3
SBWR TRACG Vessel Nodalization - Axial Levels (LOCA/ECCS)

[

Redacted

]

Table 8.1-4
TRACG Description of the SBWR Vessel Regions (LOCA/ECCS)

[

Redacted

]

Table 8.1-5
Grouping of Fuel Channels in Vessel Radial Rings (LOCA/ECCS)

[

Redacted

]

Table 8.1-6
Grouping of Fuel Channels in Vessel Radial Rings (Transients)

[

Redacted

]

Table 8.1-7
TRACG Description of the SBWR Containment (LOCA/ECCS)

[

Redacted

]

[

Redacted

]

Figure 8.1-1 Evolution of SBWR/TRACG Nodalization for LOCA/ECCS and Transients

[

Redacted

]

Figure 8.1-2 Schematic of the LOCA/ECCS Model Showing the RPV and the Containment Nodalization

[

Redacted

]

Figure 8.1-3 SBWR RPV Nodalization for LOCA/ECCS

[

Redacted

]

Figure 8.1-4 Nodalization of an SBWR Fuel Channel

[

Redacted

]

Figure 8.1-5 Nodalization of GDCS Piping

[

Redacted

]

Figure 8.1-6 Nodalization of SBWR Steamline System for LOCA/ECCS

[

Redacted

]

Figure 8.1-7 Nodalization for SBWR Feedwater System

[

Redacted

]

Figure 8.1-8 Nodalization of Steam Separators

[

Redacted

]

Figure 8.1-9 Nodalization for SBWR IC and DPV System

[

Redacted

]

Figure 8.1-10 Nodalization of Main Steamline System for SBWR Transients

8.2 Containment

The purpose of Section 8.2 is to describe the nodalization of the TRACG input model used for post-LOCA performance evaluation of the SBWR containment and to justify its adequacy on the basis of the post-test evaluations described in Sections 3 through 6. The knowledge and experience gained by modeling various SBWR test series with TRACG has been integrated into the SBWR TRACG containment model. Following the presentation of various features of the model in Tables 8.2-1 through 8.2-3, Table 8.2-4 summarizes the modeling approach for each of the test series and for the SBWR containment, and Table 8.2-5 presents a justification of the approach taken for the SBWR. The SBWR model includes all major containment systems and, specifically, the passive heat removal systems unique to the SBWR design. Important subregions of the model are schematically represented in Figures 8.2-1 through 8.2-4 and a schematic integral representation of the model is shown in Figure 8.2-5. The radial coordinates at the bottom of Figure 8.2-5 are relative to the reactor pressure vessel (RPV) centerline. The axial coordinates are relative to the RPV bottom-dead-center.

8.2.1 RPV and Containment Volumes

The main building block of the containment model is an axisymmetric VSSL component with 18 axial levels and 6 radial rings. The nodalization of the VSSL component is dictated by a combination of RPV and containment geometric features, and engineering judgment, influenced by the results of post-test evaluations described in earlier sections of this report. The correspondence between the positions of the radial and axial boundaries and geometric features of the plant is shown in Tables 8.2-1 and 8.2-2. The radial structure of the VSSL component is primarily dictated by the need to provide an upflow and downflow branch in each of the three regions (RPV, DW, and WW). The axial level structure was primarily dictated by containment geometry but the level positions also accommodate, in a reasonable manner, the important geometric features of the RPV. These include the total height of the vessel, the distance from the bottom to the top of the active fuel, and the height of the chimney.

[

Redacted

]

[

Redacted

]

8.2.2 One-Dimensional Components

In addition to the VSSL component, the SBWR TRACG containment model includes a large number of one-dimensional BREK, CHAN, FILL, PIPE, TEE, and VLVE components. These components and their interconnections are listed in Table 8.2-3. With a few exceptions, they are also shown in Figures 8.2-1 through 8.2-5. [

Redacted

]

[

Redacted

]

8.2.2.1 Lower Drywell

[

Redacted

]

8.2.2.2 Fuel Bundles

[

Redacted

]

8.2.2.3 PCCS

[

Redacted

]

[

Redacted

]

8.2.2.4 ICS

[

Redacted

1

8.2.2.5 GDCS One-Dimensional Components

[

Redacted

1

8.2.2.6 Steamlines

[

Redacted

1

8.2.2.7 SRVs

[

Redacted

1

[

Redacted

]

8.2.2.8 DPVs

[

Redacted

]

8.2.2.9 LOCA Vents

[

Redacted

]

8.2.2.10 Vacuum Breakers

[

Redacted

]

8.2.2.11 Equalization Lines

[

Redacted

]

[Redacted]

8.2.2.12 RPV Pressure Taps

8.2.2.13 Gas Generation by Radiolysis and Metal/Water Reaction

8.2.2.14 DW-to-WW Bypass Leakage

[Redacted]

8.2.2.15 Feedwater and Control Rod Drive Flow

8.2.2.16 Refill Pool

[Redacted]

[Redacted]

8.2.2.17 MSIVs

[Redacted]

8.2.2.18 Components to Simulate Other Breaks

Table 8.2-1
Radial Ring Boundaries of VSSL Component in SBWR TRACG Containment Model

[

Redacted

]

Table 8.2-2
Axial Level Boundaries of VSSL Component in SBWR TRACG Containment Model

[

Redacted

]

Table 8.2-3
SBWR TRACG Containment Model Components
 (* denotes connection is specific to main steamline break simulation)

Redacted

Table 8.2-3 (continued)
SBWR TRACG Containment Model Components

Redacted

Table 8.2-3 (continued)
SBWR TRACG Containment Model Components

Redacted

Table 8.2-3 (continued)
SBWR TRACG Containment Model Components

Redacted

Table 8.2-4
SBWR TRACG Containment Model Approach vs. Test Facility Modeling Approach

Redacted

Table 8.2-4 (continued)
SBWR TRACG Containment Model Approach vs. Test Facility Modeling Approach

Redacted

Table 8.2-4 (continued)
SBWR TRACG Containment Model Approach vs. Test Facility Modeling Approach

Redacted

Table 8.2-4 (continued)
SBWR TRACG Containment Model Approach vs. Test Facility Modeling Approach

Redacted

Table 8.2-5
Justification of SBWR TRACG Containment Model Approach

[

Redacted

]

Table 8.2-5 (continued)
Justification of SBWR TRACG Containment Model Approach

[

Redacted

]

Table 8.2-5 (continued)
Justification of SBWR TRACG Containment Model Approach

[

Redacted

]

Table 8.2-5 (continued)
Justification of SBWR TRACG Containment Model Approach

[

Redacted

]

Table 8.2-5 (continued)
Justification of SBWR TRACG Containment Model Approach

[

Redacted

]

Table 8.2-5 (cont'd)
Justification of SBWR TRACG Containment Model Approach

[

Redacted

]

[

Redacted

]

Figure 8.2-1 TRACG Model of SBWR Containment -RPV

[

Redacted

]

Figure 8.2-2 TRACG Model of SBWR Containment - IC and PCC

[

Redacted

]

Figure 8.2-3 TRACG Model of SBWR Containment - DW and GDCS

[

Redacted

]

Figure 8.2-4 TRACG Model of SBWR Containment - WW

[

Redacted

]

**Figure 8.2-5 TRACG Model of SBWR Containment - Configured for
Main Steamline Break**

9. Assessment of TRACG Qualification

The purpose of Section 9 is to provide an overall assessment of the TRACG qualification for application to the SBWR. This assessment includes an evaluation of the adequacy of TRACG models and a demonstration of coverage of the highly ranked PIRT phenomena by qualification studies presented in this report, or in the generic TRACG qualification report [9.1-1]. The assessment of model adequacy is accomplished by a quantitative review of the results of the comparisons of TRACG calculations and test measurements presented in Sections 3 through 6, and augmented by selected studies from the generic TRACG qualification report. The assessment of PIRT phenomena coverage is accomplished by demonstrating that the qualification strategy for SBWR application of TRACG, described in Section 2, was successfully carried out.

9.1 Adequacy of TRACG Models

The assessment of TRACG model adequacy is organized by specific parameters of interest for SBWR performance evaluations. The accuracy of the calculations is discussed with reference to all of the test data relevant to the calculation of a given parameter. The discussion is divided into five major categories: (1) LOCA/ECCS, (2) Transients, (3) Stability, (4) Containment, and (5) Plant Startup. Within these categories, a further distinction is made between “Key Safety Parameters” and parameters that fall into the category of “PIRT Phenomena”. For each set of test data, TRACG calculation accuracy is quantified in terms of an average difference, or bias, between the TRACG calculations and the test measurements, and a standard deviation (unbiased estimate) of the differences about that average. In most cases, a bias and standard deviation are presented for both the absolute differences and the differences relative to the measured values, expressed as percentages. (Mathematical definitions of bias and standard deviation are given in Section 2). The bias and standard deviation of the TRACG calculations are discussed and summarized in a set of tables. For each safety parameter or PIRT phenomenon, an appropriate comparison basis is presented and used to assess the adequacy of the TRACG model. Where appropriate (and available), the comparison basis includes consideration of the estimated uncertainty in the test measurements. In certain cases, the assessment of TRACG adequacy leads to the conclusion that a bounding model should be employed to cover potential uncertainties. Section 7 describes the approach used in the application of bounding models for TRACG simulations of the SBWR.

[

Redacted

]

9.1.1 LOCA/ECCS

[Redacted]

9.1.1.1.1 RPV Level

[

Redacted

]

9.1.1.2 PIRT Phenomena

9.1.1.2.1 Core Void Fraction

[

Redacted

]

9.1.1.2.2 Chimney, Lower Plenum and Downcomer Void Fraction

[

Redacted

]

9.1.1.2.3 Break Flow

[

Redacted

]

[

Redacted

]

9.1.1.2.4 GDCS Flow

[

Redacted

]

[Redacted]

9.1.2 Transients

9.1.2.1 Key Safety Parameters

9.1.2.1.1 RPV Pressure

[
Redacted
]

9.1.2.1.2 Minimum Critical Power Ratio (MCPR)

[

Redacted

]

9.1.2.1.3 Energy Deposition

[

Redacted

]

9.1.2.1.4 Level Change

[

Redacted

]

[

Redacted

]

9.1.2.2 PIRT Phenomena

9.1.2.2.1 Natural Circulation Flow

[

Redacted

]

9.1.3 Stability

[

Redacted

]

[

Redacted

]

9.1.3.1 Key Safety Parameters

9.1.3.1.1 Decay Ratio/Oscillation Amplitude

[

Redacted

]

9.1.3.2 PIRT Phenomena

9.1.3.2.1 Stability Boundary for Hydrodynamic Oscillations

[

Redacted

]

9.1.4 Containment

[

Redacted

]

9.1.4.1 Key Safety Parameters

9.1.4.1.1 Containment Pressure

[

Redacted

]

9.1.4.1.1.1 Short-Term Blowdown Response

[

Redacted

]

9.1.4.1.1.2 Long-Term Response

[

Redacted

]

[

Redacted

]

9.1.4.1.2 DW Temperature

[

Redacted

]

[

Redacted

]

9.1.4.1.3 WW Gas Temperature

[

Redacted

]

[

Redacted

]

9.1.4.2 PIRT Phenomena

9.1.4.2.1 Vent-Clearing Time

[

Redacted

]

9.1.4.2.2 WW Liquid Temperature

[

Redacted

]

9.1.4.2.3 PCC Heat Removal

[

Redacted

]

[

Redacted

]

9.1.4.2.4 PCC Pressure Drop

[

Redacted

]

9.1.5 Plant Startup

[

Redacted

]

9.1.5.1 Natural Circulation Flow (Startup Conditions)

[

Redacted

]

9.1.5.2 Low Pressure Oscillations During Startup

[

Redacted

]

9.1.6 References

- [9.1-1] J.G.M. Andersen, et al., *TRACG Qualification*, NEDE-32177P, Rev. 2, Class 3, January 2000.
- [9.1-2] M.G. Ortiz and L.S. Ghan, *Uncertainty Analysis of Minimum Vessel Liquid Inventory During a Small-Break LOCA in a B&W Plant - An Application of the CSAU Methodology Using the RELAP5/MOD3 Computer Code*, NUREG/CR-5818, December 1992.
- [9.1-3] GE Document No. 25A5113, *SBWR Standard Safety Analysis Report*, Rev. A, August 1992.
- [9.1-4] G.G. Jones, *Impact of Time-Varying Axial Power Shape on Pressurization Transients*, GENE-666-03-0393, March 1993.

Table 9.1-1
Accuracy of TRACG Calculations for RPV Level

[

Redacted

]

Table 9.1-2
Accuracy of TRACG Calculations for Core Void Fraction

[

Redacted

]

Table 9.1-3
Accuracy of TRACG Calculations for Chimney, Lower Plenum, and Downcomer
Void Fraction

[

Redacted

]

Table 9.1-4
Accuracy of TRACG Calculations for RPV Break Flow

[

Redacted

]

Table 9.1-5
Accuracy of TRACG Calculations for GDCS Flow

[

Redacted

]

Table 9.1-6
Accuracy of TRACG Calculations for IC Heat Removal

[

Redacted

]

Table 9.1-7
Accuracy of TRACG Calculations for Natural Circulation and Stability

[

Redacted

]

Table 9.1-8
Accuracy of TRACG Calculations for Peak Neutron Flux

[

Redacted

]

Table 9.1-9

Accuracy of TRACG Calculations for Short-Term Containment Pressure

[

Redacted

]

Table 9.1-10

Accuracy of TRACG Calculations for Long-Term Containment Pressure

[

Redacted

]

Table 9.1-11
Accuracy of TRACG Calculations for DW Temperature

[

Redacted

]

Table 9.1-12
Accuracy of TRACG Calculations for WW Gas Temperature

[

Redacted

]

Table 9.1-13
Accuracy of TRACG Calculations for Vent Clearing Time

[

Redacted

]

Table 9.1-14
Accuracy of TRACG Calculations for WW Liquid Temperature

[

Redacted

]

Table 9.1-15
Accuracy of TRACG Calculations for PCC Heat Removal

[

Redacted

]

Table 9.1-16
Accuracy of TRACG Calculations for PCC Pressure Drop

[

Redacted

]

Table 9.1-17

Accuracy of TRACG Calculations for Natural Circulation Flow (Startup Conditions)

[

Redacted

]

Table 9.1-18

Accuracy of TRACG Calculations of Flow Oscillations During Startup

[

Redacted

]

[

Redacted

]

Figure 9.1-1 SBWR Stability Map

9.2 Adequacy of Qualification Coverage

Section 2 described a “Qualification Strategy” for SBWR application of TRACG. Tables 2.1-7a and 2.1-7b were developed to show how the highly ranked PIRT parameters were covered by SBWR-related tests and associated TRACG post-test analyses. The purpose of this section is to present a set of conclusions which demonstrate that the TRACG qualification strategy was successfully carried out. This will be done in terms of each of the highly ranked PIRT parameters listed in Tables 2.1-7a and 2.1-7b.

9.2.1 Reactor Vessel and Core

In the discussion of PIRT phenomena for the reactor vessel and core, reference will be made to the Christensen, Wilson and Bartolomei void fraction tests. These tests are discussed individually in Section 3.3.1 and important distinguishing features of the tests are shown in Table 3.3-2.

9.2.1.1 Lower Plenum

[

Redacted

]

[

Redacted

]

9.2.1.2 Bypass

[

Redacted

]

9.2.1.3 Core

[

Redacted

]

[

Redacted

]

[

Redacted

]

[

Redacted

]

[

Redacted

]

9.2.1.4 Guide Tubes

[

Redacted

]

9.2.1.5 Downcomer

[

Redacted

]

[

Redacted

]

[

Redacted

]

9.2.1.6 Chimney

[

Redacted

]

[

Redacted

]

9.2.1.7 Separators

[

Redacted

]

9.2.1.8 ATWS

[

Redacted

]

9.2.1.9 Steamline

[

Redacted

]

9.2.1.10 Isolation Condenser

[

Redacted

]

9.2.1.11 Stability

[

Redacted

]

[

Redacted

]

9.2.1.12 RPV

[

Redacted

]

9.2.1.13 Interactions

[

Redacted

]

[

Redacted

]

9.2.2 Containment

9.2.2.1 Break

[

Redacted

]

9.2.2.2 Main Vent

[

Redacted

]

9.2.2.3 SRV

[

Redacted

]

9.2.2.4 Drywell

[

Redacted

]

[

Redacted

]

9.2.2.5 Wetwell

[

Redacted

]

[

Redacted

9.2.2.6 PCCS

[

Redacted

]

]

[

Redacted

]

[

Redacted

]

9.2.2.7 Drywell/Wetwell Boundary

[

Redacted

]

9.2.2.8 Vacuum Breaker

[

Redacted

]

[Redacted]

9.2.2.9 Equalizing Line

9.2.2.10 RPV

9.2.2.11 DPV

9.2.2.12 System Interactions

[

Redacted

]

9.2.3 References

- [9.2-1] J.G.M. Andersen et al., *TRACG Qualification*, NEDE 32177P, Rev. 2, January 2000.
- [9.2-2] *SBWR Testing Summary Report*, NEDC-32606P, Rev. 0, Class 3, August 2002.
- [9.2-3] W.J. Oosterkamp and G. Koopmans, *Startup of Natural Circulation BWRs*, ICONE-2, Tokyo, 1991.
- [9.2-4] J.G.M. Andersen, et al., *TRACG Model Description*, NEDE-32176P, Rev. 2, December 1999.
- [9.2-5] C.L. Martin, *Lattice Physics Methods*, NEDO-20913A, February 1977.

- [9.2-6] S.O. Akerlund, et al., *The GESTR-LOCA and SAFER Models for the Evaluation of the Loss-of-Coolant Accident*, Volume 1: GESTR-LOCA - A Model for the Calculation of Fuel Rod Thermal Performance”, NEDO-23785-1-A, Revision 1, February 1985.
- [9.2-7] J.F. Briesmeister, editor, *MCNP - A General Monte Carlo N-Particle Transport Code*, Version 4A, LA-12625, Los Alamos National Laboratory, March 1994.
- [9.2-8] *SBWR Vacuum Breaker Prototype Experimental Qualification General Test Report*, COMPES Report ED45913, October 1994.
- [9.2-9] *Scaling of the SBWR Related Tests*, NEDC-32288P, Revision 1, October 1995.

10. Conclusions

The objective of the TRACG qualification effort was to assess the code and demonstrate its capability to adequately calculate various classes of SBWR transient and accident events. TRACG is used for the analysis of SBWR loss-of-coolant accidents (LOCAs), including both the performance of the Emergency Core Cooling Systems (LOCA/ECCS), and containment pressure and temperature response (LOCA/containment), anticipated transients, anticipated transients without scram (ATWS) and stability.

The qualification objective was achieved through the following steps:

1. A systematic and rigorous approach was defined (Section 2) and followed.
2. Tests were performed or selected from available data sets to develop the necessary TRACG qualification database (Section 2).
3. TRACG was used to simulate the tests and modeling capabilities were evaluated quantitatively (Sections 3 through 6).
4. Limitations in TRACG models were identified, and bounding approaches developed to address these as necessary (Section 7).
5. SBWR nodalizations were developed for the TRACG analysis applications and were justified on the basis of the test simulations (Section 8).
6. The accuracy of TRACG for the analysis applications was evaluated and shown to be adequate (Section 9).
7. Coverage of highly ranked PIRT phenomena by the qualification test data was evaluated and shown to be adequate by comparison with design margins (Section 9).

An important factor in the evaluation of the adequacy of TRACG for SBWR application is that the overall performance of the SBWR for LOCAs can be readily predicted, and the key safety parameters have large design margins. The core does not uncover for any of the postulated breaks and there is no core heatup. The containment pressure can be calculated on a global thermodynamic basis, and is primarily controlled by the compression of the wetwell gas space resulting from the purging of the noncondensibles from the drywell together with the steam vapor pressure corresponding to the suppression pool surface temperature. The plant response and the performance of key safety systems have been confirmed through testing (PANTHERS, GIST, GIRAFFE, PANDA and Mark III and Mark II containment early blowdown response tests). The results were accurately calculated by TRACG. Thus, TRACG can be used with confidence to calculate the key safety parameters for LOCA (peak cladding temperature and peak containment pressure).

For operational transients, the governing physical phenomena are similar to operating BWRs. TRACG has been qualified against data from the Peach Bottom turbine trip tests, Hatch MSIV

closure tests and Hatch flow coastdown tests. The safety parameters (RPV pressure and neutron flux) were accurately calculated by TRACG. The SBWR transient response differs from operating plants in the magnitude of level swings caused by void changes in the tall chimney. This difference is addressed by separate effects tests on level changes and void fraction measurements in large pipes. These tests were calculated well by TRACG.

ATWS events involve the same physical phenomena as for operational transients. In addition, steam is discharged to the suppression pool through safety/relief valves, and shutdown of the nuclear reaction is achieved by delivery of boron to the core. All the important phenomena were covered under TRACG qualification for LOCA and transients, except for mixing and stratification of the injected borated water solution in the RPV inventory. A scaled boron mixing test was analyzed for this purpose, and a conservative modeling procedure was developed to bound stratification effects in the SBWR. [

Redacted

]

In conclusion, the qualification results documented in this report demonstrate that TRACG has been satisfactorily assessed over the defined matrix of tests, and is qualified for application to the SBWR over the intended range of applications. TRACG can, therefore, be used for the licensing analysis of transient and accident events in conjunction with an appropriate application methodology. The details of the application methodology for SBWR are documented in the TRACG Application Report [10-1]*.

10.1 References

[10-1] *Application of TRACG Model to SBWR Licensing Safety Analysis*, GE Nuclear Energy, NEDE-32178P, Rev. 1, January 1998.

*This report is not relevant to the ESBWR. It will be replaced by an ESBWR Application Report.

Appendix A

Comparison between TRACG02 and TRACG04

Pages A-1 through A-5

Redacted